Ingenieurfakultät Bau Geo Umwelt

Technische Universität München

Fachgebiet Hangbewegungen

Long-term monitoring of permafrost-affected rock walls

Towards an automatic, continuous electrical resistivity tomography (AERT) monitoring for early warning systems

Eingereicht von

Markus Keuschnig, Msc

Vollständiger Abdruck der von der Fakultät Bau Geo Umwelt, Technische Universität München zur Erlangung des akademischen Grades eines Doktor der Naturwissenschaften (Dr. rer. nat.) genehmigten Dissertation.

Vorsitzender: Prof. Dr.-Ing. habil. Thomas Wunderlich

Prüfer der Dissertation: 1. Prof. Dr. rer. nat. Michael Krautblatter

2. Prof. Dr. rer. nat. Lothar Schrott

3. Prof. Dr. rer. silv. Annette Menzel

Die Dissertation wurde am 21.09.2016 an der Technischen Universität München eingereicht und durch die Fakultät Bau-Geo-Umwelt am 11.11.2016 angenommen.

„The most rewarding researches are those which, in as much as they are a joy to the thinker, are at the same time of benefit to mankind.“

(Christian Doppler)

Comment

This Ph.D.-thesis was written in accordance with the rules for "Kumulative Promotionen" issued on February, 2014. The following articles have been fully incorporated in the thesis (* ISI listed publication):

*OTTO, J. C., **KEUSCHNIG, M.**, GOTZ, J., MARBACH, M. & SCHROTT, L. 2012. Detection of Mountain Permafrost by Combining High Resolution Surface and Subsurface Information - an Example from the Glatzbach Catchment, Austrian Alps. *Geografiska Annaler Series a-Physical Geography,* 94A**,** 43-57.

*HARTMEYER, I., **KEUSCHNIG, M.** & SCHROTT, L. 2012. A Scale-Oriented Approach for the Long-Term Monitoring of Ground Thermal Conditions in Permafrost-Affected Rock Faces, Kitzsteinhorn, Hohe Tauern Range, Austria. *Austrian Journal of Earth Sciences,* 105**,** 128-139.

***KEUSCHNIG, M.**, KRAUTBLATTER, M., HARTMEYER, I., FUSS, C. & SCHROTT, L. accepted. Automated Electrical Resistivity Tomography testing for Early Warning in Unstable Permafrost Rock Walls around Alpine Infrastructure. *Permafrost and Periglacial Processes*.

***KEUSCHNIG, M.**, HARTMEYER, I., SCHMIDJELL, A., MARBACH, M., SCHROTT, L. & KRAUTBLATTER, M. prepared for submission. A low-cost strategy for near-surface rock temperature measurements using iButtons. *Cold Regions Science and Technology*.

***KEUSCHNIG, M.**, KRAUTBLATTER, M. & HARTMEYER, I. prepared for submission. Field evidence for temperature-resistivity relationship of permafrost-affected alpine rock walls. *The Cryosphere*.

***KEUSCHNIG, M.**, HARTMEYER, I., HÖFER-ÖLLINGER, G., SCHOBER, A., KRAUTBLATTER, M. & SCHROTT, L. 2015. Permafrost-Related Mass Movements: Implications from a Rock Slide at the Kitzsteinhorn, Austria. *In:* LOLLINO, G., MANCONI, A., CLAGUE, J., SHAN, W. & CHIARLE, M. (eds.) *Engineering Geology for Society and Territory - Volume 1.* Springer International Publishing.

Additionally, the following publications have been considered in the thesis:

KEUSCHNIG, M., HARTMEYER, I., OTTO, J. C. & SCHROTT, L. 2011. A new permafrost and mass movement monitoring test site in the Eastern Alps—concept and first results of the MOREXPERT project. *In:* BORSDORF, A., STÖTTER, J. & VEULLIET, E. (eds.) *Managing Alpine future II—inspire and drive sustainable mountain regions. Proceedings of the Innsbruck Conference, 21–23 November 2011.* IGF-Forschungsberichte 4: Austrian Academy of Sciences.

OTTO, J. C. & **KEUSCHNIG, M.** 2014. Permafrost-Glacier Interaction - Process Understanding of Permafrost Reformation and Degradation. *In:* RUTZINGER, M., HEINRICH, K., BORSDORF, A. & STÖTTER, J. (eds.) *permAfrost – Austrian Permafrost Research Initiative - Final Report.* IGF-Forschungsberichte 6: Austrian Academy of Sciences.

*SUPPER, R., OTTOWITZ, D., JOCHUM, B., ROMER, A., PFEILER, S., KAUER, S., **KEUSCHNIG, M.** & ITA, A. 2014. Geoelectrical monitoring of frozen ground and permafrost in alpine areas: field studies and considerations towards an improved measuring technology. *Near Surface Geophysics,* 12**,** 93-115.

Content:

1 Abstract

Subsurface monitoring of permafrost conditions at depths up to 20-30 m is crucial to assess the safety and reliability of mountain infrastructure, because permafrost degradation critically affects rock slope stability in high mountains. Thus, developing methods to provide information on thermal and hydrostatic subsurface properties is essential, especially as boreholes provide one-dimensional (1D) thermal data in a complex 3D terrain and usually cannot be installed in actively unstable rock masses. Electrical resistivity tomography (ERT) has been proven to be a straightforward monitoring tool for near surface bedrock permafrost for monthly or longer intervals. But as rockfalls are often prepared over periods of days or hours, ERT for early warning purposes should also detect short-term triggering events such as pressurised water flow.

During the course of this Ph.D.- project, an open air laboratory (OpAL) for long-term monitoring of permafrost and mass movements was established in the summit region of the Kitzsteinhorn (3,203 m a.s.l.) and is now the best instrumented long-term monitoring site for permafrost and mass movements in Austria. The systemic and scale-oriented approach includes a combination of automated weather stations, remote sensing techniques, temperature measurements in shallow and deep boreholes, geophysical and geotechnical investigations to identify potentially critical thresholds for rock slope instabilities. The OpAL was developed and instrumented to provide answers to the following main research questions: (i) Is an automatic electrical resistivity tomography (AERT) capable to continuously monitor the state of frozen, steep permafrost affected bedrock? (ii) On which temporal and spatial scales can AERT monitor stability-relevant hydrostatic and thermal changes? (iii) Do iButtons provide sufficient accuracy to perform spatially and temporally highly resolved near-surface rock temperature (NSRT) measurements in complexly structured permafrost-affected rock walls? (iv) Is it possible to observe a temperature-resistivity (T-ρ) relationship under field conditions, what are the characteristics and are these T-ρ gradients comparable to laboratory results?

To provide stability-relevant hydrostatic and thermal information with ERT, the first permanently installed AERT system was established on a steep, unstable permafrost rock wall to monitor subsurface electrical resistivity changes continuously. ERT is measured every 4h at the up to 67° steep rock wall below the Kitzsteinhorn cable car. Wenner datasets (n=996) were analysed from February 2013 to February 2014 in terms of data stability, raw data characteristics and measurement errors coinciding with potential disturbing factors. Strong resistivity changes coincided with rapid freezing or water inundating rock fractures. Automatically detected periods with large resistivity changes produce ERT time series with low resistivities extending from the bottom upwards during times of snowmelt. Fracture inventories, visual observations of cleftwater and NSRT measurements, provide indications that the flow of pressurised water in fractures warms the surrounding rock in an upward direction. Complementary to the AERT measurements, the spatial and temporal variations of NSRT are measured in a hitherto unknown coverage using a newly developed low-cost alternative based on miniature temperature loggers (iButtons). This includes an innovative adaptation procedure including preparation, installation and maintenance of the system. To meet the requirements for spatially and temporally distributed rock temperature measurements, the measurements were analysed regarding reliability and accuracy. The combination of AERT and NSRT measurements leads to the first comprehensive field evidence of a T-ρ relationship. The T-ρ relationship can be used as a proxy for the thermal state and in further consequence for stability-relevant information on the

mechanical state of permafrost rock walls. Based on 1485 Wenner and rock temperature datasets, the T-ρ characteristics were analysed considering different depths of investigation. Linear regression modelling shows that analysed T-ρ relationships are highly significant with a *p*-value $< 2.2e^{-16}$ and a R^2 of up to 0.64. The measured T-ρ gradients of 22.9 to 27.9 %/°C under permafrost conditions, are in the range of the laboratory results of 29.8±10.6 %/°C (Krautblatter, 2009).

This Ph.D.-thesis presents (i) the first approach to monitor permafrost rock walls quasi-continuously with AERT where high apparent resistivity changes in 4h intervals may precede critical hydrostatic events confined by permafrost rocks including (ii) a newly developed strategy for spatially and temporally high resolution NSRT measurements. The combined methodological approach (AERT and NSRT measurements) results (iii) in the first comprehensive field evidence of the T-ρ relationship which has been postulated in the laboratory a few years ago. OpAL instrumentation and field monitoring techniques developed, tested and analysed in this PhD provide a framework that can be used for early warning systems in unstable permafrost-affected rock walls.

2 Zusammenfassung

Permafrostveränderungen beeinflussen die Stabilität hochalpiner Felswände und Felsflanken. Daher ist die Überwachung von Permafrostbedingungen, bis in eine Tiefe von 20-30 m, essentiell für die Sicherheitsbeurteilung alpiner Infrastruktur. Für die Überwachung thermischer und hydrostatischer Bedingungen im komplexen, alpinen Gelände ist die Entwicklung von Methoden, die über punktuelle Bohrlochmessungen hinausgehen, von großer Bedeutung. Geoelektrik (ERT) ist eine bewährte Methode zur Überwachung von Felspermafrost in monatlichen oder längeren Messintervallen. Stabilitätsrelevante Faktoren wie Felstemperaturen oder Gebirgsfeuchte können sich jedoch innerhalb weniger Tage oder Stunden maßgeblich verändern. Auch kurzfristige Auslöser, wie erhöhte Kluftwasserdrücke, müssen daher mit einem möglichen ERT-Frühwarnsystems detektiert werden können.

Im Verlauf dieser Doktorarbeit wurde ein Freiluftlabor für die Langzeitüberwachung von Permafrost und gravitativen Massenbewegungen im Bereich der Gipfelregion des Kitzsteinhorns (3.203 m ü. d. M.) eingerichtet. Dieses Freiluftlabor ist gegenwärtig der am besten instrumentierte Forschungsstandort für Permafrost und Massenbewegungen in Österreich. Basierend auf einer systemischen, skalenorientierten Überwachung von Atmosphäre (Wetterstationen), Oberfläche (Fernerkundung, Bewegung) und Untergrund (Bohrlochtemperaturen und Geophysik) werden Einflussfaktoren auf die Felsstabilität kontinuierlich überwacht um potentiell kritische Schwellenwerte zu identifizieren. Für diese Doktorarbeit bildet das Freiluftlabor die Basis für die Beantwortung der folgenden, übergeordneten Forschungsfragen: (i) Ist eine automatische ERT (AERT) geeignet den Zustand von steilen, Permafrost-beeinflussten Felswänden kontinuierlich zu überwachen? (ii) Auf welchen zeitlichen und räumlichen Skalen kann eine AERT stabilitätsrelevante hydrostatische und thermische Veränderungen detektieren? (iii) Bieten iButtons eine ausreichende Genauigkeit für die Durchführung hochaufgelöster räumlicher und zeitlicher NSRT Messungen in komplexen, Permafrost-beeinflussten Felswänden? (iv) Ist es möglich eine Temperatur-Resistivitäts-Beziehung (T-ρ) unter Feldbedingungen zu messen, welche Eigenschaften weist diese auf und sind die T-ρ Gradienten mit Laborergebnissen vergleichbar?

Um kontinuierliche, stabilitätsrelevante thermische und hydrostatische Daten mit ERT zu erfassen, wurde erstmalig ein AERT System in einer steilen, instabilen und durch Permafrost-beeinflussten Felswand für kontinuierliche Messungen installiert. Dabei werden alle 4h Geoelektrikmessungen in der bis zu 67° steilen Felswand unterhalb der Kitzsteinhorn-Seilbahn durchgeführt. 996 aufeinanderfolgende Wenner Datensätze wurden von Februar 2013 bis Februar 2014 erfasst und hinsichtlich Datencharakteristik, Messfehler und deren potenziellen Einflussgrößen analysiert. Große Veränderungen in der Resistivität stimmen mit spontanem Gefrieren oder der Infiltration von Wasser überein. Automatisch erfasste Perioden mit großen Resistivitätsveränderungen ergeben ERT Zeitreihen, in welchen sich während der Schneeschmelze niedrige Resistivitäten von größeren Tiefen nach oben hin ausbreiten. Basierend auf Trennflächenanalysen, visuellen Beobachtungen von Kluftwasser und NSRT Messungen kann auf unter Druck stehendes Kluftwasser geschlossen werden, das den Untergrund von tieferen Bereichen in Richtung Oberfläche sättigt und erwärmt. Ergänzend zu den ERT Daten wurde die räumliche und zeitliche Verbreitung der NSRT in einem bisher noch nicht erreichten Umfang mit Hilfe einer neu entwickelten „low-cost" Alternative auf Basis von Miniatur-Temperaturloggern (iButtons) erfasst. Diese beinhaltet ein innovatives Anpassungsverfahren einschließlich Vorarbeiten, Installation und Wartung. Um der hohen räumlichen und zeitlichen Variabilität der NSRT gerecht zu werden, wurden die Messungen hinsichtlich Verlässlichkeit und Genauigkeit analysiert. Mit diesem kombinierten methodischen Ansatz (AERT und NSRT Messungen) konnte erstmalig die T-ρ Beziehung unter Feldbedingungen nachgewiesen werden. Die T-ρ Beziehung kann als Proxy für den thermischen Zustand und in weiterer Folge als stabilitätsrelevante Information für den mechanischen Zustand von Permafrost-beeinflussten Felswänden verwendet werden. Basierend auf 1485 Wenner und NSRT Datensätzen wurden die T-ρ Beziehungen unter Berücksichtigung verschiedener Untersuchungstiefen analysiert. Lineare Regressionsmodelle zeigen einen hochsignifikanten T-ρ Zusammenhang mit einem *p*-value $< 2,2e^{-16}$ und einem R^2 von bis zu 0,64. Die unter Permafrostbedingungen gemessenen T-ρ Gradienten von 22,9 bis 27,9 %/°C sind im Bereich der Labormessungen mit einem Gradienten von 29,8±10,6 %/°C (Krautblatter, 2009).

Diese Doktorarbeit präsentiert (i) den ersten Ansatz für die kontinuierliche Überwachung von Permafrost-beeinflussten Felswände mit AERT ergänzt mit (ii) einer neu entwickelten Strategie für räumlich und zeitlich hochaufgelöste NSRT Messungen. Der kombinierte methodische Ansatz führt zum (iii) ersten umfangreichen Feldbeweis der bi-linearen Temperatur-Resistivitäts-Beziehung, welche bereits vor einigen Jahren unter Laborbedingungen nachgewiesen werden konnte. Die während dieser Doktorarbeit im Freiluftlabor entwickelten, getesteten und analysierten Instrumentierungen und Überwachungstechniken bilden eine Basis für Frühwarnsysteme in instabilen, von Permafrost-beeinflussten Felswänden.

3 Introduction

3.1 Motivation and problem statement

The pronounced changes of mountain glaciers and significant rockfall events during exceptional warm summers in the last decades have strongly raised awareness and interest in changing conditions of high mountain areas (Haeberli et al., 2010). Alpine regions are considered to be particularly sensitive to climate change and observations as well as projections report a rise of temperatures significantly above lowland areas. In Austria, the mean annual air temperature (MAAT) has increased approximately 2 °C (APCC, 2014) since 1880. This temperature rise is significantly higher than the global mean of 0.85 °C (IPCC, 2013). Even in the future, a greater average temperature increase up to 5.3 °C for 2085 (A1FI scenario, Nogués-Bravo et al. (2007)) is expected for alpine regions compared to global temperature change.

Extensive areas in cold mountain regions are affected by permafrost conditions. In Austria, permafrost areas cover approximately 1,600 km² (Ebohon and Schrott, 2008). Permafrost is defined as ground (soil or rock and included ice or organic material) that remains at or below 0°C for at least two consecutive years (IPA, 2015). Mountain permafrost research is a young scientific discipline that systematically started in the early seventies (Haeberli et al. 2010). In the Alps, long-term data series on permafrost conditions, comparable to meteorological data, are limited to a few monitoring test sites (e.g. the Swiss Permafrost Network – PERMOS (2015)). However, long-term monitoring is a prerequisite for an improved understanding of permafrost dynamics and particularly for permafrost and rockfall interaction.

An increasing number of rockfall events of different magnitudes have been observed and reported recently from permafrost-affected areas (Rabatel et al., 2008; Huggel, 2009; Ravanel and Deline, 2011; Fischer et al., 2013; Stoffel et al., 2014; Keuschnig et al., 2015) representing a serious risk factor for man and infrastructure (Höfer-Öllinger et al., 2015). Especially during the hot periods of 2003 and 2005 a large number of rockfall events were triggered from steep bedrock areas affected by permafrost without preceding precipitation or earthquake (Gruber and Haeberli, 2007). These studies are based on field observations and suggest an increasing occurrence of rockfall events due to rising temperatures (Figure 1).
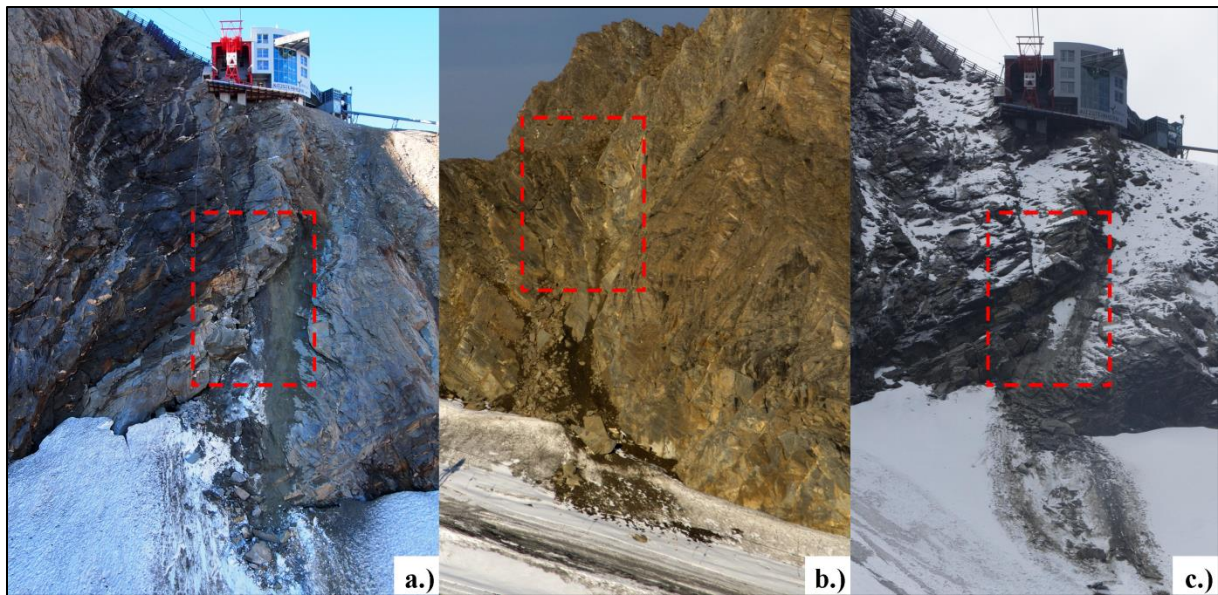
Figure 1: Observed rockfall events from permafrost-affected areas (August, 2012 (a); September, 2012 (b, c); Kitzsteinhorn, Austria). Red areas mark the detachment zones.

The Working Group II of the Intergovernmental Panel on Climate Change (IPCC, 2014) points out an increase in rock slope failures in the Western Alps (medium confidence) and a major contribution from climate change. However, for single rockfall events, the reconstruction of the failure- and the triggering mechanism is problematic due to a lack of atmospheric, ground surface and subsurface data at and before the event.

Laboratory studies show that thermal changes in frozen rock significantly alter the mechanical properties of rock and ice along potential failure planes (Krautblatter et al., 2013). For rock stability considerations, the thermal state of steep permafrost-affected rock faces has become a key issue. The development and refinement of methods capable of providing information on thermal and hydrostatic subsurface properties has gained major importance (Harris et al., 2009; Haeberli et al., 2010; Krautblatter et al., 2012). This is especially true as boreholes provide 1D thermal data in a complex 3D terrain and cannot be installed in actively unstable rock masses.

Geophysical techniques that rely on the measurement of electrical currents have become increasingly popular in this field as electrical resistivity of frozen rock is highly temperature-dependent and reacts sensitively to the gradual freezing of water in pores and fissures in bedrock from 0 to ca. -8 °C (Mellor, 1973; Krautblatter et al., 2010). Electrical resistivity tomography (ERT) with its ability to differentiate frozen from unfrozen subsurface has therefore developed into one of the most widely used methods in periglacial and permafrost research (Ishikawa, 2003; Hauck and Kneisel, 2008; Kneisel et al., 2008; Schrott and Sass, 2008; Lewkowicz et al., 2011; Otto et al., 2012). For monitoring purposes, ERT measurements are repeated at certain time intervals using the same survey geometry and identical electrodes in order to assess temporal and spatial variations of ground thermal conditions (Kneisel et al., 2014). However, the installation and maintenance of continuous AERT in steep unstable bedrock has not been achieved yet as it has high demands for near-vertical electrode and cable setups, accessibility and infrastructure, regular maintenance and safety. Seguin (1978) shows that electrical resistivity is an accurate proxy for rock temperature. Krautblatter (2009) demonstrates a bilinear temperature-resistivity (T-ρ) relationship based on sedimentary,

metamorphic and igneous rock samples from permafrost areas. A comparable field study of T-ρ relationships has not been reported yet due to the lack of accurate field monitoring data.

3.2   Main goal of the thesis and overall structure

Considering the research gaps described in Chapter 3.1, the main goal of the Ph.D.-thesis is to demonstrate the capability of a continuous and combined AERT and NSRT monitoring to provide stability-relevant thermal and hydrostatic information on a "slope" scale (Hartmeyer et al., 2012b) for potential early warning systems. For this purpose, the first permanently installed AERT system was established on a steep, unstable permafrost rock wall (Keuschnig et al., accepted). Furthermore, spatial and temporal variations of near-surface rock temperatures (NSRT) are measured in a hitherto unknown coverage using a newly developed low-cost alternative based on miniature temperature loggers (iButtons), (Keuschnig et al., prepared for submission-a). The combined methodological approach leads to the development of a temperature-resistivity calibrated system which provides subsurface thermal information based on the first field evidence of the laboratory-postulated bi-linear (Krautblatter, 2009) T-ρ relationship (Keuschnig et al., prepared for submission-b). Table 1 shows the overall structure of the Ph.D.-thesis and the incorporated publications arranged as chapters.

*Table 1: The overall structure of the Ph.D.-thesis. Partly incorporated represents < 50 % and fully incorporated 100 % of the primary publication. * ISI listed publication.*

Chapter	Publication	Incorporated
Introduction	All publications from the author are considered	Partly incorporated
The permafrost environment	All publications from the author are considered	Partly incorporated
Permafrost monitoring and observation techniques	KEUSCHNIG, M., HARTMEYER, I., OTTO, J. C. & SCHROTT, L. 2011. A new permafrost and mass movement monitoring test site in the Eastern Alps—concept and first results ft he MOREXPERT project. In: BORSDORF, A., STÖTTER, J. & VEULLIET, E. (eds.) Managing Alpine future II—inspire and drive sustainable mountain regions. Proceedings of the Innsbruck Conference, 21–23 November 2011. IGF-Forschungsberichte 4: Austrian Academy of Science	Partly incorporated
	*KEUSCHNIG, M., KRAUTBLATTER, M., HARTMEYER, I., FUSS, C. & SCHROTT, L. accepted. Automated Electrical Resistivity Tomography testing for Early Warning in Unstable Permafrost Rock Walls around Alpine Infrastructure. Permafrost and Periglacial Processes.	Partly incorporated
	*SUPPER, R., OTTOWITZ, D., JOCHUM, B., ROMER, A., PFEILER, S., KAUER, S., KEUSCHNIG, M. & ITA, A. 2014. Geoelectrical monitoring of frozen ground and permafrost in alpine areas: field studies and considerations towards an improved measuring technology. Near Surface Geophysics, 12, 93-115.	Partly incorporated
	*OTTO, J. C., KEUSCHNIG, M., GOTZ, J., MARBACH, M. & SCHROTT, L. 2012. Detection of Mountain Permafrost by Combining High Resolution Surface and Subsurface Information - an Example from the Glatzbach Catchment, Austrian Alps. Geografiska Annaler Series a-Physical Geography, 94A, 43-57.	**Fully incorporated**
Establishing an open air laboratory for long-term monitoring of permafrost and mass movements	KEUSCHNIG, M., HARTMEYER, I., OTTO, J. C. & SCHROTT, L. 2011. A new permafrost and mass movement monitoring test site in the Eastern Alps—concept and first results of the MOREXPERT project. In: BORSDORF, A., STÖTTER, J. & VEULLIET, E. (eds.) Managing Alpine future II—inspire and drive sustainable mountain regions. Proceedings of the Innsbruck Conference, 21–23 November 2011. IGF-Forschungsberichte 4: Austrian Academy of Science	Partly incorporated
	OTTO, J. C. & KEUSCHNIG, M. 2014. Permafrost-Glacier Interaction – Process Understanding of Permafrost Reformation and Degradation. In: RUTZINGER, M., HEINRICH, K., BORSDORF, A. & STÖTTER, J. (eds.) permAfrost – Austrian Permafrost Research Initiative – Final Report. IGF-Forschungsberichte 6: Austrian Academy of Sciences.	Partly incorporated
	*HARTMEYER, I., KEUSCHNIG, M. & SCHROTT, L. 2012. A Scale-Oriented Approach of the Long-Term Monitoring of Ground Thermal Conditions in Permafrost-Affected Rock Faces, Kitzsteinhorn, Hohe Tauern Range, Austria. Austrian Journal of Earth Sciences, 105, 128-139.	**Fully incorporated**

Providing stability-relevant hydrostatic and thermal information for early warning systems	***KEUSCHNIG, M.**, KRAUTBLATTER, M., HARTMEYER, I., FUSS, C. & SCHROTT, L. accepted. Automated Electrical Resistivity Tomography testing for Early Warning in Unstable Permafrost Rock Walls around Alpine Infrastructure. Permafrost and Periglacial Processes.	**Fully incorporated**
	*KEUSCHNIG, M., HARTMEYER, I., SCHMIDJELL, A., MARBACH, M., SCHROTT, L. & KRAUTBLATTER, M. prepared for submission. A low-cost strategy for near-surface rock temperature measurements using iButtons. Cold Regions Science and Technology.	**Fully incorporated**
	*KEUSCHNIG, M., KRAUTBLATTER, M. & HARTMEYER, I. prepared for submission. Field evidence for temperature-resistivity relationship of permafrost-affected alpine rock walls. The Cryosphere.	**Fully incorporated**
	*KEUSCHNIG, M., HARTMEYER, I., HÖFER-ÖLLINGER, G., SCHOBER, A., KRAUTBLATTER, M. & SCHROTT, L. 2015. Permafrost-Related Mass Movements: Implications from a Rock Slide at the Kitzsteinhorn, Austria. In: LOLLINO, G., MANCONI, A., CLAGUE, J., SHAN, W. & CHIARLE, M. (eds.) Engineering Geology for Society and Territory – Volume 1. Springer International Publishing.	**Fully incorporated**
Synoptic discussion	All publications from the author are considered	Partly incorporated
Conclusion and outlook	All publications from the author are considered	Partly incorporated

3.3   Hypotheses and research questions

3.3.1   Methodology

1. An automatic electrical resistivity tomography (AERT) is capable to continuously monitor the state of frozen, steep permafrost-affected bedrock.
    1.1. What measurement design enables self-sustained, continuous monitoring of unstable permafrost-affected rock walls?
    1.2. What are the main factors that influence measurement errors, and what time intervals and measurement settings are required to accurately monitor processes that control rock wall stability?
2. Spatially and temporally highly resolved near-surface rock temperature measurements in complex structured permafrost-affected rock walls can be achieved using a carefully designed iButtons measurement network.
    2.1. How can iButtons be adapted to provide spatially and temporally highly resolved NSRT measurements?
    2.2. What reliability and accuracy can be derived under field conditions in complex structured permafrost-affected rock walls?

3.3.2   Rock permafrost understanding

Based on the methodological research questions, the following research questions are discussed to improve rock permafrost understanding:

3. AERT is capable of continuously monitoring hydrostatic and thermal changes in permafrost rock walls
    3.1. On which temporal and spatial scales can AERT monitor stability-relevant changes?
    3.2. How can pressurised fluid flow in fractures be monitored using ERT?
4. A temperature-resistivity (T-ρ) relationship can be observed under field conditions.
    4.1. What are the characteristics of a T-ρ relationship under field conditions?
    4.2. Is the T-ρ gradient comparable with laboratory results and thus applicable for early warning purposes?

4 The mountain permafrost environment

4.1 Permafrost definition and distribution

Permafrost forms a major element of the global cryosphere (Harris et al., 2009) and is defined as ground material (soil, sediment or rock) that remains at or below 0 °C for more than two consecutive years (French, 2007; IPA, 2015). Permafrost is defined on the basis of temperature and time. This means that moisture in the form of either water or ice may or may not be present (Slaymaker and Kelly, 2009). Therefore, it is useful to distinguish between the temperature (i.e. thermal) and state (i.e. frozen, unfrozen) conditions of permafrost (French, 2007). Figure 2 illustrates a typical temperature-depth relationship with relevant permafrost-terminology.
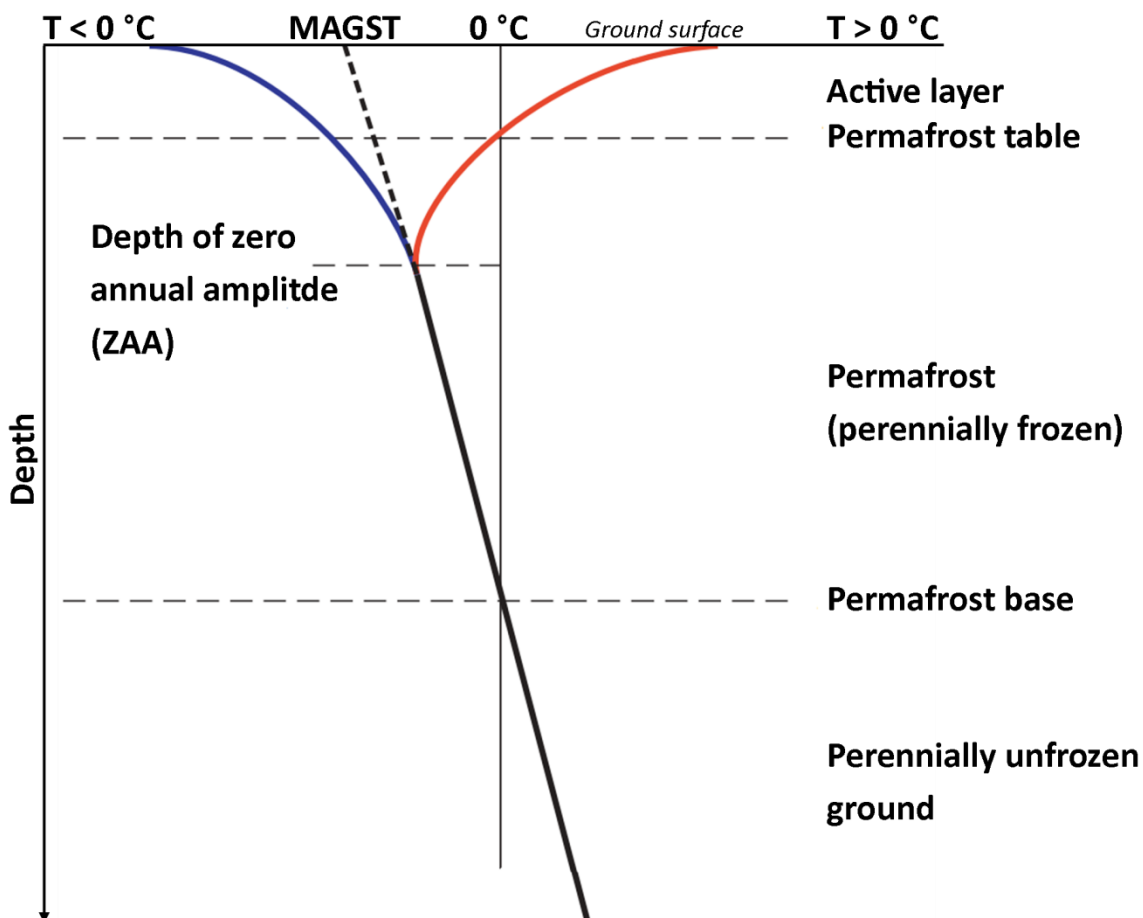

Figure 2: Idealised illustration of a typical ground thermal regime and the most important terms to describe a permafrost environment. The red and the blue line representing the warmest temperatures in summer (red) and the coldest temperatures in winter (blue), MAGST is the acronym for mean ground surface temperature. The thermal regime indicating the increase of temperature with depth, the depth of zero annual amplitude (ZAA) and the depth of seasonal thaw (active layer) (modified after ACGR (1988) and French (2007).

Permafrost occurs both on land and beneath offshore arctic continental shelves, and underlies about 22% of the Earth's land surface. In the Northern Hemisphere, permafrost covers approximately 25% (23 million km²) of the land area (Figure 3, Brown et al. (1997)).
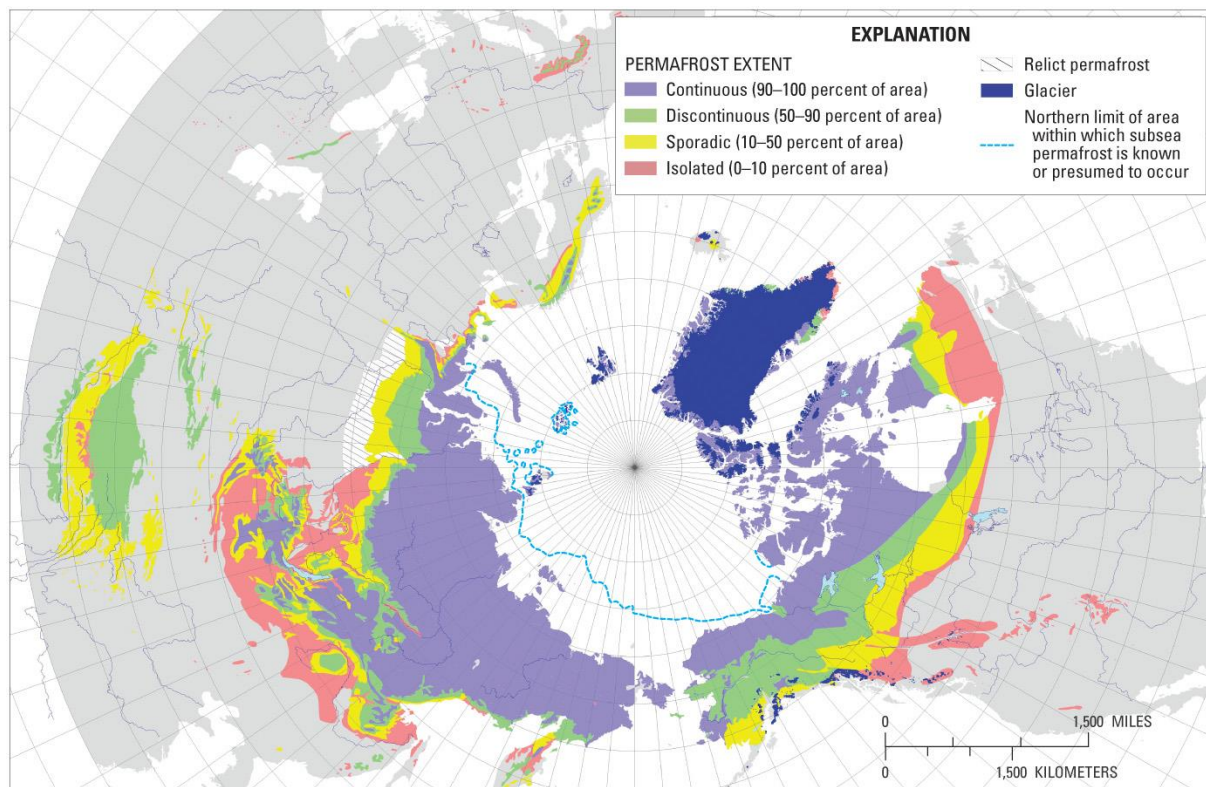
Figure 3: Generalized permafrost map of the Northern Hemisphere, including limit of subsea permafrost, based on the Circum-Arctic map (Brown et al., 1997) taken from (Williams Jr. and Ferrigno, 2012).

According to French (2007), permafrost occurs mainly in two, sometimes overlapping geographical regions, in high latitudes and high altitudes and can be classified into one of the following categories: (1) latitudinal or polar permafrost, (2) alpine or mountain permafrost and (3) plateau or montane permafrost, (e.g. Qinghai-Xizang Plateau of China). Sub-sea permafrost exists on some continental shelves, other permafrost bodies occur in terrestrial sub-arctic locations that bear no relationship to current climatic conditions (e.g. relict permafrost). A common classification for the spatial distribution of permafrost includes: (1) continuous permafrost (underlying 90-100% of the landscape), (2) discontinuous permafrost (50-90%), (3) sporadic permafrost (10-50%) and (4) isolated patches (0-10%) (Figure 3, IPA (2015)).

4.2   Mountain permafrost

Mountain permafrost is increasingly used to refer to both, alpine permafrost and polar mountain permafrost (Guodong and Dramis, 1992) and is basically permafrost in (high) mountain areas. The occurrence of mountain permafrost can be roughly characterized by the domains climate, topography and ground conditions (Figure 4, Haeberli et al. (2010)).
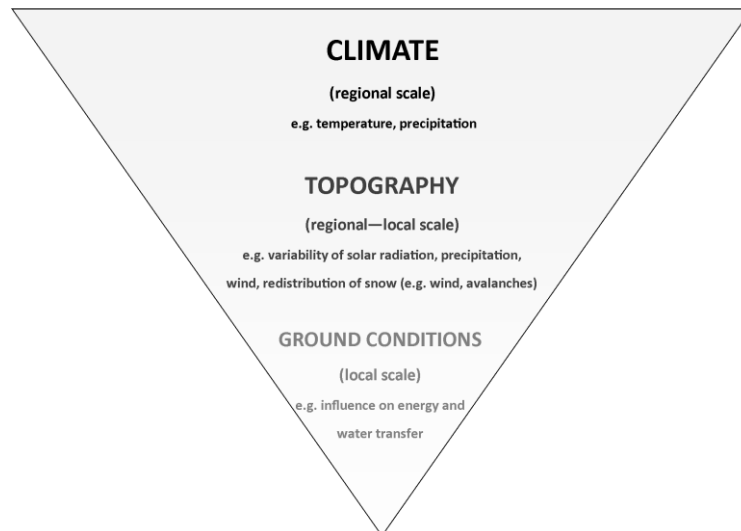
Figure 4: Influencing factors on the distribution on mountain permafrost (modified after Haeberli et al. (2010)).

Mountain topography has a great variability at a wide range of scales between regolith grains to entire mountain ranges (Otto et al., 2012). The geothermal regime of mountain permafrost is strongly influenced by ground surface characteristics (e.g. spatial and temporal variability of snow cover, vegetation, local topography, Draebing et al. (2016)), the nature of the substrate (e.g. spatial and depth variation in lithology and ice content) and the regional geothermal heat flux (Harris et al., 2009) and other factors. The factors that are controlled by local topography show a large spatial and temporal variability and their influences on ground thermal conditions leads in general to a patchier distribution of mountain permafrost than those of the arctic lowland permafrost (Figure 5).
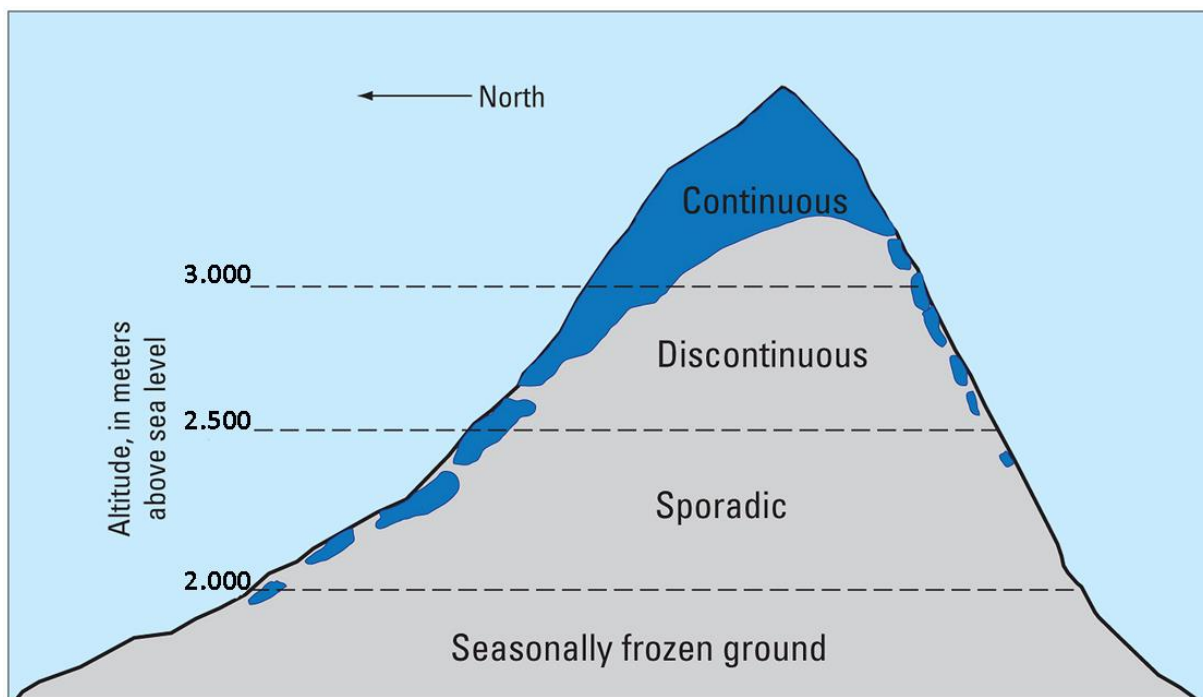

Figure 5: Idealized distribution of mountain permafrost. Modified from (Williams Jr. and Ferrigno, 2012) adapted to the Eastern Alps after Schrott et al. (2012).

4.3   Temperature-related destabilisation of alpine rock walls

Numerous rockfall events have been observed and reported recently from permafrost-affected areas (Rabatel et al., 2008; Huggel, 2009; Ravanel and Deline, 2011; Fischer et al., 2013; Stoffel et al., 2014; Keuschnig et al., 2015). The presence of massive ice in detachment zones indicates the role of permafrost in the initiation of rockfall events (Bommer et al. (2009), Figure 6).
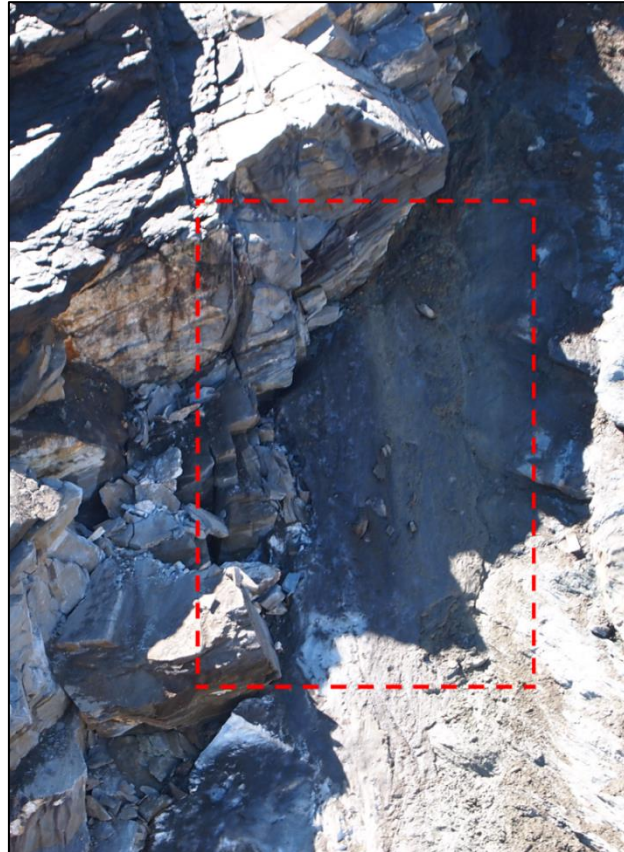

Figure 6: Visible ice on the failure plane of a rockslide event (August, 2012; Kitzsteinhorn, Austria).

It is a common approach to classify rock slope failures by volume (*Table 2*, Whalley (1974) and Whalley (1984)).

Table 2: Rock slope failure classification after Whalley (1974)

	Debris fall	**Boulder fall**	**Block fall**	**Cliff fall**	**Bergsturz**
Volume	$< 10^1\,\mathrm{m}^3$	$10^1 - 10^2\,\mathrm{m}^3$	$10^2 - 10^4\,\mathrm{m}^3$	$10^4 - 10^6\,\mathrm{m}^3$	$> 10^6\,\mathrm{m}^3$

Several case studies focus on permafrost influence on rock-ice avalanches with magnitudes $> 1 \times 10^7$ m^3 or cliff fall events (magnitudes 10^4–10^6 m³) (Bottino et al., 2002; Haeberli et al., 2004; Huggel et al., 2005; Fischer et al., 2006; Geertsema et al., 2006; Huggel et al., 2008; Lipovsky et al., 2008; Sosio et al., 2008). Furthermore, some studies show higher activities of fall processes of different magnitudes (cliff falls 10^4–10^6 m³, block falls 10^2–10^4 m³, boulder falls 10^1–10^2 m³ and debris falls < 10 m³) in permafrost-affected rock walls (Sass, 2005; Krautblatter and Dikau, 2007; Rabatel et al., 2008; Deline, 2009; Ravanel and Deline, 2011; Ravanel et al., 2011; Pudasaini and Krautblatter, 2014; Keuschnig et al., 2015).
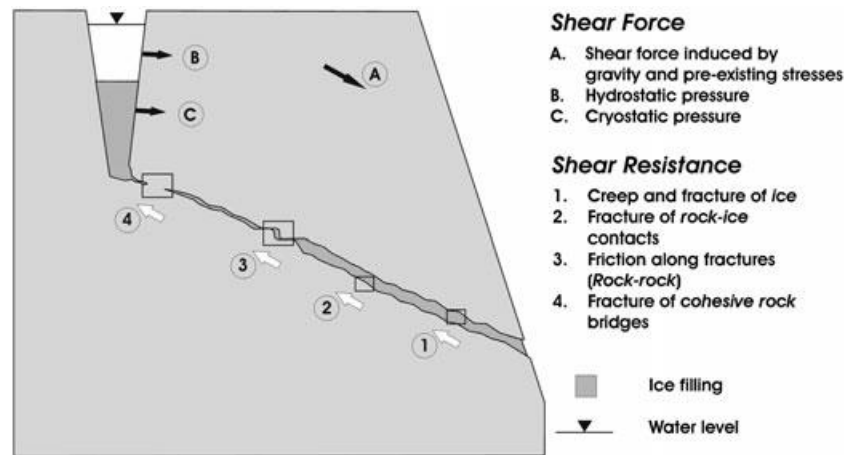
Figure 7: An idealized illustration of the rock–ice mechanical model from Krautblatter et al. (2013) .

Recently, Krautblatter et al. (2013) introduced a detailed rock- and ice-mechanical model (Figure 7) considering different temporal and spatial scales. The authors of the study point out that thermal change in frozen rock significantly alter the mechanical properties of rock and ice along potential failure planes. In detail, the destabilisation of permafrost-affected bedrock can be attributed to decreases in shear strength caused by (i) changes in rock-mechanical properties like the abrupt decrease in compressive and tensile strength as well as fracture toughness (Mellor, 1973; Dwivedi et al., 2000), (ii) changes in ice-mechanical properties of creep and fracturing due to changing thermal conditions of ice, changing water content inside the ice between -2 and 0 °C or melting (Sanderson, 1987; Budd and Jacka, 1989; Davies et al., 2001) and (iii) due to changes of the performance of the rock-ice interface. Vice versa, the shear stress applied to detachment planes can be increased by elevated hydrostatic pressures and elevated cryostatic pressures (Fischer et al., 2006; Murton et al., 2006; Matsuoka and Murton, 2008; Fischer et al., 2013). Due to the transient nature of external influencing factors, the conditions prevailing at potential failure planes may change rapidly, i.e. in a few hours, which have fundamental implications for a monitoring conception and the required temporal resolution of the measurements.

5 Permafrost monitoring and observation techniques

As described in Chapter 4.2, mountain topography has a great variability and therefore the distribution of mountain permafrost is commonly very heterogeneous. The assessment of permafrost conditions is carried out applying a broad band of methods and observation techniques.

5.1 Permafrost monitoring

Partly derived and modified from:

KEUSCHNIG, M., HARTMEYER, I., OTTO, J. C. & SCHROTT, L. 2011. A new permafrost and mass movement monitoring test site in the Eastern Alps—concept and first results of the MOREXPERT project. In: BORSDORF, A., STÖTTER, J. & VEULLIET, E. (eds.) Managing Alpine future II—inspire and drive sustainable mountain regions. Proceedings of the Innsbruck Conference, 21–23 November 2011. IGF-Forschungsberichte 4: Austrian Academy of Science

Mountain permafrost research is a young scientific discipline that systematically started in the early seventies (Haeberli et al., 2010). Long-term data series on permafrost conditions, comparable to meteorological data, are limited, but essential for understanding of permafrost dynamics and related processes. Unfortunately, most geomorphic studies or processes are carried out fewer than three years (Selby, 1993), hence the validity of short-term process measurements is at best uncertain, at worst they are irrelevant (Conacher, 1988). In context to mountain permafrost, the correlation between air and subsurface temperatures is not straightforward since surface characteristics and cover (e.g. snow cover), subsurface ice content, and mountain topography mask changes in atmospheric conditions when they propagate into the subsurface (Haeberli et al., 2010; Otto et al., 2012; PERMOS, 2015). In order to deal with this factors, long-term monitoring strategies and projects like Permafrost and Climate in Europe (PACE, Harris et al. (2001)), the Swiss Permafrost Network (PERMOS, Noetzli and Vonder Muehll (2010)) and the Permafrost Long-term Monitoring Network (PermaNET, 2015) were initiated in the European Alps. Especially high mountain summits in the western European Alps like Schilthorn (CH), Matterhorn (CH), or Aiguille du Midi (F) have been instrumented for continuous monitoring of permafrost (Noetzli and Vonder Muehll, 2010; Ravanel and Deline, 2011). In Austria, continuous permafrost long-term monitoring activities with deep boreholes and geophysics are limited to the sites Hoher Sonnblick (Schoner et al., 2012) and Kitzsteinhorn (presented in this Ph.D.-thesis, Hartmeyer et al. (2012b)). All permafrost monitoring sites with one or more boreholes contribute to the Global Terrestrial Network for Permafrost (GTN-P, Figure 8).
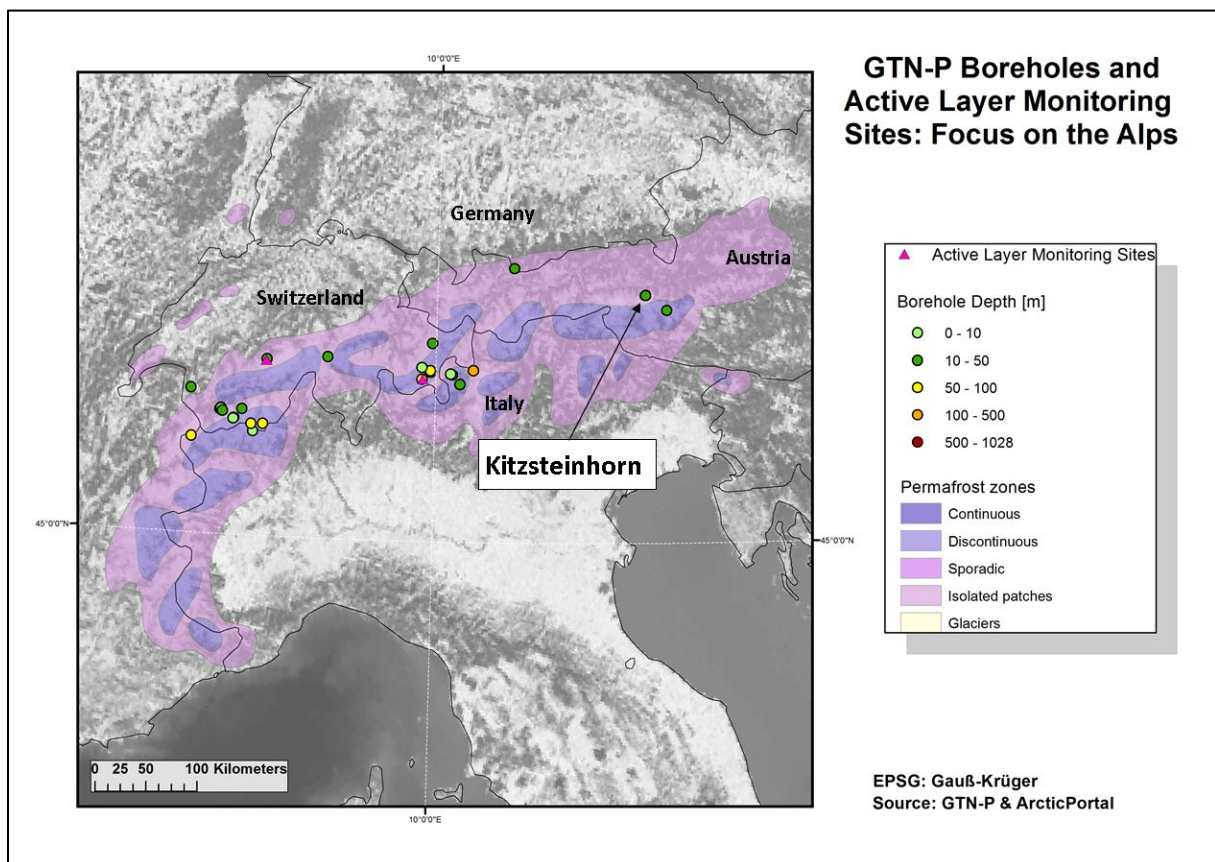

Figure 8: GTN-P monitoring test sites including boreholes in the European Alps (modified after: GTN-P (2015).

GTN-P is the primary international program concerned with monitoring permafrost parameters. The program was developed in the 1990s by the International Permafrost Association (IPA) under the Global Climate Observing System (GCOS) and the Global Terrestrial Observing Network (GTOS), with the long-term goal of obtaining a comprehensive view of the spatial structure, trends and variability of changes in the active layer thickness and permafrost temperature (GTN-P, 2015).

5.2 Monitoring domains and observation techniques

5.2.1 Atmospheric conditions

Weather and climate conditions have the most important influence on variations of the ground surface and the subsurface thermal regime (ground thermal regime). Air temperature, solar radiation and precipitation (solid and fluid) are important parameters and are commonly measured by automatic weather stations. The occurrence of a snow cover has a large influence on the ground-thermal regime (Rodder and Kneisel, 2012; Park et al., 2013; Zhou et al., 2013). The snow cover insulates the ground from atmospheric influences, the time of the first snow fall, the duration and thickness of the snow cover, and the time when the ground surface becomes snow free in spring are relevant (PERMOS, 2013).

As a first approximation, the long-term mean annual air temperature (MAAT) can be used to delineate mountain regions with permafrost occurrences (Haeberli et al., 2010). For instance, a MAAT of -3 to -4 °C is a good estimate for the regional limit of the lower mountain permafrost boundary in southern Norway (King, 1986; Etzelmüller et al., 2003; Harris et al., 2009). Accordingly, MAAT below –3 °C indicates areas with significant amounts of permafrost (continuous, discontinuous permafrost distribution, while a few occurrences exist around –1 °C (sporadic permafrost) (Haeberli et al., 2010). For empiric-statistical permafrost distribution modelling, permafrost evidences are used to develop a topoclimatic key (Figure 9) for a specific mountain (Keller, 1992; Schrott et al., 2012).
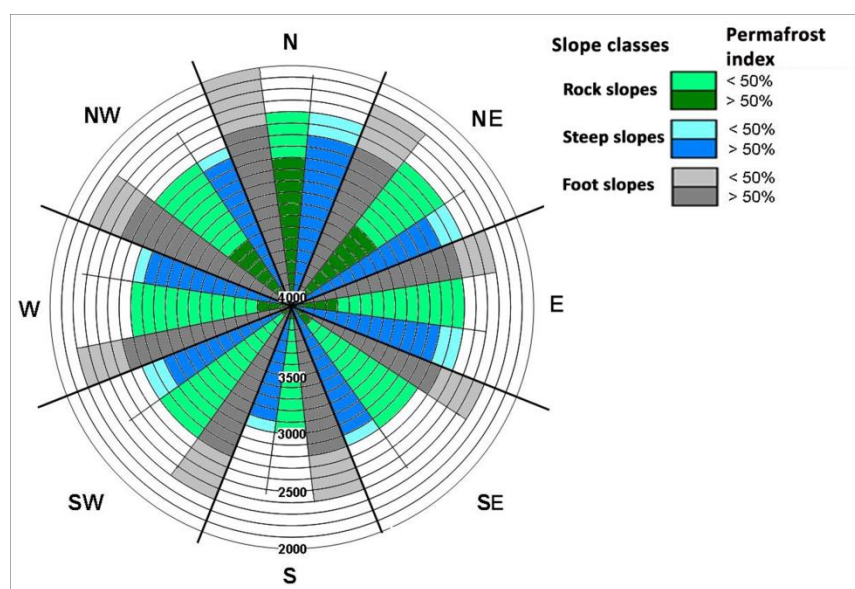

Figure 9: Topoclimatic key for the Kitzsteinhorn region (Hohe Tauern, Schrott et al. (2012)).

5.2.2   Ground surface thermal conditions

According to French (2007) permafrost changes are reflecting a negative or positive heat balance at the surface of the earth. The thickness to which permafrost can develop is mainly determined by a balance between the internal heat gain with depth (geothermal gradient) and heat loss from the surface. Using the ground surface temperature and the geothermal gradient, it is possible to calculate the ground temperature at any depth (French, 2007):

$$T_Z = T_S + G_g \times Z \qquad\qquad\qquad (1)$$

Equation 1 represents a one-dimensional heat flow equation, where T_Z is the ground temperature (°C) at depth Z (m), T_S is the mean annual ground surface temperature (°C), G_g is the geothermal gradient (°C m−1) and Z is depth (m).

The ground surface temperature (GST) is defined as the surface or near-surface temperature of the ground (PermaNET, 2015). GST are usually measured with miniature data loggers (Hoelzle et al., 1999; Ishikawa, 2003; Gubler et al., 2011) in the uppermost centimetres of the ground to avoid direct radiation influences (Figure 10).

Figure 10: Miniature data logger for continuous GST measurements, placed in a depth of 10 cm to avoid direct radiation (Maurergrat, Kitzsteinhorn area).

Continuous GST measurements provide information of the first snow fall, the duration and thickness of the snow cover, the winter equilibrium temperature (WEqT), the so called zero curtain effect caused by latent heat release and the time when the ground surface becomes snow free (Otto et al., 2012; Schoner et al., 2012; Schrott et al., 2012; PERMOS, 2013) (Figure 11).

GST is a proxy for estimating potential permafrost occurrence and can be used for calibrating and validating permafrost models (Schrott et al., 2012). GST is an indirect method for permafrost detection and a certain degree of uncertainty has to be taken into account. However, GST is well suited to complement borehole measurements in order to capture the influence of differing surface cover types and topographic settings, which cause a high spatial variability of ground surface temperatures (PERMOS, 2013).
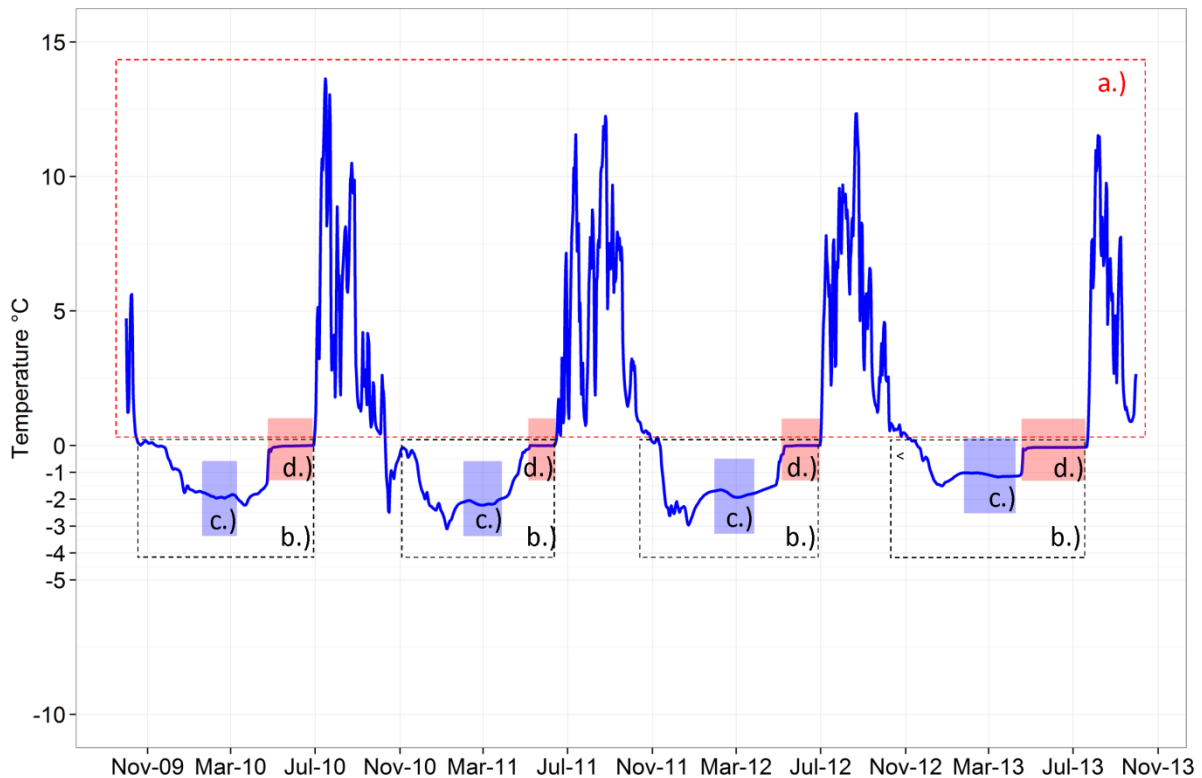
Figure 11: Typical annual ground surface temperature (GST) evolution at the lower limit of the permafrost distribution (Kitzsteinhorn area, 2,623 m a.s.l., exposition: N): a.) high diurnal variations during the snow free period from early summer to fall caused by high air temperature variations; b.) period of snow cover which provides isolation from atmospheric influences - fluctuation of temperature is damped to a minimum; c.) the winter temperature is reached with heat flux coming from the subsurface (WEqT), the GST temperature increases again in spring due to the decrease of snow cover thickness and the percolation of meltwater and d.) GST remains at approx. 0 °C over weeks because of latent heat release (zero curtain effect).

Another method to predict the occurrence of permafrost is the measurement of the bottom temperature of the winter snow cover (BTS). BTS was introduced by Haeberli (1973) and applied in several studies (Haeberli, 1978; King, 1983; Ikeda and Matsuoka, 1999; Otto et al., 2012; Schoner et al., 2012; Schrott et al., 2012) to measure the temperature at the snow-ground interface as a proxy for permafrost occurrence. BTS measurements are usually conducted at in spring (typically between February/March) where a sufficient insulation against solar radiation and air temperature is provided by a snow depth of 80 to 100 cm (Figure 12, a).
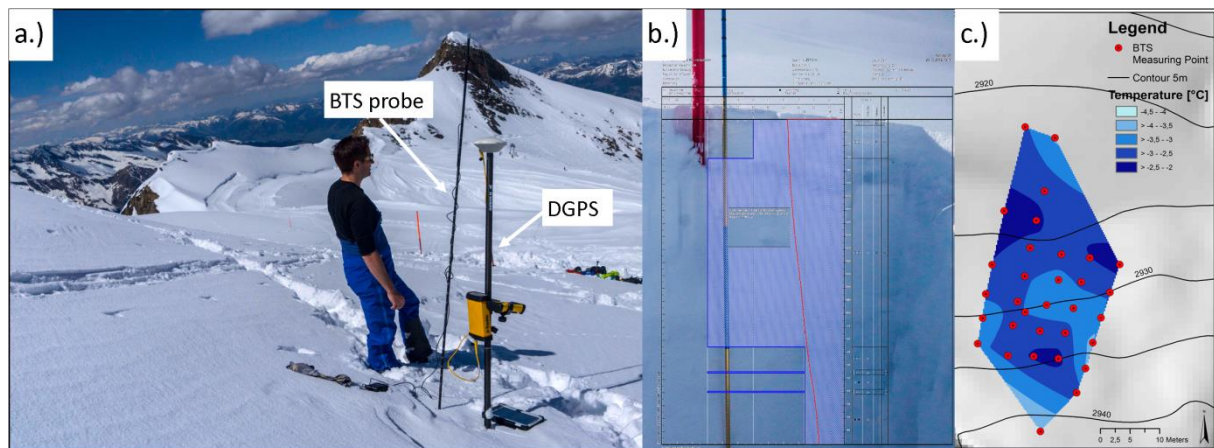
Figure 12: BTS measurements (Kitzsteinhorn area, 2,900 a.s.l.): a.) BTS measurement at a point of interest, positioning is carried out using a differential global positioning system (DGPS); b.) snow profile as proxy for the qualitative interpretation of the measured BTS values and c.) interpolated BTS measurements indicating permafrost occurrence (approx. -2 to -4 °C).

Hoelzle (1992) applied the following "rules of thumb" for BTS: values of < −3 °C indicate that permafrost is "probable", values of −2 °C to −3 °C that permafrost is "possible" (uncertainty range) and values of >−2 °C that permafrost is "unlikely" (*Figure 12*, c).

Complementary, important parameters for BTS can be delivered by snow profiles. Stratigraphy, density, grain size and shape, temperature gradients and thermal conductivity can be assessed from a representative snow profile, which is located within the BTS measurement setting (*Figure 12*, b). The snow profile is a meteorological archive and can be used as a proxy for qualitative interpretation of the measured BTS values. For example, an isothermal snow cover with temperatures of about −1° C indicate wet snow conditions and water availability at the bottom of the snow cover which has significant influences on the measured BTS values (Hiller et al., 2014).

5.2.3 Subsurface thermal conditions

Subsurface temperatures in mountain permafrost are usually measured in boreholes and are typically only a few degrees below 0 °C (Harris et al., 2003; Christiansen et al., 2010; Haeberli et al., 2010; Noetzli and Vonder Muehll, 2010; Schoenreich et al., 2010; Zhao et al., 2010). Ground temperature data from permafrost boreholes are particularly well suited to the detection of changes in the surface boundary condition that can be interpreted as climate signals (Lachenbruch and Marshall, 1986; Harris and Isaksen, 2008; Harris et al., 2009). Boreholes provide direct evidence of permafrost and are often the core observation technique of a permafrost monitoring network.

In the last decades, mountain permafrost boreholes with depths up to 100 m and more (Noetzli and Vonder Muehll, 2010; Keuschnig et al., 2011; PERMOS, 2013) were drilled in the European Alps (Figure 8). Borehole temperatures are measured at different sites, covering bedrock and loose material ground conditions. To assess e.g. depth of active layer or the zero annual amplitude (ZAA), boreholes are instrumented with thermistor chains in certain depths (Figure 13).
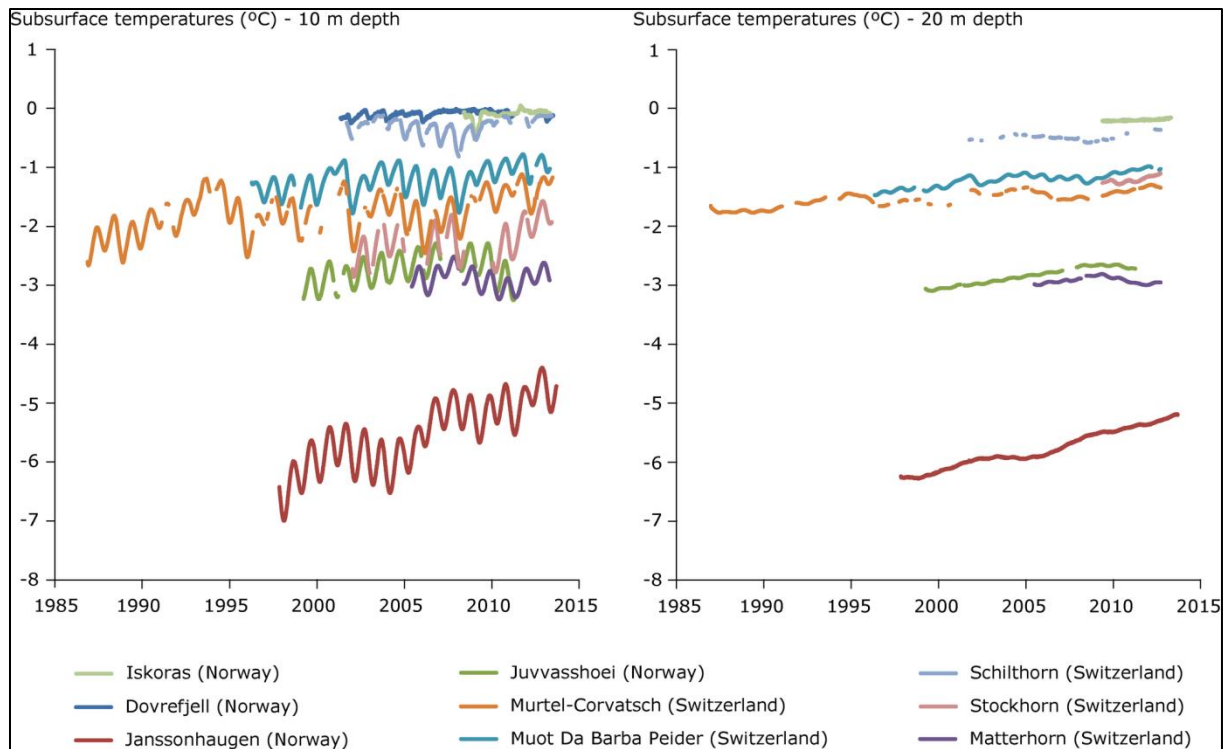
Figure 13: The Figure shows trends in observed permafrost temperatures from 10 m (left) and 20 m (right) depth for selected boreholes in European mountains: the sites include the PACE transect and two additional sites in the Swiss Alps(and two in Norway (Dovrefjell and Iskoras) (PERMOS, 2013).

Geophysical methods like electrical resistivity tomography (ERT), ground penetrating radar (GPR) or seismic are standard techniques for indirect permafrost investigations (Hauck and Kneisel, 2008; Schrott and Sass, 2008). In order to reduce uncertainties using geophysical methods, the application of complementary geophysical methods or direct borehole measurement is highly recommended (Otto and Sass, 2006; Schrott and Sass, 2008; Hartmeyer et al., 2012b).

5.2.4   The role of ERT in permafrost monitoring

Partly derived and modified from:

KEUSCHNIG, M., KRAUTBLATTER, M., HARTMEYER, I., FUSS, C. & SCHROTT, L. accepted. Automated Electrical Resistivity Tomography testing for Early Warning in Unstable Permafrost Rock Walls around Alpine Infrastructure. Permafrost and Periglacial Processes.

SUPPER, R., OTTOWITZ, D., JOCHUM, B., ROMER, A., PFEILER, S., KAUER, S., KEUSCHNIG, M. & ITA, A. 2014. Geoelectrical monitoring of frozen ground and permafrost in alpine areas: field studies and considerations towards an improved measuring technology. Near Surface Geophysics, 12, 93-115.

Electrical resistivity tomography (ERT) can differentiate frozen from unfrozen rock in the subsurface, and therefore has become widely used in periglacial and permafrost research (Ishikawa, 2003; Hauck and Kneisel, 2008; Kneisel et al., 2008; Schrott and Sass, 2008; Lewkowicz et al., 2011; Otto et al., 2012). Electrical resistivity of frozen rock is highly temperature-dependent and reacts sensitively to the gradual freezing of water in pores and fissures in bedrock between 0 and ca. -8 °C (Mellor, 1973; Krautblatter et al., 2010).

For monitoring purposes, ERT measurements are repeated at certain time intervals using the same survey geometry and identical electrodes in order to assess temporal and spatial variations of ground temperature (Kneisel et al., 2014). ERT monitoring of permafrost in steep rock faces was first conducted in 2005 (Krautblatter and Hauck, 2007). Most ERT permafrost monitoring studies have been carried out either on unconsolidated material (e.g. talus, soil) or on gently inclined rock slopes with debris cover (Supper et al., 2014) (Table 3). But ERT monitoring during repeated field campaigns also provides a powerful tool for detecting monthly changes of permafrost in solid rock walls (Krautblatter et al., 2010). However, continuous monitoring by Automated ERT (AERT) in steep unstable bedrock has not been achieved yet as it imposes stringent demands for near-vertical electrode and cable setups, accessibility and infrastructure, and regular maintenance and safety.

Table 3: Overview on published permafrost monitoring activities, modified after Supper et al. (2014). Dark grey area highlights the study presented in the Ph.D. thesis.

	Kitzsteinhorn (Keuschnig et al., accepted)	Kitzsteinhorn (Supper et al., 2014)	Mölltaler Glacier (Supper et al., 2014)	Schilthorn E-W (Hilbich et al., 2011)	Zugspitze (Krautblatter et al., 2010)	Murtèl (Hilbich et al., 2009)	Schilthorn (Hilbich et al., 2008)	Steintälli (Krautblatter and Hauck, 2007)	Val Muragl (Kneisel et al., 2014)	Brüeltobel (Kneisel et al., 2014)	Murtèl \ Corvatsch (Kneisel et al., 2014)
System	Geotom	GEOMON4D	GEOMON4D	Geotom	ABEM SAS 300C	Syscal	Syscal	ABEM SAS 300C	Syscal	Syscal	Syscal; Geotom
Material (Electrode coupling)	Bedrock	Debris	Debris	Debris	Bedrock	Debris	Debris	Bedrock	Debris	Debris	Debris
Number of electrodes	37	81	81	30	127; 3 arrays overlapping (41, 61, 41)	48	30	41	36	36	36
Electrode type	Stainless Steel Climbing Bolts	Stainless Steel	Stainless Steel	Stainless Steel	Stainless Steel	Stainless Steel	n/a	Stainless Steel Screws	Stainless Steel	Stainless Steel	Stainless Steel
Spacing	2 m	1 m	1 m	2 m	1.53 m, 4.6 m, 1.53 m	5 m	2 m	1.5 m	1 m, 2 m	1.8 m	2 m
Profile length	72 m	80 m	80 m	58 m	276 m	235 m	60 m	60 m	35 m	63 m	70 m
Configuration	Wenner, Schlumberger, Coupling	Gradient	Gradient	Wenner, Schlumberger, Dipole - Dipole	Wenner, Schlumberger, Gradient	Wenner	Wenner	Wenner	Wenner, Schlumberger	Wenner, Dipole – Dipole	Wenner
Number of data sets	> 3.000	544 (at date 29.03.2013)	250	180	7	4	110	4	20	16	5; 58
Number of data points	210	2.600	2.600	135	1.550	n/a	135	190	n/a	n/a	n/a
Measurement frequency	6 per day	daily	daily	daily since April 2009 (summer 3, winter 2 per day)	once per month in February, May, June, July, August, September, and October 2007	sporadic; at least one measurement every Aug./Sept.	variable, yearly, with some monthly and daily periods	sporadic, August - September	annually - snowfree period	4–8 times a year (weekly)	sporadic \ daily
Observation period	02/2013–2015, with some breakes	10/2011–2013	09/2010 - 09/2011	04/2009– 04/2010, with some breaks	February–October	2006–2008	1999–2006	Summer 2005	2005–2009	2009–2011	08/2010– 02/2011; 03– 06/2011
Current range [mA]	0.001 – 200	0.001 –2	0.03 –2	0.001 –200	> 0.2	0.02 –2	n/a	> 0.2	n/a	n/a	n/a
Resistivity range [kΩm]	1–28.000	50–1.500	1–200	0.6–3.5	1–2.000	10–1.000	1–2	1–80	1–25	1–1.000	2–300
Contact resistance	n/a	n/a	n/a	< 10 kΩ	1–100 Ω	up to 500 kΩ	n/a	n/a	3–40 kΩ	5–400 kΩ	20–500 kΩ
Data error estimation	raw data statistics	raw data statistics	data statistics	Filtering, de-Spiking of app. Res.	reciprocity principle (Slater et al., 2000)	DOI index (Oldenburg and Li, 1999)	n/a	n/a	n/a	n/a	n/a
RMS error	2–30 %	4–25 %	3–26 %	3 %	10 –20 %	4–5 %	2–4 %	6–18 %	2–3 %	2.2–15 %	2.5–8.5 %
Inversion software	Res2DInv	EarthImager	EarthImager	Res2DInv	CRTomo	Res2DInv	Res2DInv	Res2DInv	Res2DInv	Res2DInv	Res2DInv
Active layer thickness	2–3 m	n/a	n/a	5 m	n/a	4–7 m	5 m	2–6 m	5 m	1 m	2 m
min. Temperature (1 m)	-8 °C	-12 °C	-7.5 °C	-1.5 °C	-4 °C	no successful measurements in winter	-3 °C	only summer	-0.85 °C	-8.5 °C	-0.8 °C

5.3 Case study: combining ground surface and subsurface thermal information

Fully incorporated: OTTO, J. C., KEUSCHNIG, M., GOTZ, J., MARBACH, M. & SCHROTT, L. 2012. Detection of Mountain Permafrost by Combining High Resolution Surface and Subsurface Information - an Example from the Glatzbach Catchment, Austrian Alps. Geografiska Annaler Series a-Physical Geography, 94A, 43-57.

5.3.1 Abstract

Permafrost distribution in mid-latitude mountains is strongly controlled by solar radiation, snow cover and surface characteristics like debris cover. With decreasing elevation these factors have to counterbalance local positive air temperatures in order to enable permafrost conditions. We combine high resolution surface data derived from terrestrial laser scanning with geophysical information on the underground conditions using ground penetrating radar and electrical resistivity tomography and ground surface temperature data in order to understand the effects of surface characteristics on permafrost distribution in an Alpine catchment, Austrian Alps (Glatzbach, 47°2'23.49" N; 12°42'33.24" E, 2,700–2,900 m a.s.l.). Ground ice and permafrost is found above an elevation of 2,780 m a.s.l. on north-east facing slopes in 2009, previous studies detected permafrost at the same site at 2,740 m a.s.l. in 1991. Analysis of surface roughness as a proxy for grain size distribution reveals that the lower boundary of discontinuous and sporadic permafrost is lowered on rough surfaces compared to fine-grain zones. At the same location modelled potential summer solar radiation in coarse grain zones is reduced by up to 40% compared to surfaces of fine grain sizes. The mostly patchy permafrost distribution at the Glatzbach can therefore be attributed to local surface cover characteristics, particularly regolith grain size and its influence on solar radiation. We conclude that the analysis of ground surface characteristics using very high resolution terrain data supports the assessment of permafrost in Alpine areas by identifying rough surface conditions favouring permafrost occurrence.

5.3.2 Introduction

Permafrost distribution in mid-latitude mountains is strongly controlled by solar radiation, snow cover and surface characteristics like debris cover (Hoelzle, 1994; Keller, 1994). With decreasing elevation these factors have to counterbalance positive air temperatures in order to enable permafrost conditions. Mountain terrain is often characterized by highly variable geological, geomorphological, climatic and topographic conditions. Mountain topography has a great variability at a wide range of scales between regolith grains to entire mountain ranges. Snow distribution, solar radiation, surface material composition, vegetation cover and other factors influence ground thermal regimes. The factors that are controlled by local topography show a large spatial variability and their influences on ground thermal conditions should be considered in the investigation of permafrost at a local scale. Therefore, subsurface information, like temperature or resistivity, needs to be linked to surface characteristics.

Spatial distribution of mountain permafrost is generally acquired using geophysical techniques, as well as measurements of Bottom Temperature of Snow Cover (BTS) and Ground surface Temperature (GST) (Hoelzle, 1992; Keller, 1994; Ishikawa and Hirakawa, 2000; Gruber et al., 2004b; Brenning et al., 2005; Krautblatter and Hauck, 2007; Hauck and Kneisel, 2008; Gubler et al., 2011; Hartmeyer et al., 2012b). Analysing the influence of regolith characteristics on ground thermal

conditions has been limited to point measurements in many previous studies, mainly in boreholes and at single blocks (Hanson and Hoelzle, 2004; Gruber and Hoelzle, 2008; Phillips et al., 2009; Schneider et al., 2012). On a locale scale, at the lower limit of permafrost, Nyenhuis (2006) investigated permafrost distribution in a hanging valley in the Turtmanntal, Swiss Alps and considers a mean block size of <50 cm to be unfavourable for permafrost occurrence. A spatial approach to quantify surface characteristics in mountain regions with permafrost occurrence is however necessary to fully understand this factor (Etzelmuller et al., 2001; Nyenhuis, 2006). The combination of high resolution subsurface information with detailed surface data can help to understand heterogeneous ground ice distribution in alpine environments, especially at the lower boundary of discontinuous permafrost.

Controlling surface characteristics, mainly grain/block size, on permafrost distribution have been acknowledged by several authors, most of them working on rock glaciers (Ishikawa, 2003; Hanson and Hoelzle, 2004; Nyenhuis, 2006; Lambiel and Pieracci, 2008). Block fields which results from rockfall activity, or aggregated by periglacial creep, are considered as accumulators of cold temperatures (Gorbunov et al., 2004). High porosity and low thermal conductivity lead to a significantly different thermal subsurface regime compared to fine-grained surface material. A high surface roughness of blocky material prevents or retards a closed and deep snow cover. Holes in the snow and boulders that stick out of the snow cover enable an increased temperature exchange between the atmosphere and the ground compared to snow covered areas. Consequently, cold winter air is accumulated between coarse blocks. Several processes have been described from blocky surface material that lead to ground cooling for example the Balch effect (cold air sinks down due to higher density), free convection, the chimney effect or the reduction of insulation effect of the snow cover (Wakonigg, 1996; Harris and Pedersen, 1998; Ishikawa, 2003; Gorbunov et al., 2004; Delaloye and Lambiel, 2005; Phillips et al., 2009). Gruber and Hoelzle (2008) showed that ground cooling results from a preservation of low temperatures through winter and summer due to the low thermal conductivity of coarse debris. Apparently, coupling between atmosphere and ground is stronger in the cold season than in summer allowing cold temperatures to penetrate the blocky layer through free convection (Herz, 2006). These findings suggest that regolith composition is one of the governing factors for discontinuous, sporadic and isolated permafrost distribution in the European Alps.

Topography impacts on the accumulation and duration of snow. Snow deposition and redistribution is mainly influenced by wind conditions, while duration of snow cover depends on snow depth, solar radiation and the local energy balance (Grunewald et al., 2010). Snow cover affects ground temperatures in two ways: Thin early winter snow cover (<15 cm) removes energy from the ground by increased long wave emissivity at the snow surface and increased heat flux from underground (Zhang, 2005). This phenomena leads to intense ground cooling in autumn, termed autumn-snow effect by Keller (1994), which is preserved by a deeper snow cover in winter. Thick snow cover represents a thermal insulator due to its low thermal conductivity that shields energy exchange between the ground and the atmosphere (Keller, 1994; Ishikawa, 2003; Keller and Tamas, 2003; Zhang, 2005). Snow conditions consequently influence the local permafrost occurrence and can be responsible for local uncertainties in regional permafrost models.

Furthermore, terrain roughness resulting from coarse boulders generates highly variable conditions of shading and solar radiation impact. Consequently, area-wide data on surface material needs to be included in permafrost distribution models, especially with increasing model resolution. High

resolution surface data from airborne or terrestrial laser scanning can be used to quantify surface characteristics (Heritage and Milan, 2009). The morphometric variable surface roughness describes the variability of surface changes and can be taken as surrogate for grain size composition. Boulders and blocks stick out of the surrounding surface and create an irregular surface which causes high roughness, while small and equally sized grain compositions create smooth surfaces. Roughness is frequently analysed in studies of fluvial dynamics where gravel bed characteristics are studied in detail (Heritage and Milan, 2009; Hodge et al., 2009). Computation of surface roughness is scale-dependent according to the size of the object of interest (Grohmann et al., 2011). With respect to grain size (>cobbles, i.e. >128 mm), very high resolution surface data is required that can only be provided by Terrestrial Laser Scanning (TLS) delivering highly accurate data at cm resolution. Various mathematical solutions exist to quantify surface roughness from digital elevation data. An overview and a comparison of different techniques is provided by Grohmann et al. (2011).

In this study we combine geophysical information using Ground Penetrating Radar (GPR) and Electrical Resistivity Tomography (ERT) with high resolution surface data derived from TLS and GST data, in order to assess and understand local permafrost distribution at the Glatzbach test site, Austrian Alps (Figure 14).

Figure 14: Panoramic view of the Glatzbach site in southeastern direction (July 2009). Permafrost investigations have been carried out on the slope towards the right, which is facing north-east. The highest peak along the ridge to the right is at 2910 m a.s.l..

Permafrost occurrence shows a strong correlation with rough surface conditions and reduced modelled solar radiation values. Additionally, the observed permafrost distribution is compared to data on permafrost occurrence from the same catchment published by Rennert (1991) showing an upward shift of around 50 m of the lower permafrost boundary between 1991 and 2009.

5.3.3 Study site

The Glatzbach catchment (47° 2' 23.49" N; 12° 42' 33.24" E) is located within the central Austrian Alps (Figure 14, a) south of Austria's highest peak (Großglockner, 3,798 m a.s.l.). We have focused our investigation on a north-east facing slope at the northern limit of the catchment (Figure 14, b).
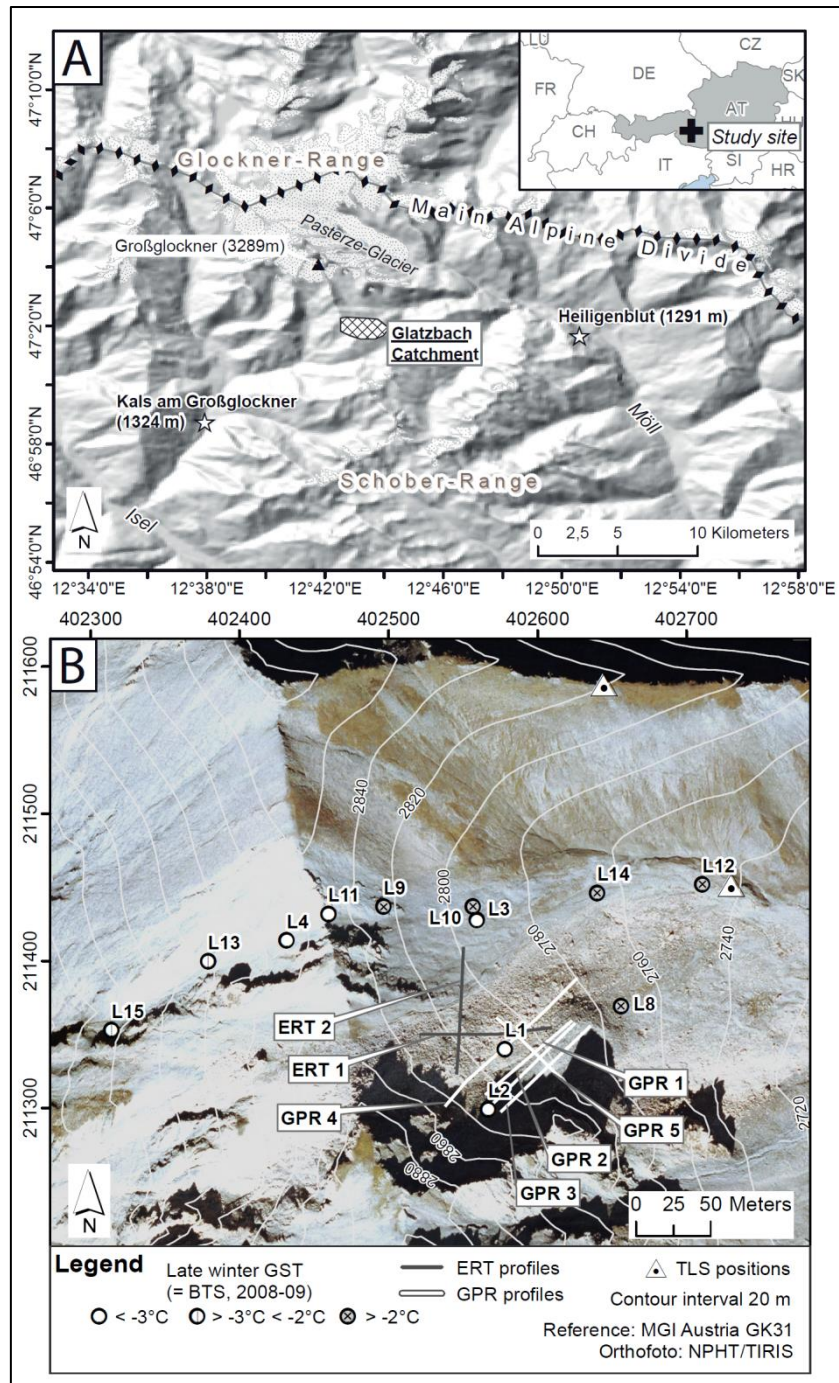
Figure 15: (a) Location of the study area; (b) aerial image of the study site and location of geophysical profiles (ERT = electric resistivity tomography; GPR = ground penetrating radar) and GST (ground-surface temperature) data loggers (L1-L15). L1 and L2 are located close to the geophysical survey and are presented here in more detail.

Within an elevation range between 2,700 and 2,900 m a.s.l. over a distance of 500 m, the study site covers the highest slopes and ridges in the north-western part of the Glatzbach catchment. The slope has a mean inclination between 25° and 45° and an overall straight profile with small concave and convex features. As a consequence of the regional lithological setting, the rather shallow topography of the Glatzbach catchment stands out from the surrounding valleys, which depict the typical high mountain imprint of Pleistocene glacial erosion with deep cirques and hanging valleys. The area is

situated at the border between the crystalline rocks of the Penninic Tauern window(mainly gneiss and schist) and the Schober Mountains a Palaeozoic formation of mica schist. Lithology at the Glatzbach is part of the "Bündnerschist", dominated by quartz- and calcareous phyllite, quartzite, as well as dolomitic- and calcareous marble (Hoeck et al., 1994). Phyllites are especially prone to physical and chemical weathering producing fine-grained regolith. In areas dominated by quartzite and dolomitic marble, blocky debris covers the surface. The surface and lithology of the investigated slope is characterized by fine-grained, platy debris of phyllite less than 10 cm in diameter in northern parts and of blocky debris larger than 30 cm in diameter resulting from rockfall events of the dolomitic marble outcrops toward the southwest. Towards the southern boundary low bedrock steps exist resulting from dipping of the Penninic rocks towards southwest. Central parts of the catchment hold vegetation covered soils, mainly cambric and calcic cryosol and regosol and shallow podsol of up to 1 m thickness. Numerous periglacial landforms have developed in the Glatzbach area including solifluction lobes and earth hummocks (Rennert, 1991). Solifluction has been studied and monitored intensively in the last two decades (Jaesche, 1999; Jaesche et al., 2002; Jaesche et al., 2003; Stingl et al., 2010). Climate data for the Glatzbach site have been collected since 1997 by the University of Natural Resources and Life Sciences, Vienna, Austria. A mean annual air temperature between 1997 and 2010 of -1.4 °C was recorded at an elevation of 2,650 m a.s.l. (Figure 16). Total annual precipitation is around 1,120 mm recorded between 1987 and 1997 (Jaesche et al., 2003) with an assumed 70% of snow precipitation (Böhm et al., 2008). The site is located at the assumed lower boundary of discontinuous permafrost in this region (Ebohon and Schrott, 2008), due to its relatively low elevation between 2,700 and 2,900 m a.s.l..
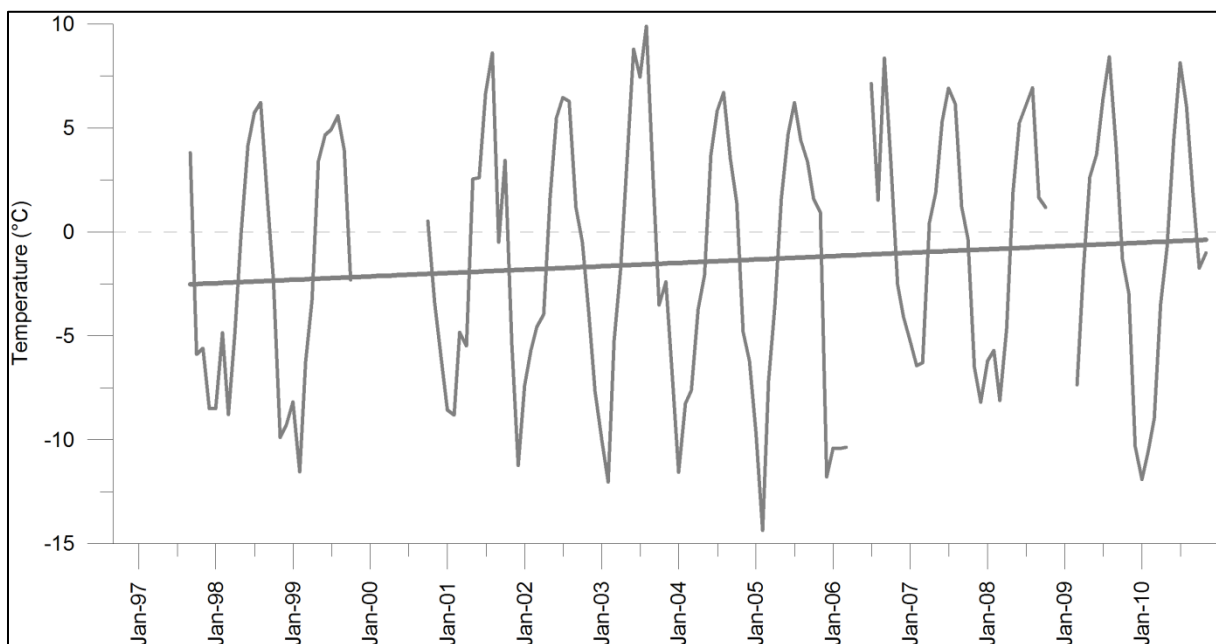
Figure 16: Monthly average air temperature and linear trend at the Glatzbach site (data: University of Natural Resources and Life Sciences, Vienna).

Previous permafrost investigation around the Glatzbach catchment

The Glatzbach catchment in the central Hohe Tauern range is among the few locations in the Austrian Alps where permafrost conditions and periglacial processes are studied outside of rock glaciers. Here, investigations started more than 20 years ago (Stingl, 1971; Veit, 1993; Jaesche et al., 2002; Jaesche et al., 2003). Ground movement on a NE-facing slope measured between 1985 and 2008 at two solifluction lobes located at 2,650 and 2,700 m a.s.l., respectively, reached values up to 200 cm per year with mean values around 2–20 cm per year, (Jaesche, 1999; Jaesche et al., 2003; Stingl et al., 2010). Previous investigation on permafrost distribution and subsurface conditions has been performed around the Glatzbach catchment within a Diploma project in 1991. The unpublished thesis by Rennert (1991) documents the permafrost detection using sediment cores and pits (at 12 locations), BTS-temperatures (36 locations), continuous measurements of ground temperature at different depths up to 2m (12 locations) and geophysical surveying (refractions seismic at 42 locations and 1-D resistivity sounding at 11 locations). The lower boundary of permafrost was determined at 2,715 m a.s.l. within the Glatzbach catchment. The study documents a heterogeneous permafrost distribution at the site attributed to locally changing ground surface conditions affecting permafrost occurrence. Based on these observations Rennert (1991) concludes that two main factors control the permafrost conditions in this area: local aspect and regolith characteristics.

Methods, field survey and data

Permafrost detection at the Glatzbach site is based on geophysical field measurements from winter and summer 2009. A total of 15 GST data loggers have been installed at the study site logging ground surface temperature at an interval of 1-hour since 2008 (Figure 15, b). The loggers have been buried within the upper 5 cm of the ground for shielding of direct radiation.We used new UTL-1 and UTL-3 loggers (Universal Temperature Logger, Geotest) with a factory provided accuracy of +/-0.1 °C (www.utl.ch). The locations of most of the GST loggers can be viewed on Figure 15, b. For the analysis we used only two loggers that are in close proximity to the geophysical surveys. Snow depths at the two logger sites used have been measured in mid- March 2009 using BTS probes and are also observable in the GPR soundings (Figure 17 and Figure 18).
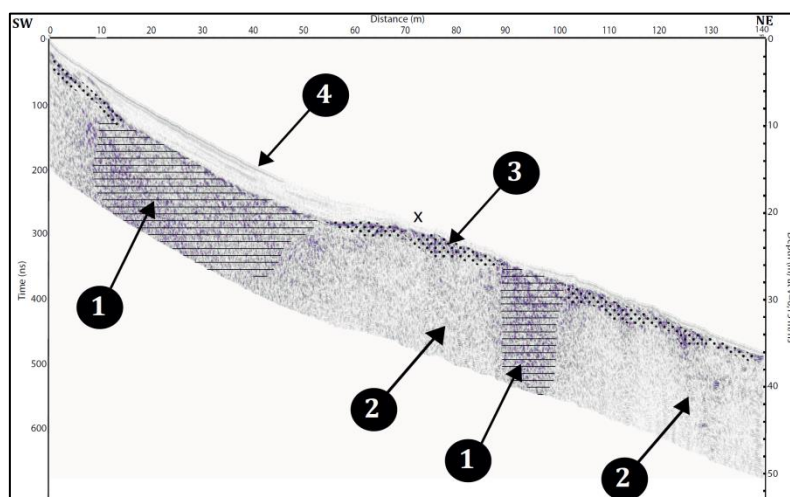
Figure 17: Radargram of GPR profile 4 (GPR4). (1) Dense pattern of reflections indicating ice lenses (velocity 0.15–0.16 m ns^{-1}, hatched zone), (2) unfrozen zone (velocities 0.11–0.12 m ns^{-1}), (3) dense reflection patterns at the surface interpreted as seasonal frost layer (velocity 0.15–0.22 m ns^{-1}, stippled zone), (4) snow cover above slope surface, (X) crossover with GPR5.
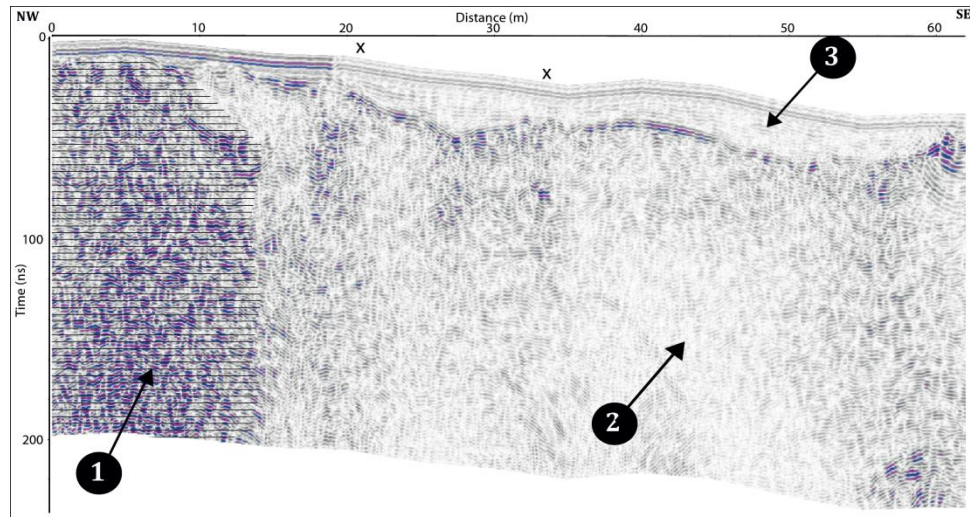
Figure 18: Radargram of GPR profile 5 (GPR5). (1) Dense pattern of reflections indicating ice lenses (velocity 0.15–0.16 m ns^{-1}, hatchedzone), (2) unfrozen zone (velocities 0.11–0.12 m ns^{-1}), (3) snow cover above slope surface, (X) crossover with GPR4 and GPR1 (from left). (The seasonal frost layer is less well developed underneath the snow cover compared to GPR4 and cannot be distinguished in the radar data).
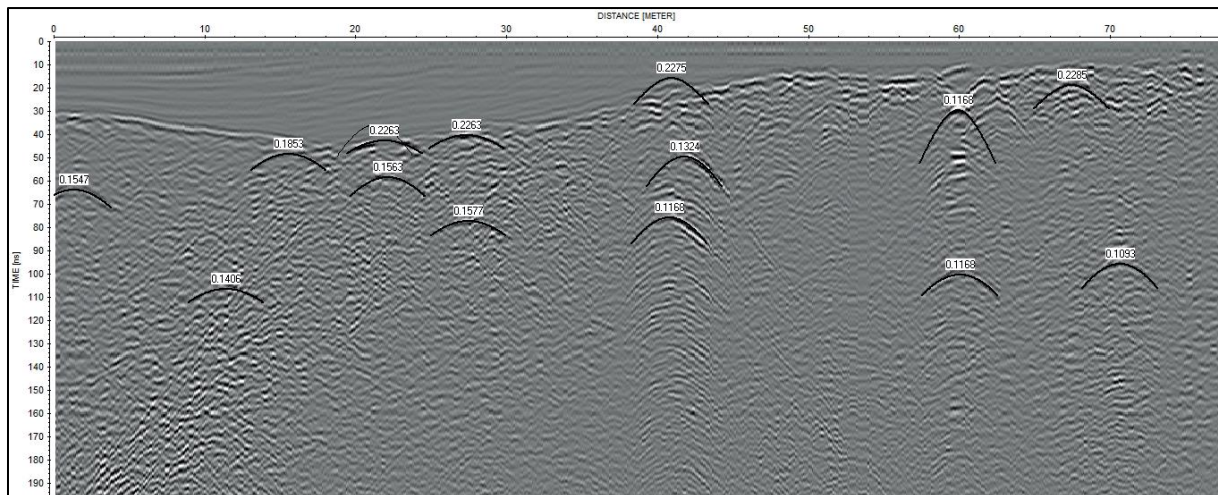

Figure 19: GPR3 radargram with parabolas representing single objects smaller than the GPR footprint in the given depth. Numbers represent propagation velocities in m ns^{-1}.

Ground penetrating radar was applied on the snow covered ground in March 2009. Five GPR profiles were measured with length between 60 and 140 m (Figure 15, b). We used a MALA RAMAC system with a 250 MHz shielded antenna system. The continuous measurement was applied with a station spacing of 5 cm triggered by a string and using a sample frequency of 2,553 MHz. Within a time window of 204 ns a total of 32 stacks were obtained. Applying this measurement configuration we can expect a vertical resolution of about 20 cm and a lateral resolution of about 50 cm (for permafrost environment, v ~ 0.13 m ns^{-1} at 1 m depth (Mcquillin et al., 1984; Trabant, 1988). GPR raw data were analysed using REFLEXW software applying standard filter routines, migration and topographic correction. Due to the use of the shielded antenna electronics no Common Midpoint (CMP) or Wide Angle Reflection and Refraction (WARR) measurements were made. Because of the vertically and horizontally heterogeneous ground velocity and the lack of accurate CMP and WARR

measurements a detailed data migration was not applied. However, in order to assess the penetration depth, we performed an overall migration using a single velocity of 0.15 m ns-1 for GPR4 only (Figure 18). The data interpretation is based on the propagation velocity of the radar waves. The following velocity measurements are based on hyperbola analyses. Winter conditions, subsequent closed snow cover and low subsurface water content, facilitated the application of GPR and significantly improved the data quality. The measurements generated high resolution, low noise data that also contain the snow depth and the accurate position of the slope topography. In order to compensate for possible uncertainties when using just one indirect prospection technique, the application of additional geophysical methods is recommended (Otto and Sass, 2006; Schrott and Sass, 2008). Consequently, in July 2009 subsurface resistivity was recorded at two locations using a GeoTom MK8E1000 multielectrode resistivity system with 25 electrodes and 4 m electrode spacing resulting in profile lengths of 96 m each. ERT was analysed with the Res2DInv software package. However, an exact overlap of the GPR and ERT profiles was not possible due to the different measurement times.

In order to estimate surface roughness and regolith grain size, a 20 cm digital elevation model (DEM) was generated applying TLS. We used a RIEGL LMS-Z620 laser scanner with a factory provided accuracy of 10 mm and a maximum range of 2,000 m. The calculated DEM results were generated by two scans positions, each containing more than 9 million points. The scans were referenced using four fixed reflectors positioned by differential GPS (GPS positioning accuracy: vertical <0.7 m, horizontal: <0.8 m, standard deviation between tie points (scan position 1) and control points (scan position 2): 0.02 m, standard deviation between local coordinates and global coordinate system: 0.39 m). Point data was filtered using a 2.5D minimum filter applying a 20 x 20 cm analysis window in RiSCAN Pro software. This filter separates the lowest values within the analysis window and generated a data set of 1.6 million points that were homogeneously distributed throughout the study area. Point data were exported as x,y,z and interpolated using the topo2raster function (TOPOGRID algorithm) in ArcGIS with a 20 x 20 cm cell size. All spatial data analysis and visualisation was performed with ArcGIS. Serving as a proxy for regolith grain size, surface roughness was quantified using the standard deviation of residual topography (Haneberg et al., 2005; Grohmann et al., 2011). Residual topography results from the difference between the original and a smoothed DEM. We applied a lowpass filter using a 3 x 3 window in order to generate a smoothed DEM. Residual topography represents local variation between the highest and the lowest point in the neighbourhood without being influenced by locale slope. Solar radiation of the study site was modelled using ArcGIS Solar Analyst for the summer period between 15 June and 15 September. We used a sky map of 40 m, simulated a standard overcast sky using diffusion portion of 0.3 and transmissivity of 0.5 for the calculation (ArcGIS settings). The time period was chosen in correspondence to comparable studies showing that during the summer months, when snow cover is reduced completely or to a great extent at this elevation, albedo is low and solar radiation is the most important energy input affecting subsurface conditions (Hoelzle, 1994; Schrott, 1994).

5.3.4 Results and interpretation

Ground penetrating radar
In total 5 GPR profiles have been acquired in winter 2009 (Figure 15, b). All profiles show a similar pattern of reflections and energy propagation velocities with signals returning from up to 14 m below the snow surface. Beneath the snow cover the topography of the slope is clearly represented by the

first strong reflector (Figure 19). The slope at this location is concavely shaped in the upper section with a snow cover of up to 4 m, followed by a straight section in the lower part, where snow depth decreases to 0.2–1 m (Figure 17). At the ground surface, all profiles show multiple reflections beneath the snow cover hinting at a boulder surface with voids. Propagation velocity within this upper layer is between 0.18 and 0.23 m ns-1 indicating the presence of ice and snow in these voids (cf. Figure 17). This zone has a thickness of upper 1–2 m which increases where the snow cover decreases (dotted area, marked with 3 in Figure 17 and Figure 18). Due to the propagation velocity that indicates ground ice, we interpret this first layer as seasonal frost at the surface. The depth of this layer corresponds with previous thermal measurements by Jaesche et al. (2003) who observed winter frost up to depths of about 80 cm at the Glatzschneid. Locally, this dense reflection pattern extends to deeper zones along the slope (hatched area, marked with 1 in Figure 17 and Figure 18). Here, propagation velocities are 0.13–0.16 m ns-1, representing typical values for ground ice (Musil et al., 2002; Berthling and Melvold, 2008). These zones are interpreted as active permafrost zones, where seasonal frost reaches the permafrost table. Other areas where energy propagates with velocities between 0.09 and 0.11 m ns-1 (Figure 19), marked with 2 in Figure 17 and Figure 18 and few reflections are observable are interpreted as unfrozen zones. These are located below the layer of seasonal frost. No distinct boundary between regolith and bedrock can be observed. We assume that due to the high resolution of the GPR measurement the rough bedrock surface is apportioned into diffraction hyperbolas of single edges and cavities and not represented by a continuous reflector. In profile GPR4 two zones of dense reflectors and higher velocities are visible, one in the upper section and another starting at around 90 m downslope of a convex part of the section (Figure 17). GPR5 profile is placed across the slope starting on the blocky material and running towards southeast which consists of finer grain sizes at the surface (Figure 18). Reflection patterns are comparable to the downslope profiles revealing a zone of dense reflections from the surface into deeper parts of the slope.

Electrical resistivity tomography

In summer 2009 we carried out electrical resistivity soundings close to the zone where GPR has been applied in the previous winter. Two perpendicular profiles have been placed across the coarse grain zone of the slope (Figure 15, b). ERT1 runs downslope from W to E, crossing GPR4 and GPR5 at its lower end. Inversion results show higher resistivity in the central part of the section with resistivity values up to 80,000 Ωm, with its maximum about 5 m below the surface (Figure 20). This zone of higher resistivity is observable in the upper section of ERT2 as well. However, here maximum values do not exceed 40,000 Ωm. Downslope of this zone in ERT2 resistivity strongly decreases below 5,000 W m. We interpret resistivity values >10,000 Ωm as ground ice occurrence, following general observations by previous studies (Hauck and Kneisel, 2008). Regions of resistivity below 10,000 Ωm can be regarded as non-frozen regolith; lower resistivity values (<1000 Ωm) suggest moisture within the slope, probably due to rainy weather conditions, snow/frost melt or subsurface drainage. The measurement was taken in early summer, before the maximum thickness of the active layer is reached. Since seasonal frost is assumed to penetrate only up to a maximum of 1 m into the ground (see above), we are convinced to identify permafrost in the deeper ground and not remains of seasonal frost. At the time of measurement, active layer thickness in profile ERT1 is of a few decimetres while in profile ERT2 a maximum of 2 m of the surface shows resistivity below 10,000 Ωm and appears to be unfrozen (Figure 20).
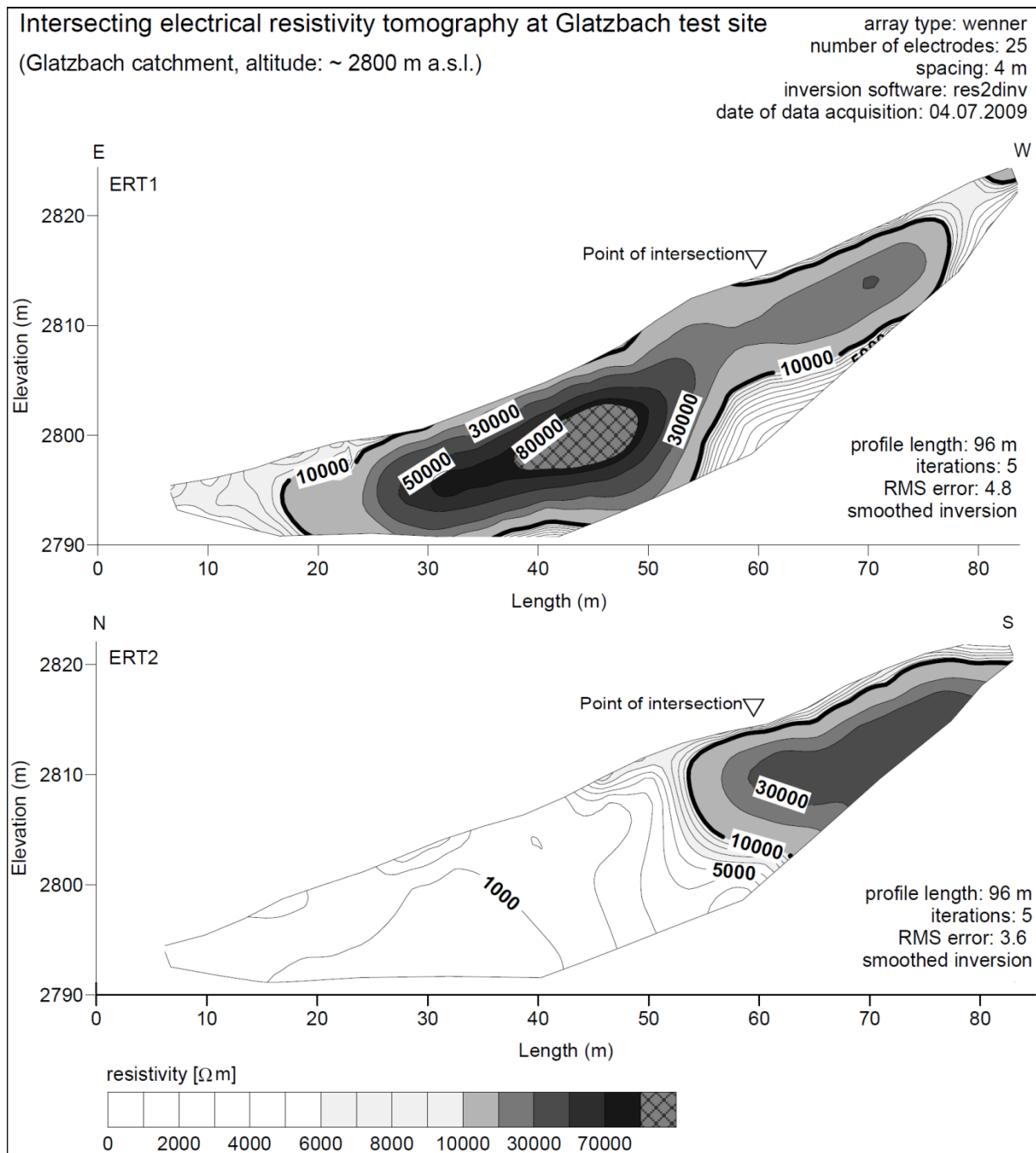
Figure 20: Intersecting ERT profiles at Glatzbach site. Profile lengths of both measurements were 96 m with a 4 m electrode spacing. The bold black line marks the 10.000 Ωm contour line.

Ground surface temperature records

Assuming a thick winter snow cover (>1 m), which has not been constantly monitored, we can interpret the GST data similar to BTS measurements, looking at GST below snow in late winter: Five out of 15 loggers have measured mean temperatures below -3 °C in late winter with minor temperature changes in February and March, indicating permafrost conditions based on the BTS principle. Another two loggers recorded mean temperatures between -2 and -3 °C in this period, which can be interpreted as possible permafrost occurrence, while the remaining loggers measured temperatures between 0 and -2 °C and do not allow for permafrost interpretation. Loggers L1 and L2

have been placed in late August 2008 in close proximity to the GPR survey lines (*Figure 15*, b) documenting the ground surface temperature development in winter 2008/2009 (*Figure 21*).
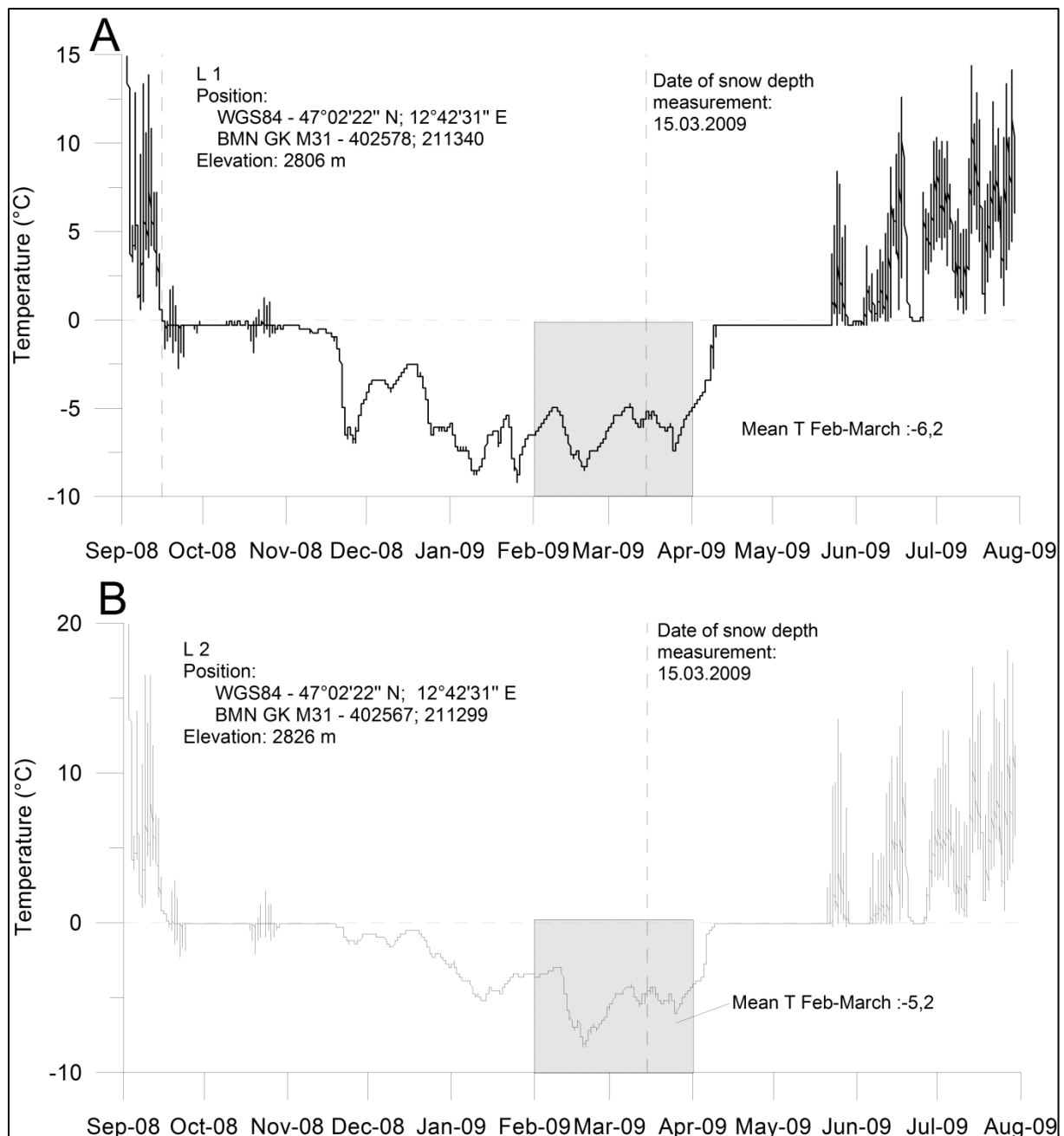
Figure 21: Ground surface temperature at site L1 (a) and L2 (b) between September 2008 and July 2009.

Unfortunately, the local climate station failed between late-October 2008 and late-March 2009, preventing a comparison of GST and air temperatures throughout the winter. GST dropped to almost constant 0 °C between 16 September and 18 October (Figure 21, a, b). October 2008 ended in a mild period with positive daytime air temperatures around 5 °C and around 0 °C at night. The 0 °C constant indicates the first shallow, short term snow cover in early autumn, where latent heat release generates the so called zero curtain effect. GST dropped sharply below -5 °C at L1 in mid-November, while at L2 temperature slowly decreased towards -5 °C not until mid- January (Figure 21, a, b). Winter GST at L1 reveals short term fluctuations between -2.5 and -8.5 °C (Figure 21, a). In

contrast, L2 shows fewer fluctuations until end of December and a slower decrease of temperatures between -0.5 and -3 °C (Figure 21, b). From early February 2009 to April 2009 both curves depict symmetrical GST fluctuations, however, with deeper absolute values at L1. Logger L1 was covered by approximately 1.5 m of snow, while L2 had at least 3–4 m of snow cover at that time. As of the beginning of April, snow melt produces the zero curtain effect producing a constant GST of 0 °C. Snow melt lasted until 25 May and 21 May at L1 and L2, respectively. L1 was positioned on a coarse grain surface, while surface material underneath L2 is finer. To conclude, we interpret both logger locations as permafrost sites due to mean temperatures below -3 °C in late winter (February-March). Higher surface roughness at site L1 may have prevented a continuous snow cover in early winter leading to strong downcooling, larger temperature changes and lower maximum temperatures compared to L2, where winter temperatures more slowly adapt to subsurface thermal conditions. However, we acknowledge that due to the large fluctuation within the data we cannot exclude ventilation effect and influence of air temperature on the GST and thus GST data does not provide a highly certain permafrost indicator here.

High resolution terrain analysis

In order to analyse influences of surface characteristics on the permafrost distribution we quantified morphometric variables and potential solar radiation for the study site using a 20 cm DEM. Quantification of surface roughness using the standard deviation of residual topography within an analysis window of 60 x 60 cm displays the location of boulders when compared with digital aerial photographs (compare Figure 15, b). Roughness values are around 0.01–0.02 m in smooth, fine-grained terrain, whereas coarse grained terrain shows values between 0.03 and 1 m (Figure 22, a). Solar radiation input on the study slope during the summer period (15 June–15 September) was modelled between less than 20 kWh m^{-2} on the steeper inclined upper parts of the slope and more than 50 kWh m^{-2} on southern slopes and flat areas (Figure 22, b). The impact of large boulders on the energy input is clearly reflected in the modelled values of solar radiation. In areas with large boulders, hence high surface roughness, solar radiation values vary between around 50 kWh m^{-2} at the illuminated sides of boulders and less than 30 kWh m^{-2} on the shaded side. Due to local shading effects of large boulders, modelled energy input is reduced by up to 40% on rough surfaces compared to surfaces covered by fines (Figure 22, b).
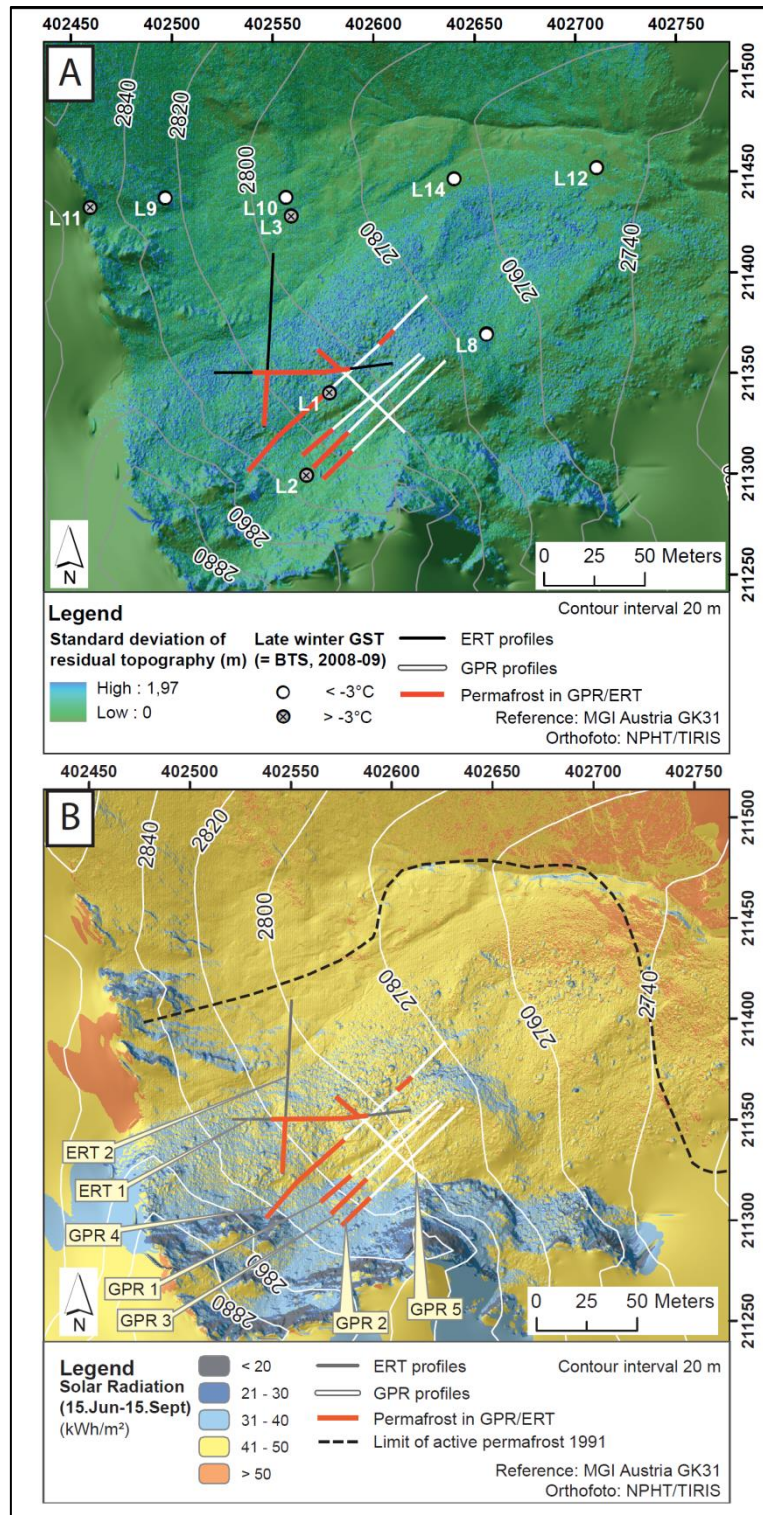
Figure 22: (a) Map of surface roughness expressed as standard deviation of residual topography (3 x 3 window). Coarse blocks stick out in green compared to low smooth surfaces in light brown. (b) Map of solar radiation input between 15 June and 15 September (kWH m⁻²) based on a 20 cm DEM. Lowest values are modelled for the steep rock faces oriented in northern directions and for the block field in the centre of the slope. Highest values are observed on south facing slopes.

5.3.5   Discussion

Based on the field data we could detect and accurately localize permafrost occurrence at the Glatzbach site on the northeast facing slope above 2,780 m a.s.l.. However, GPR4 shows that some sporadic ice lenses can also occur below this zone. High resolution terrain analysis indicates that small scale variations of the surface are responsible for the permafrost occurrence. Figure 23 depicts a comparison of solar radiation, slope, roughness and snow depth along profile GPR4. The curves of surface roughness and solar radiation vary almost diametrically opposed indicating the negative influence of large boulders on the energy input. In contrast, surface roughness and slope angles show similar patterns. Modelled solar radiation along the profile ranges from 20 to 50 kWh m^{-2} for the summer period. In the underlying GPR image, two zones of dense reflections patterns indicate the occurrence of subsurface ground ice. Their location corresponds well to areas of lower solar radiation and increased surface roughness at the surface. The upper zone of low solar radiation is influenced by a steep inclination, the general orientation towards NE and shading effects by the proximate steep rock wall towards southwest (Figure 22, b). The influence of shading effects can have significant impact on local permafrost occurrence in mountain regions (Schrott, 1994; 1996). With increasing distance from the ridge solar radiation increases towards a first plateau of high energy between 53 and 62 m where solar radiation surpasses 50 kWh m^{-2}. The observed zone of reflections in GPR4 corresponds also to a convex part of the slope with greatest snow depths. At 80 m, ground ice occurrence falls into a second zone of reduced solar radiation and increased surface roughness (Figure 23).
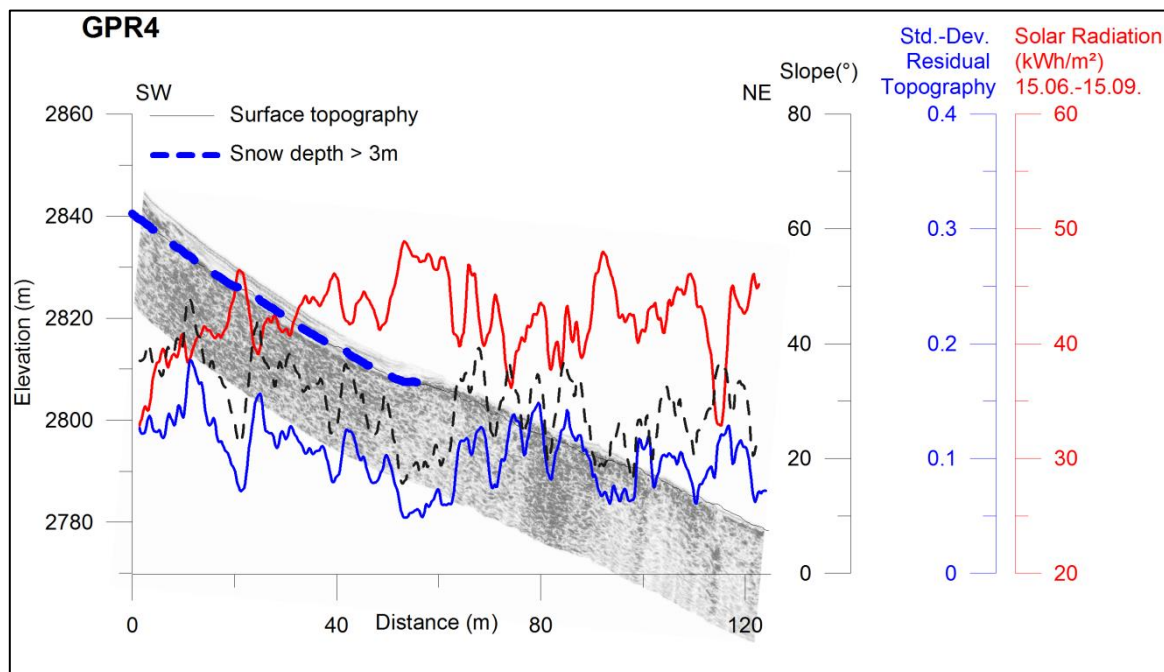
Figure 23: Comparing surface roughness, solar radiation, slope and snow depth at 15 March 2009 (thick dashed line) along profile GPR4. Curves of solar radiation, surface roughness and local slope have been smoothed using a running average of 3 m for better visualization. Permafrost areas are represented by dense reflection patterns in the radargram (compare to Figure 17).

Modelling the solar radiation at this resolution enables to identify local surface influences on the distribution of permafrost. Single large boulders as well as a cluster of larger blocks on a slope reduced overall solar input through local shading effects, leading to cooler surface conditions in

shaded areas and higher insolation on sun-facing parts of the boulders. This effect may either add to the influence of slope angle and aspect, or may counterbalance them. With respect to permafrost formation, decreased solar radiation on coarse-grain surfaces may lower the limit of permafrost compared to locations of similar elevation and aspect with fine-grain regolith. In case of GPR4 we observed that surface conditions enable the occurrence of isolated ground ice about 10 m lower compared to the potentially continuous occurrence in the upslope area. However, it needs to be verified to what extend the other potential influences on permafrost caused by surface boulders affect the permafrost distribution here. We can mostly exclude air circulation between the rocks since large amounts of fine material fill the voids. On the other hand, large blocks that stick out of the winter snow surface may influence the local conditions here as well. Additionally, it needs to be analysed to what extend increased insolation on the one side of the blocks counterbalances the shading effect on the other side. This would probably require some modelling to estimate this effect and is surely depending on the size of the block.

Comparing permafrost distribution between 1991 and 2009

In 1991 Rennert mapped permafrost distribution at the Glatzbach catchment (cf. Figure 22, b). Based on 1D-electrical resistivity, refraction seismic, BTS and ground temperature measurements, and pits he estimated the lower limit of active permafrost at 2,740 m a.s.l. on the easterly and north-easterly part of the slope (Rennert, 1991). Based on our investigation we detect permafrost at elevation above 2,790 m a.s.l. limited to steep parts of the north-easterly exposed slope and on surfaces characterized by coarse regolith (Figure 22, b). Even though we cannot judge the accuracy of the previous study by Rennert, we can assume a rise of permafrost of around 50 m in elevation between 1991 and 2009. Between 1997 and 2010 mean annual air temperature rose from -2.1 °C (1997–2003) to -1.2 °C (2004–2010).

5.3.6   Conclusion

The Glatzbach site in the central Eastern Alps of Europe can be considered as an area with sporadic and discontinuous permafrost occurrence. Ground ice and permafrost is found above an elevation of 2800 m a.s.l. on slopes facing north-east. The strongly varying pattern of permafrost distribution at the Glatzbach results from local surface cover characteristics, mostly influenced by regolith grain size and variation of solar radiation. Analysis of surface roughness as a proxy for grain size distribution using very high resolution (grid resolution 20 x 20 cm) terrestrial laser scan data reveals that the lower boundary of discontinuous and sporadic permafrost is lowered on rough surfaces compared to fine-grain zones. At the same location modelled potential summer solar radiation in coarse grain zones is reduced by 40% compared to surfaces of fine grain sizes and between the illuminated and the shaded side of the boulders. This effect adds up to previously considered influences of coarse blocks on ground thermal conditions including snow cover development and air circulation that in combination lead to localized ground cooling and permafrost conditions despite positive air temperatures.

The study shows that a combination of high resolution geophysical information with very high resolution surface information significantly supports the understanding of local permafrost conditions in alpine terrain. Digital elevation data derived from laser scanning, especially from terrestrial surveys provides sufficiently detailed surface data in order to analyse local regolith conditions. Modelling of permafrost conditions on large scales therefore should include the analysis of surface conditions in order to consider surface influences on the local permafrost distribution. It

has to be mentioned however, that special attention is required concerning accurate positioning of the surface and subsurface data in order to provide precise data overlap. This includes the application of GPS for surveying of geophysical profiles, referencing of laser scans, and a high resolution consideration of topography within geophysical analysis software.

6 Establishing an open air laboratory for long-term monitoring of permafrost and mass movements

Partly derived and modified from:

KEUSCHNIG, M., HARTMEYER, I., OTTO, J. C. & SCHROTT, L. 2011. A new permafrost and mass movement monitoring test site in the Eastern Alps—concept and first results of the MOREXPERT project. In: BORSDORF, A., STÖTTER, J. & VEULLIET, E. (eds.) Managing Alpine future II—inspire and drive sustainable mountain regions. Proceedings of the Innsbruck Conference, 21–23 November 2011. IGF-Forschungsberichte 4.

OTTO, J. C. & KEUSCHNIG, M. 2014. Permafrost-Glacier Interaction - Process Understanding of Permafrost Reformation and Degradation. In: RUTZINGER, M., HEINRICH, K., BORSDORF, A. & STÖTTER, J. (eds.) permAfrost – Austrian Permafrost Research Initiative - Final Report. IGF-Forschungsberichte 6: Austrian Academy of Sciences.

6.1 The MOREXPERT project and monitoring concept

The major part of this Ph.D.-thesis is an outcome of the MOREXPERT and MOREXPERT 2 project. The project MOREXPERT (Monitoring expert system for hazardous rock walls, 2010 - 2014) established an "open air laboratory" for long-term monitoring of permafrost and rockfall interaction at the summit region of the Kitzsteinhorn (3,203 m a.s.l., Hohe Tauern range, Austria). The systemic approach includes atmospheric, surface and subsurface monitoring using a combination of automated weather stations, terrestrial and airborne laser scanning, temperature measurements in shallow and deep boreholes, geophysical and geotechnical investigations. By combining these methods, MOREXPERT aims at identifying the short- and medium-term responses of slope stability in steep permafrost-affected bedrock to climate forcing (Figure 24).
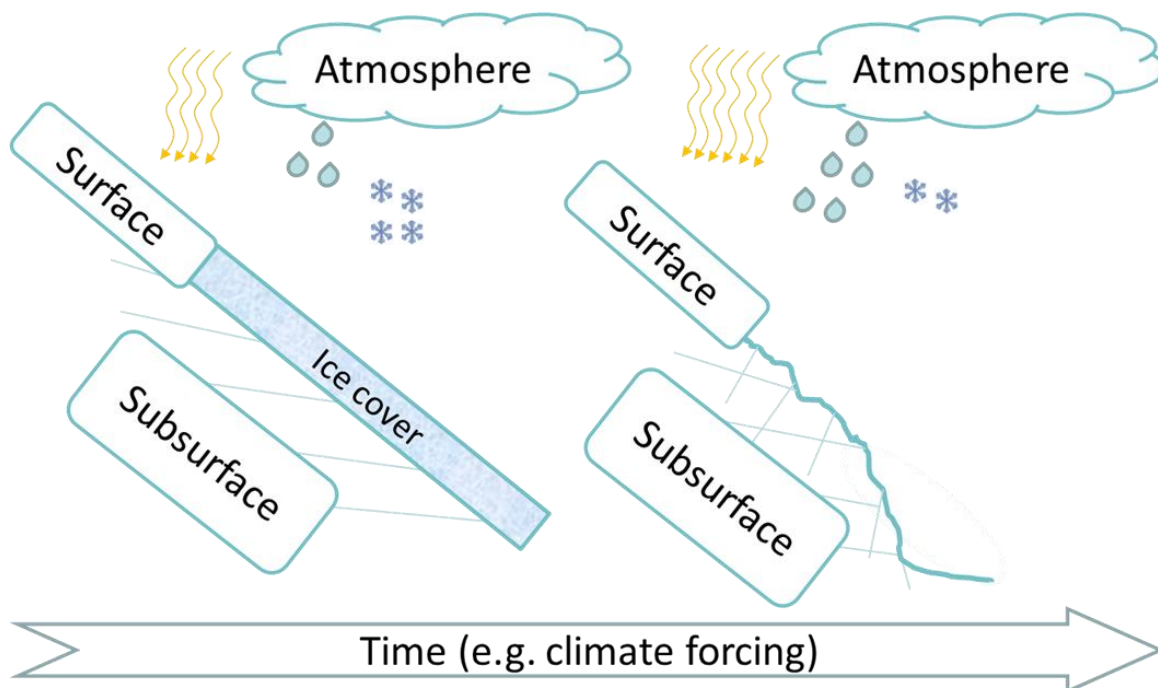
Figure 24: Expected surface and subsurface changes caused by climate forcing.

To meet the requirements of a complete adaptation strategy MOREXPERT 2 (2014 – 2017) is focused on risk management as key tool for climate change adaptation. The overall aim is to establish a dynamic, integrated risk management system on an individual operational unit (e.g. company, Gletscherbahnen Kaprun AG) which is capable to manage spatially and temporally changing environmental conditions.

Based on a preliminary risk analysis and considering cost/benefit of different instrumentation strategies, an adequate monitoring intensity was chosen. The monitoring intensity depends on the level of risk –e.g. in the area with the highest risk, the highest instrumentation density was applied. According to Schrott and Sass (2008) and Otto and Sass (2006) a combined methodological strategy is highly recommended to decrease uncertainties resulting from the use of one single method. This was taken into account, Figure 25 shows the current monitoring configuration based on a preliminary risk analysis.

Region: Summit		**Region: Magnetköpfl**		**Region: Summit station**	
Area: approx. 30 ha		Area: approx. 3 ha		Area: approx.. 0,5 ha	
Estimated risk: low		Estimated risk: medium		Estimated risk: high	
Boreholes:	-	Boreholes:	o	Boreholes:	++
GST/NST:	+	GST/NST:	++	GST/NST:	++
BTS:	o	BTS:	+	BTS:	+
ERT:	o	ERT:	+	ERT:	++
GPR:	o	GPR:	o	GPR:	o
Passive seismic:	o	Passive seismic:	o	Passive seismic:	+
Geotechnical mapping:	+	Geotechnical mapping:	++	Geotechnical mapping: :	++
TLS:	o	TLS:	+	TLS:	++
ALS:	++	ALS:	+	ALS:	+
Crackmeter:	-	Crackmeter:	o	Crackmeter:	+
Weather Station:	+	Weather Station:	+	Weather Station:	++

Figure 25: Schematic overview of the monitoring intensity based on a preliminary risk analysis. "++" to "-"represents the instrumentation intensity of each method relatively to each other. GST/NST: Ground-Surface/Near-Surface Temperature; BTS: Bottom Temperature Snow Cover; ERT: Electrical Resistivity Tomography; GPR: Ground Penetrating Radar; TLS: Terrestrial Laser Scanning; ALS: Airborne Laser Scanning.

One of the most important observation techniques is represented by the permanently installed ERT below the Kitzsteinhorn summit station which provides the data for this Ph.D.-thesis.

6.2 Monitoring site

The study site is located at the Schmiedingerkees cirque at the Kitzsteinhorn (3,203 m a.s.l.; 47°11'17'' N, 12°41'15'' E) ski area in the Federal Province of Salzburg, Hohe Tauern Range, Austria. The cirque opens in north-eastern direction from the summit of the Kitzsteinhorn (3,203 m a.s.l.), covering approximately 3 km² and a vertical elevation difference of 1,500 m between the summit and the glacier forefield limits (1,700 m maximum Little Ice Age (LIA) extent) (Figure 26).

Figure 26: Kitzsteinhorn sudy site (3.203 m a.s.l.; 47°11'17'' N, 12°41'15'' E).

The Kitzsteinhorn is located just north of the main Alpine divide and has no directly adjacent summits. The Schmiedingerkees glacier has a size of approx. 1.05 km² (2012), covering around 40 % of the cirque area. The glacier is a flat cirque type glacier with a maximum thickness of 90 m and is surrounded by steep bedrock slopes of up to 250 m height.

6.2.1 Climate and permafrost distribution

Three weather stations are located within the study area, permitting continuous observation of external forcing of ground thermal conditions. The weather stations are located at the Alpincenter (2,446 m a.s.l.) of the ski station at the Kammerscharte (2,561 m a.s.l.) in the neighbouring cirque towards the southeast and directly on the Schmiedingerkees glacier (2,920 m a.s.l.). The stations show mean annual air temperature (MAAT) values of 1.0 °C, -3.0 °C and -2.7 °C, respectively (**Fehler! Verweisquelle konnte nicht gefunden werden.**). The mean annual precipitation is

Table 4: Climate data of the reference climate stations around the Kitzsteinhorn.

Location	Altitude [m a.s.l.]	Time period	MAAT [°C]	Mean snow height [m]	Max snow height [m]	Mean solar radiation [W/m²]
Alpincenter	2.446	01.2005-01.2015	1.0	0.9	2.8	-
Kammerscharte	2.561	11.2008-01.2015	-3.0	1.1	3.7	160.2
Glacier Plateau	2.920	11.2008-01.2015	-2.7	1.5	4.1	-

Compared to the MAAT at Sonnblick Observatory (3.106 m a.s.l) of -4.7 C° (mean values for 1971-2000) (Schoner et al., 2012) the MAAT of -2.7 °C at the Schmiedingerkees glacier (2.940 m a.s.l.) is in

a reasonable range. MAAT differences could be the result of local influences on the measurement, e.g. the impact of warming of buildings or special thermal conditions. The weather station at the Kammerscharte provides robust data with a MAAT of -3.0 °C, which indicates the lower limit of areas with significant amounts of permafrost (continuous, discontinuous permafrost distribution) (Haeberli et al., 2010).

Applying a statistical model of permafrost distribution (Permakart 3.0) based on empirical permafrost data from the Hohe Tauern range (Schrott et al., 2012) shows that large areas of the Kitzsteinhorn summit region are within the potential zone for permafrost (Figure 27, 1.2 km²). Below 2.600 m front of the Schmiedingerkees glacier, the probability of permafrost occurrence drops below 20%. Below 2,500 m only very isolated patches provide permafrost conditions.
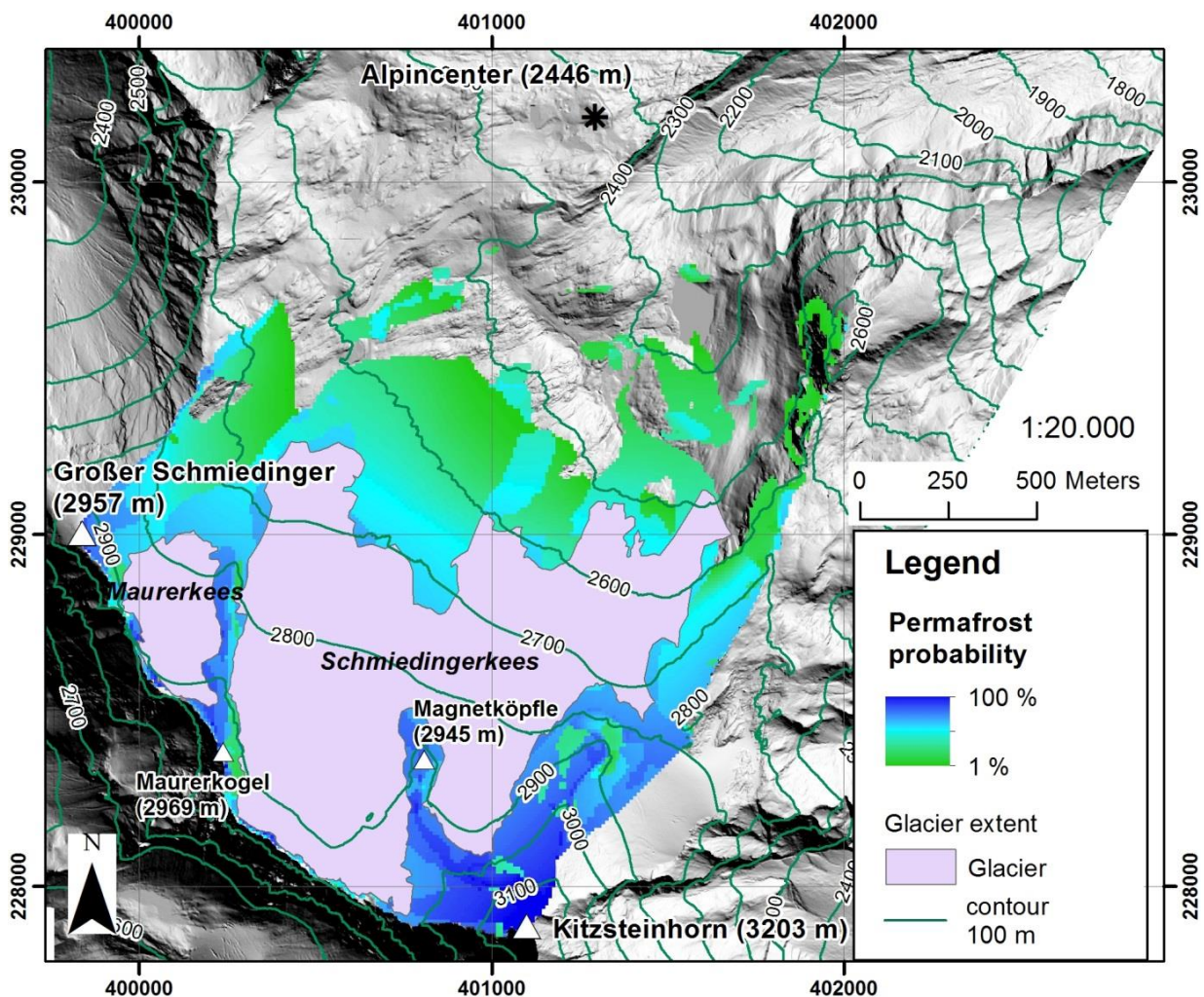
Figure 27: Map of potential permafrost distribution at the Kitzsteinhorn around the glacier extent of 2012.

6.2.2 Geology and geomorphology

The Kitzsteinhorn is constituted of rock of the Bündner schist formation and belongs to the Glockner Nappe, specifically the Glockner Facies. The study area primarily consists of calcareous mica schist with minor parts of prasinite, amphibolite, phyllite and serpentinite (Hoeck et al., 1994; Schober et al., 2012). Rising temperatures have led to a substantial glacier retreat that has been particularly

pronounced since the 1980s. Due to intense ablation the surface of the Schmiedingerkees glacier has been lowered by approximately 30 m over the last 40 years.

Glacial debuttressing represents a major long-term destabilising factor for the rock faces. In combination with the loss of the ice cover these processes have led to the exposure of oversteepened rock to atmospheric influences and intensified mechanical weathering. Geological discontinuities have become subject to a different thermal regime which includes the development of an active layer and convective heat transport in unfrozen clefts. As a consequence, the exposed rock faces are frequently affected by rockfall events (Hartmeyer et al., 2012a; Keuschnig et al., 2015) (Figure 28).
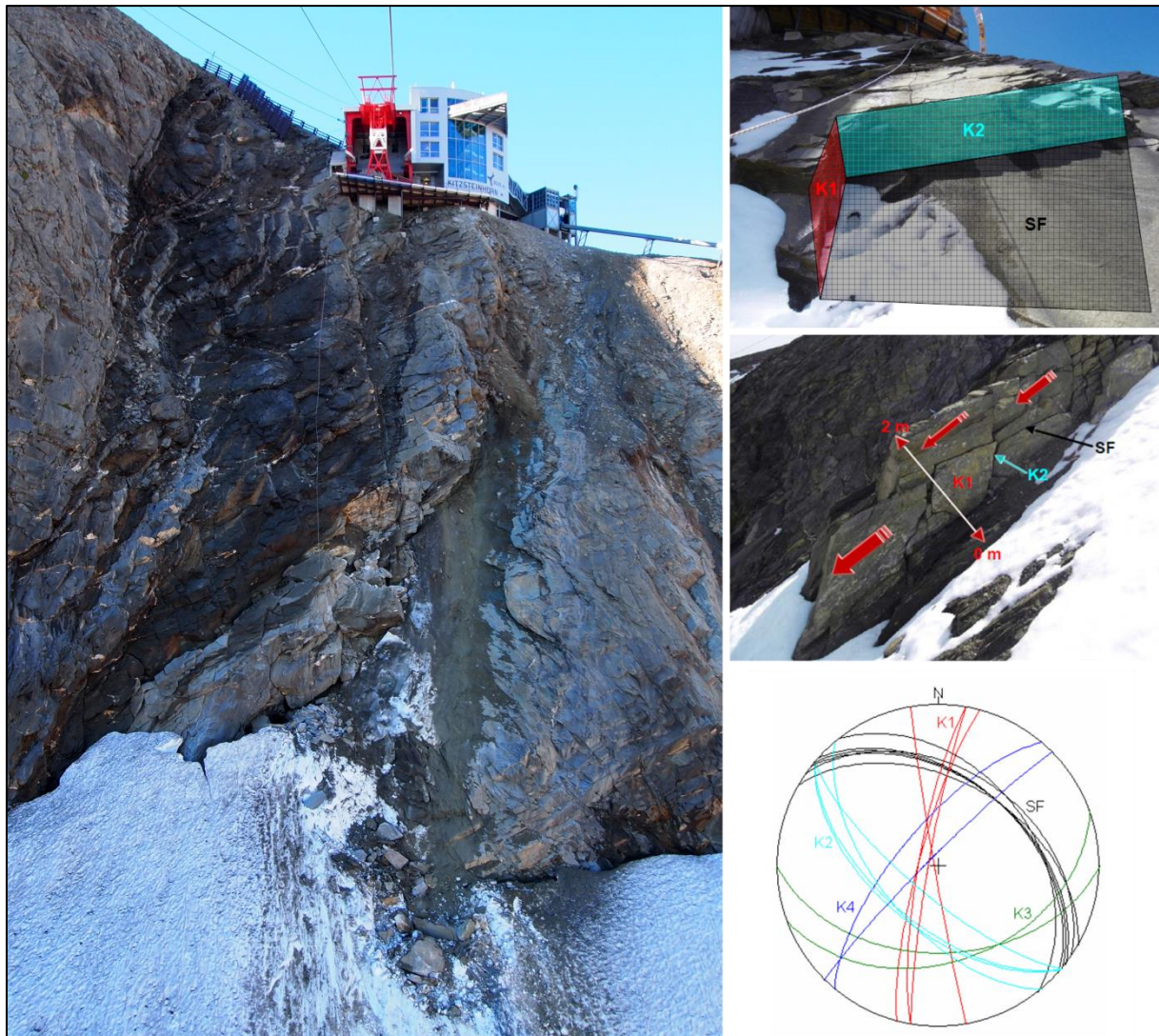
Figure 28: Rockfall detachment areas below the Kitzsteinhorn summit station (left side) and geotechnical setting of the affected north face (dip slope, right side).

The recently exposed glacier forefield is characterised by large areas of exposed bedrock (Figure 29). Only lateral and lower parts are debris covered and contain surface indicators for previous glacier extent (lateral, frontal moraines). Apparently, the Schmiedingerkees has a low debris production compared to other glaciers. The largest area of thick debris cover is located in the eastern part of the glacier forefield, east of the Schmiedinger lake. The steep cirque side walls are characterised by

intense rockfall and avalanche activity. Especially the eastern ridge, descending from the Kitzsteinhorn peak shows intense erosion leading to debris cover on the eastern part of the glacier. This debris input is most probably responsible for the debris accumulation in the forefield at the eastern side. Prominent lateral moraines that indicate the LIA ice maximum can be observed south of the Alpincenter (2,446 m a.s.l.) and within the descending valley north of the lake.
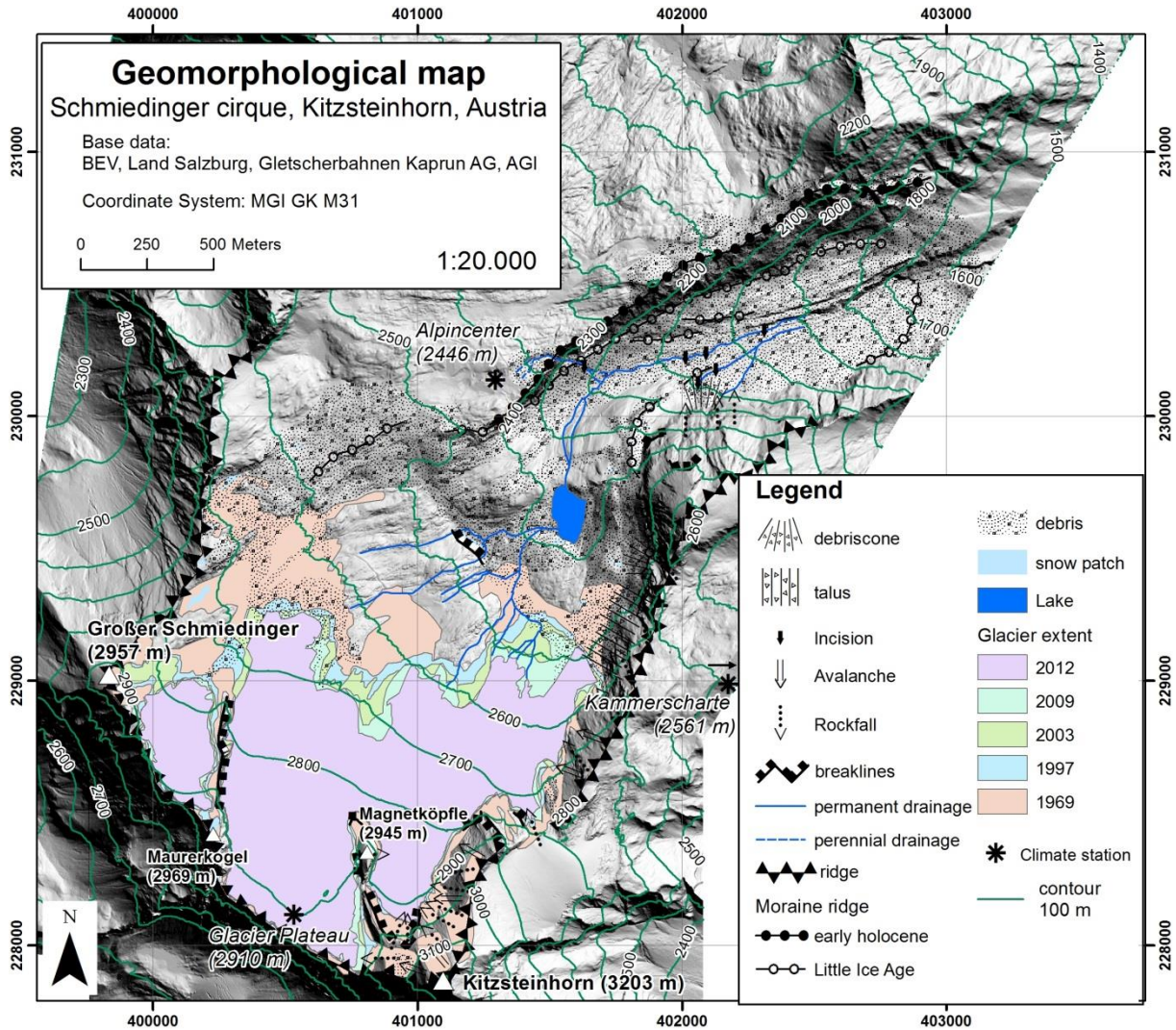
Figure 29: Decreasing glacier extent and ice cover in the area of the release zone during the last decades (Otto and Keuschnig, 2014).

6.3 A scale-oriented approach

6.3.1 Abstract

Within the research project MOREXPERT ('Developing a Monitoring Expert System for Hazardous Rock Walls') a new study site for long-term bedrock permafrost monitoring has been initiated. Surface and subsurface thermal conditions in steep rock faces are monitored based on a combination of borehole, geophysical and meteorological measurements. MOREXPERT was launched in September 2010, the study area is located at the Kitzsteinhorn (3,203 m; 47°11'17'' N, 12°41'15'' E), Hohe Tauern Range, Austria. Within the research project ground thermal conditions are monitored on three complementary scale levels: the 'borehole scale', the 'slope scale' and the 'mountain scale'. At each scale level ground thermal conditions are studied applying different methodical approaches and, therefore, with different spatial and temporal resolutions. At the 'borehole scale' five deep boreholes provide ground temperatures from depths of up to 30 m. At the 'slope scale' data from two ERT (Electrical Resistivity Tomography) arrays are used to derive information on ground thermal conditions. At the 'mountain scale' spatially distributed temperature measurements with miniature loggers in a maximum depth of 80 cm deliver information on the heterogeneity of near-surface rock temperatures. The introduced scale-oriented monitoring approach explicitly takes into account the high lateral and vertical variability of ground temperatures in high-alpine rock faces. Complementary analysis of data obtained at different scale levels allows (constrained) validation and extrapolation of information, eventually yielding a quasi-spatial model of the thermal state of the Kitzsteinhorn's surface and subsurface. Due to its generic design the presented monitoring approach is considered to be transferable to comparable high-mountain study sites.

6.3.2 Introduction

Ground surface temperatures (GST) vary largely over short distances depending on topographic variables (elevation, slope aspect, slope inclination), ground surface cover (fine-grained, coarse-grained material) and snow distribution (Brenning et al., 2005; Luetschg et al., 2008; Otto et al., 2012). Recent studies show that even within an altitudinal belt of 300 m variation of, mean annual ground surface temperatures (MAGST) can be as high as 6 °C, not taking into account steep rock faces where variation is likely to be even larger (Gubler et al., 2011). Apart from its considerable spatial heterogeneity, GST also varies strongly over short observations periods due to the transitory nature of high-mountain climatic and microclimatic conditions (Schneider et al., 2012).

Temperatures at depth are governed by the high spatial and temporal heterogeneity of thermal conditions at and near the surface. However, as temperatures propagate downwards into the ground they become progressively attenuated and phase-shifted, yielding thermal patterns that differ significantly from those at the surface. This vertical variability of thermal conditions is controlled primarily by the thermal properties of the subsurface, the prevalent mechanism of heat transport (heat conduction vs. advection) and the persistence of past climatic conditions large depths (Isaksen et al., 2000).

Within this contribution a permafrost monitoring approach is presented that explicitly takes into account both, lateral and vertical variability of ground thermal conditions in bedrock. The introduced approach is currently implemented within the MOREXPERT project ('Monitoring Expert System for Hazardous Rock Walls'). MOREXPERT started in September 2010 and initiates a new long-term monitoring site focusing on permafrost and rockfall interaction in steep bedrock. Long-term data series on ground thermal conditions, comparable to meteorological data, are essential since permafrost distribution potentially responds very slowly to changing climatic conditions. For this reason the projects Permafrost and Climate in Europe (PACE) (Kellerer-Pirklbauer et al., 2008), the Swiss Permafrost Network (PERMOS) (Noetzli and Vonder Muehll, 2010) (Noetzli and Vonder Muehll, 2010)and the Longterm Permafrost Monitoring Network (PermaNET) (Mair et al., 2011) have initiated long-term permafrost monitoring sites in the European Alps. Particularly high mountain peaks in the western European Alps (e.g. Schilthorn, Matterhorn, Aiguille du Midi) have been instrumented for continuous monitoring of permafrost (Gruber et al., 2004c; Ravanel et al., 2011). In Austria, extensive permafrost monitoring with deep boreholes and geophysics was limited to one site, situated at Hoher Sonnblick (3,105 m). The Sonnblick is located approximately 25 km southeast of the MOREXPERT site and features a permanently installed ERT profile and three 20 m deep boreholes (Klee and Riedl, 2011). By establishing a new site at the Kitzsteinhorn, which includes five 20-30 m deep boreholes and comprehensive geophysical monitoring, the MOREXPERT project addresses the need for a larger number of extensive permafrost monitoring sites in Austria (Otto and Keuschnig, 2014). Nonetheless, the establishment of new monitoring sites and the expansion of the borehole network remain crucial issues in Austrian permafrost research.

6.3.3 Study area

The study area of the MOREXPERT project is located in the Federal Province of Salzburg, in the Hohe Tauern Range, Austria's highest mountain range (Figure 30). It encompasses the entire summit region of the Kitzsteinhorn (3,203 m), covering approximately 3.5 ha and a vertical elevation difference of 300 m.
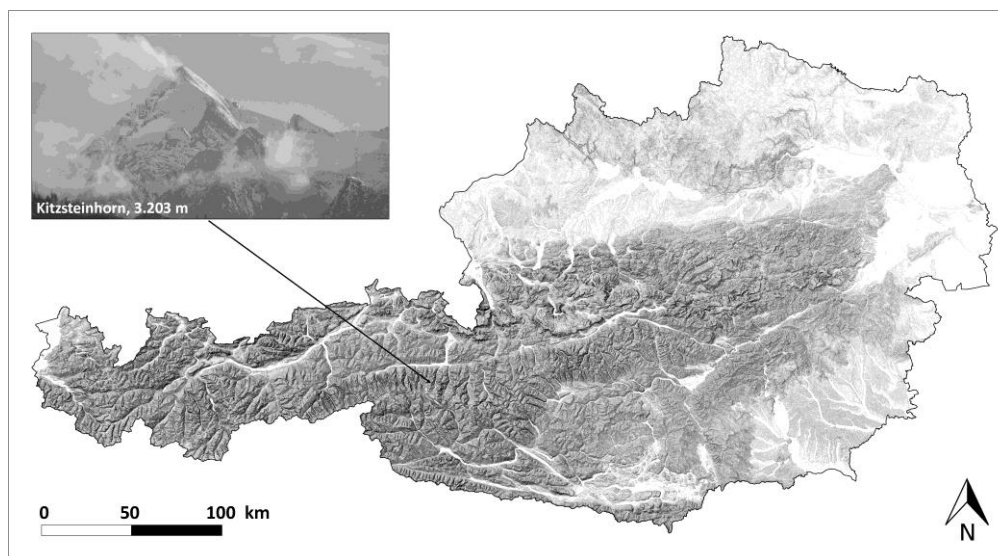
Figure 30: The study area of the MOREXPERT project is located at the Kitzsteinhorn (3,203 m), Hohe Tauern Range, Austria.

The Kitzsteinhorn is located just north of the main Alpine divide and has no directly adjacent summits. In combination with its pronounced pyramidal shape these topographical features make the Kitzsteinhorn ideal for the investigation of the influence of aspect and elevation on ground thermal conditions. The small-scale lateral variability of ground thermal conditions in alpine terrain has contributed to the selection of a comparatively small study area.

The Kitzsteinhorn primarily consists of calcareous-micaschists (Hoeck et al., 1994). Stress release and intense physical weathering processes, typical for periglacial environments, resulted in the formation of an abundance of joint sets with large apertures. Intense retreat of the Schmiedingerkees glacier in recent decades led to the exposure of oversteepened rock faces, which in turn are frequently affected by minor rockfall events (Hartmeyer et al., 2012a).

The tourism infrastructure existing within the study area (cable car, ski lifts, ski slopes etc.) provides easy access and convenient transportation of measuring equipment, an essential prerequisite for an extensive long-term monitoring program. The west ridge of the Kitzsteinhorn is tunneled by a gallery ('Hanna-Stollen'), which allows the acquisition of thermal information from depths of up to 80 m below the terrain surface (Figure 31).
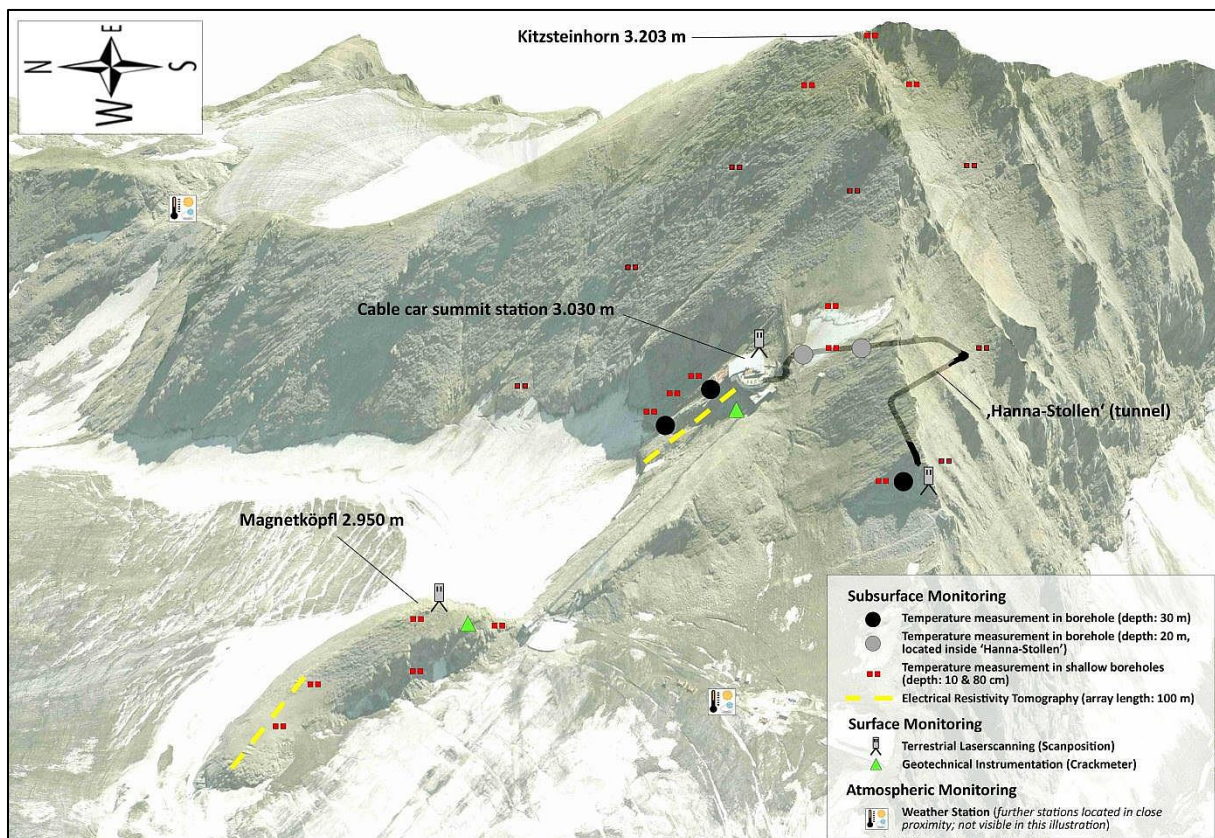
Figure 31: 3D-Overview of monitoring sites and investigation scales at the Kitzsteinhorn.

Six weather stations are located within the study area or in its direct vicinity (< 2 km away), permitting continuous observation of external forcing of ground thermal conditions. At the weather stations, which are located at altitudes between 2,400 m and 2,940 m, air temperature, humidity, wind speed, wind direction, snow height and precipitation are recorded.

Furthermore, an abundance of historical data on glaciology and climate allow the compilation of long time series to estimate the influence of changing climatic conditions over the last century (Tollner, 1951).

6.3.4   Preliminary investigations

The success of a monitoring campaign hinges greatly on the suitability of the selected measurement sites. The more pre-information can be attained, the better the monitoring system can be adapted to local conditions and the more efficiently long-term changes can be monitored. For this reason a large number of preliminary investigations had been carried out prior to the start of the actual monitoring.

Permafrost Modeling

To get a theoretical overview of the thermal state of the Kitzsteinhorn, permafrost distribution has been modeled using an advanced version of the 'Permakart' model (Version 3.0) (Keller, 1992; Schrott et al., 2012). 'Permakart 3.0' is an empirical-statistical model that calculates the probability of permafrost occurrence based on a topo-climatic key. The underlying topo-climatic key analyses the relation between altitude, slope and aspect while also taking into account foot-slope positions. Modeling results reveal that large areas of the Kitzsteinhorn summit pyramid are underlain by permafrost. Particularly the northwest face and to a lesser degree the northeast face display a very high probability of permafrost occurrence (> 75%). South-facing slopes do not seem to be affected by permafrost according to the modeling results (Figure 32).
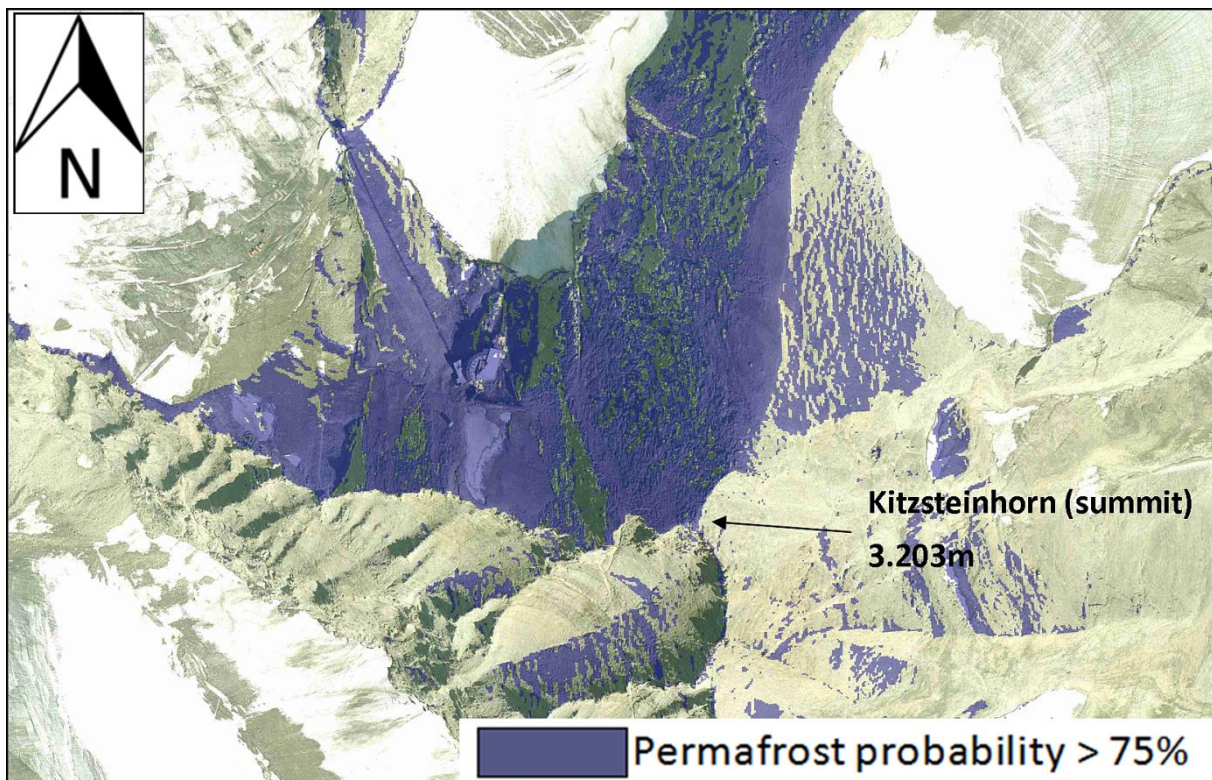
Figure 32: Modeled distribution of permafrost at the Kitzsteinhorn summit region based on a DTM with a resolution of 1 m.

Electrical Resistivity Tomography

In order to attain first geophysical evidences of permafrost occurrence at the Kitzsteinhorn, ERT measurements have been carried out inside the 'Hanna-Stollen'. The 'Hanna-Stollen' connects the north side of the mountain (cable car summit station) to the south side at an altitude of approximately 3,000 m. It constitutes a cross-section through the mountain and therefore represents an intriguing opportunity to investigate the influence of aspect on permafrost occurrence along a single ERT profile line (northern vs. southern exposure).

The vertical distance between the ceiling of the gallery and the terrain surface ranges from approximately 15 m at the north/south ends of the gallery to approximately 70 m in the middle section of the gallery (below the ridgeline). The ERT array was installed in the eastern side wall of the gallery yielding a horizontal (eastward) direction of investigation. Maximum depth of investigation was 21 m during measurements conducted in June 2010. Analysis of ERT data showed high resistivity values of up to 40,000 Ωm in the north section of the tomography. These values correlated well with temperatures below the freezing point, therefore indicating the existence of permafrost in this section (Figure 33).
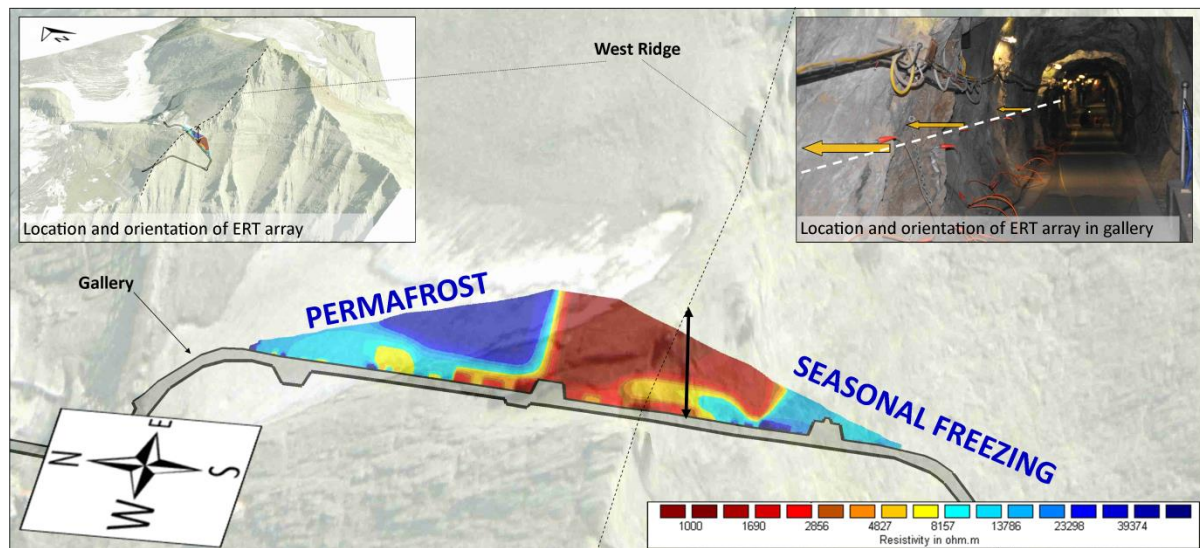
Figure 33: Location and orientation of ERT measurements conducted inside the 'Hanna-Stollen'.

The central and south part of the tomography shows unfrozen rock as electrical resistivity values in this area clearly correspond to temperatures above the freezing point. The presence of permafrost-affected rock north of the ridgeline corresponds very well with the permafrost boundary attained through modeling of the permafrost distribution with 'Permakart 3.0'. The south end of the gallery/tomography is influenced by its vicinity to the south wall. Electrical resistivity values in this area correlate to subzero temperatures, which might be attributed to seasonal freezing (remaining winter frost) and/or the effects of a prolonged cold spell prior to the measurements. Further ERT measurements and direct temperature monitoring are certainly necessary to verify these assumptions.

Geotechnical Survey
Joints and fractures constitute pathways for circulating melt water or air and therefore represent zones of potentially intensified heat propagation (Moore et al., 2011). Heat transfer properties of

calcareous-micaschist are furthermore influenced significantly by the direction of schistosity (Robertson, 1988). For an investigation that addresses the thermal state of a large rock mass (e.g. Kitzsteinhorn summit pyramid) it is therefore of crucial importance to gather detailed information on these geotechnical parameters. For this reason a mapping campaign has been carried out by GEOCONSULT ZT GmbH (persons in charge: Mag. Giorgio Höfer-Öllinger, Mag. Andreas Schober), which delivered valuable data on joint orientation/aperture and schistosity direction. Two major joint sets exist, dipping steeply to W and SW, respectively. Furthermore, two minor joint sets have been mapped, dipping slightly to SSE and steeply to NW. The joint sets can be grouped into two generations: an older generation which is filled with either quartz or calcite and a recent generation with joint apertures ranging from a few millimetres to up to 20 centimetres. The younger joint generation carries important heat transfer implications due to its large apertures. Schistosity dips moderately steep to NE. Direction of schistosity therefore was an important criterion for the selection of the sites for deep and shallow drilling. The borehole located at the west side of the mountain (Figure 34) was drilled parallel to the schistosity. Both boreholes located at the north-facing slope below the summit station were drilled perpendicular to the schistosity.

6.3.5   Scale-oriented monitoring of permafrost-affected rock faces

Due to methodical deficiencies and/or a lack of physical understanding we usually do not have the ability to capture a geomorphic system in its entirety. It is therefore necessary to define levels or scales of observation to separately investigate specific aspects of the system (e.g. sub-systems, sub-processes). Measurement techniques applied at one scale level are not necessarily suitable for studies at other scale levels; equally, conclusions drawn from an examination at one scale do not necessarily apply to other scales (Otto et al. 2008). Careful selection of specific scales of investigation and thorough consideration of possible transferability of information gained at each scale level is therefore of crucial importance.

An assessment of the responses of permafrost-affected rock faces to climatic change requires a comprehensive understanding of their current thermal state. For an accurate characterization of a high-mountain ground thermal regime it is necessary to identify both, (i) the lateral variability of thermal conditions, i.e. small-scale, short-term thermal changes that occur at or near the surface, and (ii) the vertical variability of thermal conditions, i.e. the variation of ground temperatures with depth. Geomorphic processes relevant to this problem vary significantly over space and time meaning that one spatio-temporal perspective (scale level) is not sufficient to investigate the problem. Hence, three different scales of investigation have been defined within the MOREXPERT project, which are introduced within this chapter.

The 'Borehole Scale'

In boreholes temperature data are recorded along a vertical line (thermistor chain). Thus, boreholes can be viewed as 1D-point sources that have no horizontal/lateral extent. Temperature measurements in (deep) boreholes therefore represent the smallest scale of investigation within the MOREXPERT project in terms of areal extent. Furthermore, the 'borehole scale' is the only scale level where direct temperature measurements are conducted within the actual permafrost body. For this reason it is the only scale that provides direct permafrost evidence.

The 'borehole scale' consists of a total number of five boreholes that have been drilled into permafrost-affected bedrock (Figure 34). Two of the five boreholes were drilled inside the 'Hanna-

Stollen'. Both 'gallery boreholes' (20 m in depth) were drilled to enable ground temperature measurement in depths that otherwise could not be reached from the surface (distance to terrain surface up to 80 m) and for the validation of geophysical measurements (electrical resistivity tomography, reflection seismology). As the gallery boreholes do not cover thermal conditions at or near the surface they play a minor role in this contribution. The main emphasis is put on the three boreholes located outside the gallery. Two of them were drilled below the cable car summit station on a north-facing rock slope at an altitude of 3,030 m and 3,000 m, respectively. The remaining borehole was drilled on a west-facing rock slope, at an altitude of 2,970 m. All three boreholes located outside the gallery were drilled perpendicular to the terrain surface and reach a depth of 30 m.

By all accounts a borehole depth of 30 m is sufficient to clearly surpass the depth of the zero annual amplitude (ZAA), i.e. the depth where the seasonal temperature amplitude is attenuated to 0 °C (Gruber et al., 2004c). Since the Kitzsteinhorn boreholes have not been completely instrumented yet, there is no temperature data available to confirm the actual depth of the ZAA. However, data from Alpine boreholes (e.g. Hoher Sonnblick, located 25 km SE of Kitzsteinhorn) and Scandinavian boreholes document that temperature signals below a depth of 15-20 m are free of any seasonal or shorter-term temperature variation (Gruber et al., 2004c; Harris et al., 2009; Klee and Riedl, 2011).

Below the ZAA heat transfer is dominated by conduction due to the frozen state of water. Thermal 'disturbance' through non-conductive heat transfer (e.g. heat advection by circulating ground water) is impeded causing the preservation of thermal signals for long time periods. Near-surface warm-side deviations from the linear temperature gradient below the ZAA deliver a valuable indication of recent warming trends at the surface (Harris et al., 2003). Temperature data from deep boreholes therefore provide important evidence of past surface temperatures and long-term climatic changes that frequently date further back than local recordings of climatic conditions (Kellerer-Pirklbauer et al., 2008). In addition, a downwardly directed analysis of permafrost temperatures may deliver valuable information as well. If the borehole reaches deep enough to identify the local geothermal lapse rate, it is possible to estimate the depth of the permafrost bottom via downward, linear integration of the gradient (Gruber et al., 2004c). As permafrost thickness typically reacts very slowly to climatic changes it provides important information on past climatic conditions on a century time scale.

Above the ZAA thermal conditions are subject to seasonal variations as involved processes operate on significantly shorter time scales than in great depths. Here, borehole temperatures serve to identify important variables such as active layer thickness or the mean temperature at the top of permafrost. The latter represents an important indicator for the sensitivity of a permafrost body, particularly if it displays values close to 0 °C. Active layer thickness is primarily controlled by summer temperatures and has a high environmental and geomorphological significance. A thickening of the active layer, induced for instance by extreme summer temperatures, is likely to increase the scale and frequency of mountain slope instabilities, as evidenced during the heat summers of 2003 and 2005 (Gruber et al., 2004a; Gruber and Haeberli, 2007; Noetzli and Vonder Muehll, 2010).

Within the active layer non-conductive heat transfer plays an increased role due to the periodical availability of liquid water (Gruber and Haeberli, 2007). Intensive freeze-thaw cycles and rapidly changing ground surface temperatures have a large significance for shallow weathering of bedrock and in further consequence for the triggering of small rockfall events (Matsuoka, 2008). Barring a

thick snow cover, which is rather uncharacteristic for steep rock faces, near-surface thermal dynamics are directly coupled to climatic forcing and therefore display very short lag times and large amplitudes (Williams and Smith, 1989; Isaksen et al., 2007).

In general, thermal gradients in boreholes are influenced by past and present ground surface temperatures, regional geothermal heat flux and variations of lithology with depth (Harris et al., 2003). Particularly the influence of lithology on the type and rate of heat transfer is often overlooked and therefore plays a prominent role within the present study. Thus, well cuttings have been collected during drilling to identify potential variations of thermal bedrock properties with depth. In addition, borehole imaging has been conducted with an optical scanner by TERRASCAN GmbH to localize and assess geotechnical discontinuities (joints, fractures). During optical scanning a probe was lowered into the borehole which delivered continuous, detailed, and scaled images of the borehole walls. Recorded parameters include dip, dip direction, joint frequency and aperture. Complementary analysis of borehole temperatures and data on discontinuities has the potential to deliver valuable information on the relevance of non-conductive heat transfer and therefore is of major importance for the understanding of subsurface heat fluxes (Ravanel et al., 2011). All boreholes were drilled by 90 mm diameter air flush rotary drilling (Figure 34).

Figure 34: Air flush rotary drilling at the Kitzsteinhorn west face in September 2010 (borehole depth 30 m) (Photograph by Ingo Hartmeyer).

For temperature measurement Pt100 thermistors with an accuracy of ±0.1°C are used. The depths of the temperature sensors were selected in accordance with the PACE borehole strategy (Harris et al., 2001). Thus, attenuation of thermal variability with depth is taken into account by a down-hole increase of the sensor spacing. Temperatures will be recorded in two-hour intervals to resolve short-term variations at and near the surface (Table 5).

Table 5: Details of the locations, orientations and dimensions of the boreholes.

	Borehole Depth	Borehole Diameter	Depth of Temperature Sensors	Aspect of Slope	Gradient of Slope	Altitude (mouth of bore)
Borehole 1 *located next to cable car summit station*	30 m	90 mm	0.1, 0.4, 1, 2, 3, 5, 7, 10, 15, 20, 25, 30 m	North	45° (borehole drilled perpendicular to terrain surface)	3.030 m
Borehole 2 *located 50 m north of cable car summit station*	30 m	90 mm	0.1, 0.4, 1, 2, 3, 5, 7, 10, 15, 20, 25, 30 m	North	45° (borehole drilled perpendicular to terrain surface)	2.990 m
Borehole 3 *located 50 m north of west gallery exit*	30 m	90 mm	0.1, 0.4, 1, 2, 3, 5, 7, 10, 15, 20, 25, 30 m	West	45° (borehole drilled perpendicular to terrain surface)	2.970 m
Borehole 4 *located inside gallery, approx. 40m south of cable car summit station*	20 m	90 mm	0.1, 0.4, 2, 4, 6, 8, 10, 12, 14, 16, 18, 20 m	Borehole located inside gallery, drilled perpendicular to eastern side wall of gallery		3.020 m
Borehole 5 *located inside gallery, approx. 80m south of cable car summit station*	20 m	90 mm	0.1, 0.4, 2, 4, 6, 8, 10, 12, 14, 16, 18, 20 m	Borehole located inside gallery, drilled perpendicular to eastern side wall of gallery		3.015 m

Currently, the boreholes are instrumented with a purpose-built system for borehole temperature measurement which has been developed by GEODATA ZT GmbH. The measurement system consists of a polyethylene casing that prevents water entry into the borehole. The casing is segmented by non-corrosive brass rings that are connected to the temperature sensors. The insertion of brass rings enables improved thermal coupling between the temperature sensors and the ambient rock. The annulus (space between casing and bedrock) is filled with concrete to allow good thermal connection to the surrounding rock (Figure 35).
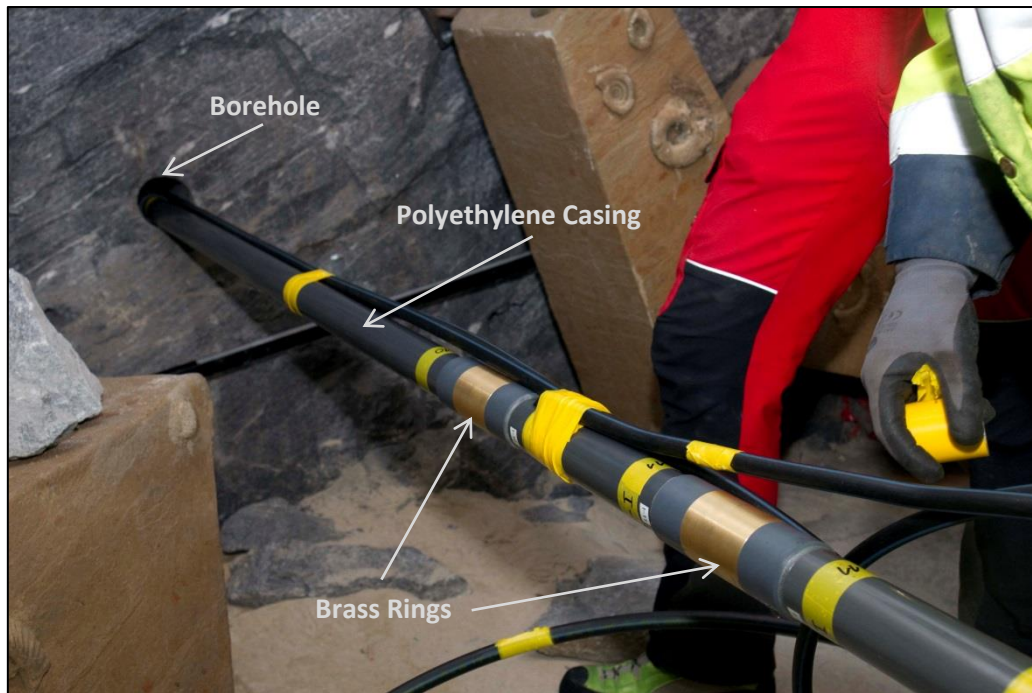
Figure 35: Borehole instrumentation inside the 'Hanna-Stollen' with a purpose-built temperature measurement system developed by GEODATA ZT GmbH (December 2011). The black tube serves to fill up the annulus with concrete after the insertion (Photograph by Robert Delleske).

In conclusion, the 'borehole scale' can be characterized as an investigation level with a very long 'thermal memory'. Due to the large investigated vertical spectrum it is possible to study both, (i) thermal fluctuations in near-surface areas that result from short-term variations of atmospheric conditions and (ii) deep-seated ground thermal 'signals' that reflect past climatic conditions and long-term climatic variations. Since boreholes deliver point information only, it is – at this scale level – not possible to factor in the high lateral heterogeneity of thermal conditions typical for complex, high-alpine terrain. To account for the spatial heterogeneity other investigation scales have to be taken into consideration.

The 'Slope Scale'

At the 'slope scale' subsurface electrical resistivity is monitored by the application of (2D) ERT (Electrical Resistivity Tomography). During ERT measurements an electric current is injected into the ground using two electrodes. The resultant voltage difference is then recorded at two potential electrodes. Repeated measurements with changing electrode location and spacing provide a dataset of the apparent subsurface resistance. The underlying resistivity distribution can then be calculated through inverse modeling (Hauck and Kneisel, 2008; Krautblatter et al., 2010).

ERT is well-suited to distinguish between frozen and unfrozen subsurface regions as a marked increase of electrical resistivity occurs at the freezing point of water-containing materials such as moist rock or soils (Mellor, 1973; Sass, 2004; Krautblatter and Hauck, 2007). For this reason ERT is one of the most commonly applied geophysical methods for permafrost-related investigations (Hauck and Kneisel, 2008). Within the MOREXPERT project ERT data will primarily be utilized to identify the intra- and interannually varying thickness of the active layer as well as near-surface freeze-thaw cycles.

For monitoring purposes, ERT measurements are repeated at certain time intervals using the same survey geometry (time-lapse ERT). Thus, temporal and spatial permafrost variability can be assessed (Hilbich et al., 2008; Krautblatter et al., 2010). Rock faces are particularly well-suited for the quantitative interpretation of ERT data as bedrock has a relatively homogenous constitution and an accurately defined pore volume. Joints and fractures however represent distortions that potentially alter the subsurface electrical field considerably (Krautblatter et al., 2010).

Two permanent ERT profiles have been installed on north-facing rock slopes. The first array is situated directly below the cable car summit station at an altitude between 2,950-3,030 m (Figure 36). Stainless steel screws and rock bolts were drilled into the rock to ensure firm electrode-rock contact. The profile is 100 m in length and has an electrode spacing of 2 m. The second profile is located on the north ridge of the Magnetköpfl at an altitude between 2,860-2,900 m. It is 80 m long, electrode spacing is 1 m. The Magnetköpfl profile is operated by the 'Geological Survey of Austria' (person in charge: Mag. Robert Supper).
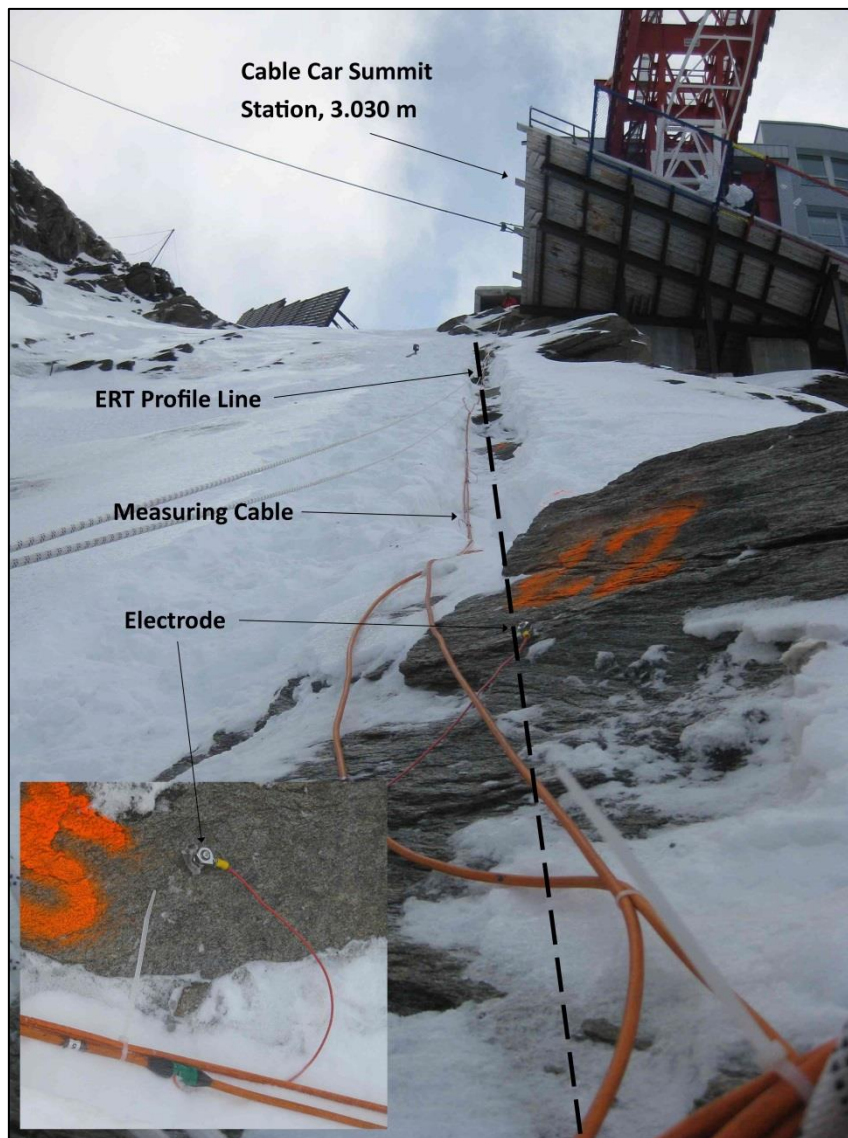
Figure 36: Permanently installed ERT array below the cable car summit station (3,030 m) (Photograph by Markus Keuschnig, view towards south.

Measurements are performed applying Wenner and Schlumberger configurations. To account for the transitory nature of near-surface thermal changes, ERT data is acquired in time intervals of two to three hours. Data acquisition runs fully automatic and is controlled via remote access. In addition to permanent ERT monitoring, sporadic ERT measurements are conducted in the 'Hanna-Stollen' and at the Magnetköpfl west face. These measurements are repeated with longer time intervals creating seasonal or annual time-sections of the monitored rock face.

Since ground temperatures are the principle parameter in any permafrost monitoring campaign, boreholes as only means of direct measurement play a crucial role. However, due to high costs and considerable technical efforts, drilling in remote high mountain areas is unfeasible within the scope of many studies. Even in the European Alps, the best-studied mountain range worldwide, only a very limited number of deep boreholes (> 10 m) exist (Noetzli and Vonder Muehll, 2010; Mair et al., 2011). Furthermore, borehole temperatures may not always be representative for the surrounding area (e.g. due to topographic effects). Thus, geophysical approaches for the characterization of ground thermal conditions represent an essential complement to borehole measurements.

While ERT field measurements do not provide direct information on ground temperatures, it is possible, under laboratory conditions, to measure electrical resistivity as a function of temperature (Mellor, 1973; Krautblatter et al., 2010). Laboratory calibration of numerous rock samples has been carried out at the cryo-laboratory at the University of Bonn (person in charge: Dr. Michael Krautblatter). During laboratory calibration different rock samples from the study area were subjected to multiple controlled freeze-thaw cycles. During freezing and thawing electrical resistivity was recorded in short intervals, which eventually produced a bilinear temperature-resistivity relationship for the investigated rock samples.

Two 30 m deep boreholes are located on the ERT array below the cable car summit station. This overlap allows parallel analysis of electrical resistivity values and borehole temperature data. Dual temperature calibration of ERT data using laboratory data and in-situ borehole temperatures significantly adds to the validity and significance of ERT results. Conversely, analysis of ERT data serves to assess the spatial representativeness of the boreholes by revealing the spatial heterogeneity of thermal conditions within the tomography.

As a rule of thumb the depth of investigation in ERT is restricted to about one sixth of the array length. Depth of investigation at the 'slope scale' is therefore reduced by half (approx. 15 m) compared to the borehole scale (30 m). Hence, the 'thermal memory' of the investigated vertical section is reduced significantly. However, as information on ground thermal conditions is collected along a two-dimensional profile line, a 'lateral dimension' is added at the 'slope scale'. In contrast to the 'borehole scale' information is not derived from a 1D-point-source (i.e. borehole). At the 'slope scale' it is therefore possible to take into account the lateral variability of ground thermal conditions typical for alpine terrain.

The 'Mountain Scale'

At the 'mountain scale' GST (10 cm depth) and NST (near-surface temperatures) (80 cm depth) are measured at a large number of sites covering different elevations, slope aspects and slope inclinations. In terms of areal extent the 'mountain scale' therefore represents the largest scale of investigation.

Despite not being a direct measure of permafrost occurrence, GST and NST are important parameters for the understanding of the ground thermal regime as they provide valuable information on the thermal evolution of both active layer and permafrost (Noetzli and Vonder Muehll, 2010). In steep rock faces GST is strongly coupled to atmospheric temperatures and solar radiation effects. This strong coupling can be attributed to the general absence of buffering mechanisms (i.e. sediment cover, thick snow cover) in steep bedrock (Williams and Smith, 1989; Kellerer-Pirklbauer et al., 2008). GST therefore varies markedly over short distances and short observation periods, which in turn has a significant influence on permafrost distribution (Luetschg et al., 2008; Gubler et al., 2011).

Due to the high spatial and temporal variability of GST and NST, measurement at a single site is of low significance. Thus, a large number of temperature measurements are required to adequately resolve the heterogeneity of GST and NST. For this reason a new methodological strategy for near-surface rock temperature measurement has been developed, following approaches by Gruber et al. (2003) and Kellerer-Pirklbauer et al. (2008). The newly developed strategy involves the distribution of several dozens of miniature loggers over the entire summit pyramid of the Kitzsteinhorn. Temperature measurement is carried out in depths of 10 cm (GST) and 80 cm (NST). For practical purposes each borehole is equipped with just one miniature logger. Every measurement site therefore consists of two shallow boreholes with respective depths of 10 cm and 80 cm. The large number of deployed loggers contributes to the reduction of uncertainty when measured GST and NST are extrapolated to areas not covered by measurements. Thus, an accurate estimation of near-surface ground thermal conditions for the entire summit of the Kitzsteinhorn is facilitated. In addition, spatially distributed measurements of GST in the vicinity of the drill sites help to evaluate the spatial representativeness of the deep boreholes (Noetzli and Vonder Muehll, 2010).

Until now 28 shallow boreholes with a maximum depth of 80 cm have been drilled (Figure 37).

Figure 37: Drilling of a shallow borehole for iButton temperature measurement at the Kitzsteinhorn south face (Photograph by Ingo Hartmeyer).

The drilling of approximately 50 further shallow boreholes is currently in progress. To enable a small drilling diameter (18 mm) and therefore minimize the extent of the drilling works, iButtons are used for temperature measurement. The iButton is a coin-sized, commercially available miniature temperature logger that integrates a battery, a computer chip, a real-time clock and a temperature sensor in stainless steel can. To the authors' knowledge the present study represents the first time that iButtons are applied for temperature measurement in bedrock.

iButtons are well-suited for monitoring purposes as a total of 8192 8-bit readings or 4096 16-bit readings can be stored in a protected memory section. The integrated digital thermometer measures temperature with a resolution of 0.0625°C. The operating temperature range reaches from -40 °C to 85 °C, with an accuracy of ±0.5 °C from -10 °C to 65 °C. To validate the measurement accuracy of the deployed iButtons, parallel temperature measurements with iButtons and UTL3-loggers (accuracy ±0.1 °C) were conducted in the study area for several months. These measurements clearly demonstrated that the accuracy of the iButtons is significantly higher than specified by the manufacturer. All temperature data acquired with iButtons stayed well within the accuracy range of the UTL3 (±0.1 °C) (Keuschnig et al., 2012).

Each iButton was attached to the lower end of a polyethylene rod (17 mm diameter) with a cold-resistant adhesive. After insertion only the upper end of the rod sticks out of the borehole allowing convenient removal and reinsertion during memory readout. In accordance with iButton measurements of GST carried out in Switzerland, the recording interval was set to three hours, enabling an operation period of 512 days (Gubler et al., 2011). Water entry represents a prominent reason for iButton measurement errors (Lewkowicz, 2008). To avoid water entry as well as advection of water and air in the borehole, the mouth of bore was sealed with weather-proof silicone. Programming and readout of all iButtons is performed using the 'Thermo23' software by Maxim Integrated Products, Inc. In comparison to the 'borehole scale' and the 'slope scale' vertical investigation depth is further reduced and amounts to less than one metre (80 cm) at the 'mountain scale'. 'Thermal memory' of the investigated vertical section therefore is at a minimum at the 'mountain scale' allowing only the identification of short-term thermal variations (e.g. diurnal and seasonal cycles). Ground thermal responses to conditions that date back further in time are not preserved near the surface and thus cannot be resolved at the 'mountain scale'.

6.3.6 Synthesis

Ground thermal conditions in high-alpine rock faces vary considerably over short distances and short observation periods. Reactions to environmental changes tend to be similarly variable in space and time, implying fast, sensitive responses at some locations and slow, lagged responses at other locations (Haeberli et al., 2010). This problem has been tackled with a monitoring approach that explicitly investigates the spatial and temporal heterogeneity of ground thermal conditions on three complementary scale levels.

At the 'borehole scale' ground thermal conditions are investigated along a vertical line (borehole thermistor chain). Due to the large depth of investigation (30 m) vertical attenuation and phase-shifting of ground temperatures can be examined at this scale level. As a consequence past climatic conditions which are preserved as deep-seated ground thermal signals can be studied. The 'borehole scale' is therefore provided with a long 'thermal memory' ('thermal inheritance'). Since boreholes have no horizontal extent, lateral variability of ground thermal conditions cannot be resolved.

The 'mountain scale' is set up diametrically opposite to the 'borehole scale'. Here, spatially distributed monitoring of GST and NST in bedrock facilitate the investigation of the small-scale lateral heterogeneity of ground thermal conditions. At the 'mountain scale' Investigation depth is reduced to a minimum as attention shifts from a vertical analysis towards an investigation of lateral variability.

In terms of its spatial and temporal extent the 'slope scale' can be viewed as a transitional scale between the 'borehole scale' and the 'mountain scale'. Compared to the 'borehole scale' depth of investigation is reduced considerably (to 15 m) while a 'lateral dimension' is added as information on thermal conditions is collected along a two-dimensional profile line (ERT array).

Within the MOREXPERT project all three methodical approaches (deep boreholes, shallow boreholes, ERT) have been implemented in complementary fashion (Figure 38).
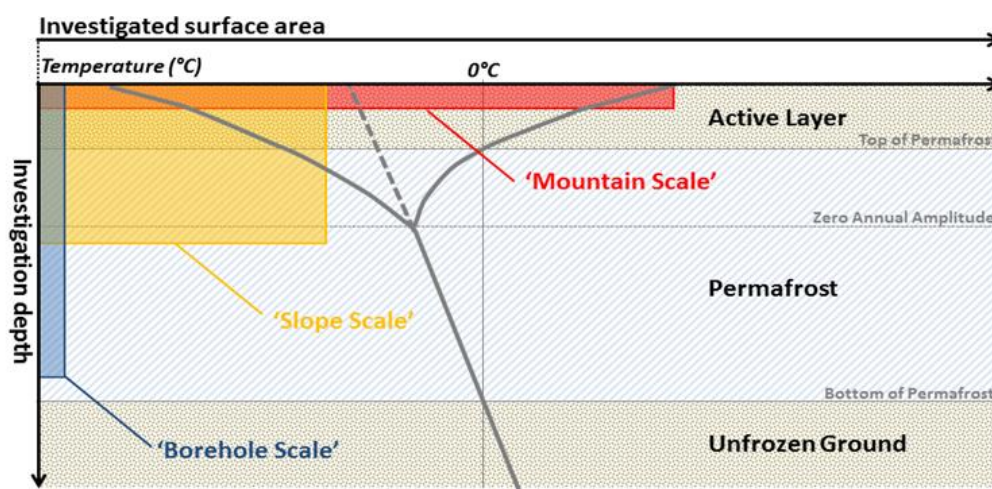
Figure 38: At the Kitzsteinhorn the ground thermal regime is investigated at three different investigation scales (conceptual illustration).

Temperatures measured in deep boreholes can be used to calibrate ERT data. Conversely, ERT data deliver information on the lateral heterogeneity of ground thermal conditions and therefore serve to assess the representativeness of measured borehole temperatures. The combination of information from the 'borehole scale' and the 'mountain scale' plays an equally important role as thermal gradients from deep boreholes can be used to estimate temperatures in large depths for areas that are covered only by near-surface temperature sensors.

Thus, the chosen monitoring approach facilitates complementary analysis of data obtained at different scale levels and therefore allows (constrained) validation and extrapolation of information. Ultimately, the chosen approach is intended to yield a quasi-spatial model of the thermal state of the surface and subsurface at the Kitzsteinhorn. Due to its generic design it is considered to be transferable to comparable high-mountain study sites.

7 Providing stability-relevant hydrostatic and thermal information for early warning systems

7.1 Electrical resistivity tomography monitoring

7.1.1 Abstract

Subsurface monitoring of permafrost conditions at depths up to 20-30 m is crucial to assess the safety and reliability of mountain infrastructure, because permafrost degradation critically affects rock slope stability in high mountains. Electrical resistivity tomography (ERT) provides a straightforward tool for monitoring near-surface bedrock permafrost at monthly or longer intervals. But as rockfalls are often prepared over periods of hours or days, ERT for early warning purposes should also detect short-term triggering events such as pressurised water flow.

Here, we present the first approach to monitor steep permafrost rock walls quasi-continuously with ERT. We measured ERT every 4h at the up to 67° steep rock wall below the Kitzsteinhorn cable car, Austria. Wenner datasets (n=996) were analysed from February 2013 to February 2014 in terms of data stability, raw data characteristics and measurement errors coinciding with potential disturbing factors. Strong resistivity changes coincided with rapid freezing or water inundating rock fractures. Automatically detected periods with large resistivity changes produce ERT time series with low resistivities extending from the bottom upwards during times of snowmelt. We infer that flow of pressurised water in fractures warms the surrounding rock in an upward direction, based on fracture inventories, visual observations of cleftwater and near-surface temperature measurements. We develop a strategy for ERT monitoring suitable for potential early warning systems, where high apparent resistivity changes in 4h intervals may precede critical hydrostatic events confined by permafrost rocks.

7.1.2 Introduction

The thermal state of steep permafrost-affected rock faces is a key control on slope stability (Gruber and Haeberli, 2007; Hasler et al., 2012; Huggel et al., 2012), because thermal changes in frozen rock significantly alter the mechanical properties of rock and ice along potential failure planes (Mellor, 1973; Davies et al., 2001; Krautblatter et al., 2013). Thus, developing methods to provide information on thermal and hydrostatic subsurface properties is essential, especially as boreholes provide one-dimensional (1D) thermal data in a complex 3D terrain and usually cannot be installed in actively unstable rock masses.

Electrical resistivity tomography (ERT) can differentiate frozen from unfrozen rock in the subsurface, and therefore has become widely used in periglacial and permafrost research (Hauck and Kneisel, 2008; Schrott and Sass, 2008; Otto et al., 2012). Electrical resistivity of frozen rock is highly temperature-dependent and reacts sensitively to the gradual freezing of water in pores and fissures in bedrock between 0 and ca. -8 °C (Mellor, 1973; Krautblatter et al., 2010).

For monitoring purposes, ERT measurements are repeated at certain time intervals using the same survey geometry and identical electrodes in order to assess temporal and spatial variations of ground temperature (Kneisel et al., 2014). ERT monitoring of permafrost in steep rock faces was first conducted in 2005 (Krautblatter and Hauck, 2007). Most ERT permafrost monitoring studies have been carried out either on unconsolidated material (e.g. talus, soil) or on gently inclined rock slopes with debris cover (Supper et al., 2014). But ERT monitoring during repeated field campaigns also provides a powerful tool for detecting monthly changes of permafrost in solid rock walls (Krautblatter et al., 2010). However, continuous monitoring by Automated ERT (AERT) in steep unstable bedrock has not been achieved yet as it imposes stringent demands for near-vertical electrode and cable setups, accessibility and infrastructure, and regular maintenance and safety.

AERT monitoring is one of the most promising methods to assess permafrost-affected rock faces. As soon as resistance measurements are transformed into spatial tomographies, by means of inversion, the outcome critically depends on the amount and distribution of measurement errors. Changing measurement errors can significantly influence ERT results and inhibit comparability of subsequent measurements as inversion of subsequent time steps would be strongly biased (LaBrecque et al., 1996; Krautblatter et al., 2010; Rosset et al., 2013). Trends could then also derive from a change of measurement errors (Koestel et al., 2008). To apply AERT as a potential early warning signal, it is essential to understand the conditions under which signal distortions occur, as these might needlessly activate a warning. Thus, consistent control of the ERT raw data is essential to generate meaningful and comparable ERT results.

The destabilisation of permafrost-affected rock masses depends on their geologic, tectonic, geomorphologic, hydrostatic and thermal histories (Krautblatter and Moore, 2014). Such destabilisation can be attributed to decreased shear strength caused by changes in (i) rock-mechanical properties such as the abrupt decrease in compressive and tensile strength as well as fracture toughness (Mellor, 1973; Dwivedi et al., 2000; Draebing et al., 2014); (ii) ice-mechanical properties of rock subject to creep and fracture due to changing ice temperature, changing water content within the ice between -2 and 0 °C or melting (Sanderson, 1987; Budd and Jacka, 1989; Davies et al., 2001); and (iii) the mechanical performance of the rock-ice interface (Krautblatter et al., 2013). The shear stress applied to detachment planes can be increased by elevated hydrostatic and cryostatic pressures (Murton et al., 2006; Matsuoka and Murton, 2008; Fischer et al., 2013). Changes in hydro- and cryostatic forcing play a key role as the shear stresses exerted by them can increase by a magnitude or more in hours and simultaneously pressurised fluid flow in fractures will act to decrease normal stress (i.e. friction) and the stability of ice infillings. Hereafter, we define pressurised water as a piezometric head of > 10 m or a pressure > 105 Pa. As a result, the conditions prevailing at potential failure planes may change rapidly (within a few hours). AERT could increase the time available to anticipate deformation or potential failures of rock slopes, which is essential for effective warning (Magnin et al., 2015; Sättele et al., 2015).

Here, we investigate the feasibility of permanently installing an automated ERT system for the first time in a steep alpine rock wall to continuously monitor the state of frozen bedrock and stability-relevant changes. We address the following questions: (1) What measurement design enables self-sustained, continuous monitoring of unstable permafrost-affected rock walls? (2) What are the main factors that influence measurement errors, and what time intervals and measurement settings are required to accurately monitor processes that control rock wall stability? (3) How can pressurised fluid flow in fractures (a major destabilising factor in permafrost rock walls) be monitored using ERT?

7.1.3 Study site

The study site is located in the summit region of the Kitzsteinhorn, Hohe Tauern Range, Austria (Figure 39 a, b). The Kitzsteinhorn summit pyramid (K in Figure 39 a, b; 3,203 m above sea level (a.s.l.); 47°11'17'' N, 12°41'15'' E), consists of rocks of the Penninic Bündner Schist Formation in the Tauern Window. This formation belongs to the Glockner Facies of the Glockner Nappe and comprises calcareous mica schist, prasinite, amphibolite, phyllite and serpentinite (Hoeck et al., 1994; Schober et al., 2012).
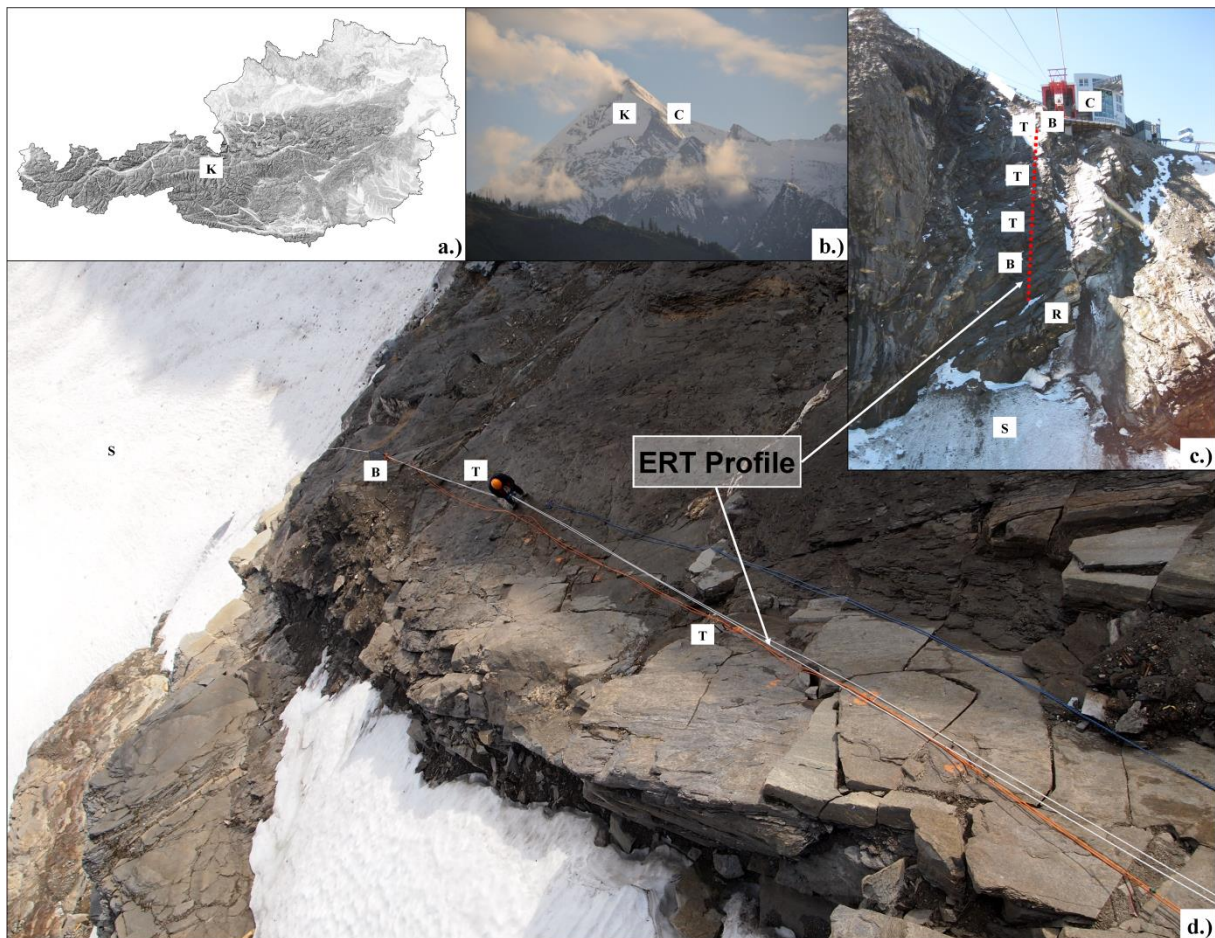
Figure 39: Location of ERT profile at the Kitzsteinhorn (K in a, b), Hohe Tauern Range, Austria. Letters show the position of the Schmiedingerkees Glacier (S in c, d), the cable car station (C in b, d), the 30 m boreholes (B in c, d), and the 10 and 80 cm near-surface temperature measurements (T in c, d, see Figure 3 for details) as well as a recent rockfall detachment of a 500 m³ rock bar (R in c).

The rock face contains a permafrost body whose core temperature is approximately -2 °C, as evidenced by five boreholes up to 30 m deep (B in Figure 39 c, d) and by the thermal regime of dozens of near-surface temperature measurements close to the ERT array (T in *Figure 39* c, d) (Hartmeyer et al., 2012). A lightning strike destroyed the temperature sensors in the deep borehole (B in Figure 39 d) close to the ERT array in autumn 2012, and so data from this borehole are unavailable for this study. Over the last decades the rock face below the cable car has been affected by a rapid glacier retreat at the base (S in Figure 39 c, d) and the complete loss of its ice cover on the rock surface recorded by orthophotographs. Several rockfall detachments with single blocks of up to 100 m³ were observed in the past few years. One major event (1000 m³) occurred directly below the ERT survey, and subsurface conditions during its detachment were recorded by ERT measurements (R in Figure 39 c, Schober et al. (2012); Keuschnig et al. (2015)).

The AERT array is installed at an altitude between 2,965 and 3,017 m a.s.l. on a north-facing, slightly convex back wall of a glacial cirque. The rock face has an average gradient of 47° (maximum 67°; Figure 39 d) and extends from the summit station of the local cable car (C in Figure 39 b, c, 3,029 m a.s.l.) down to the upper margin of the Schmiedingerkees Glacier (2,950 m a.s.l., S in Figure 39 b, d).

The study site is part of a comprehensive long-term monitoring program for permafrost and rockfall interaction, established within the research project MOREXPERT ("Developing a Monitoring Expert System for Hazardous Rock Walls") administered by "alpS – Centre for Climate Change Adaptation". Surface and subsurface conditions in the Kitzsteinhorn summit region are monitored by geotechnical, thermal, geophysical and laboratory methods (Keuschnig et al., 2011; Hartmeyer et al., 2012b) to identify the short- and medium-term responses of slope stability in steep permafrost-affected bedrock to climatic change.

7.1.4   Measurement setup, data acquisition and data processing strategy

Measurement setup

We installed an automated AERT GeoTom-MK1E100 multielectrode resistivity system (GEOLOG2000), designed to operate in high-mountain conditions. This system is robust and weather resistant, protected by a hard-case and includes all required components such as transmitter, receiver, µ-controller, AD-converter, power supply and charging unit. The resolution of the AD-converter can theoretically resolve potentials of 10 nV, while simultaneously applying up to 500 V at the current electrodes peak to peak. The GeoTom operates at frequencies from 1.04 to 25 Hz and can effectively filter railway current effects (16 2/3 Hz) and net-power influence (50/60 Hz), which is important close to infrastructure. In addition, capacitive or inductive coupling between the transmitter and receiver can be avoided. The output current ranges from 1 µA to 200 mA and the overall system accuracy is 0.5%. The measurements are performed with two multicore cables with 25 takeouts spaced 2 m apart.

The AERT profile consists of 37 electrodes and follows the rock face topography, with an overall length of 72 m. A rock slide event (Figure 40 c) prevented the installation of the lower 13 of the planned 50 electrodes. The AERT profile is a compromise between permafrost-relevant investigation depths of more than 10 m and the required resolution for active-layer measurements with a median depth of investigation of ca. 1 m.

Stainless steel climbing bolts 90 mm long and 10 mm in diameter, rather than fixed stainless screws of the same size (Krautblatter and Hauck, 2007) were drilled into the bedrock to enhance mechanical resistance and consistent electric coupling. Measurement cables were attached to anchors and aligned to minimise damage from rockfall and snow pressure (Figure 40 b). The control system was deployed inside the summit station with network access, power connection and overvoltage protection (Figure 40 a). Data acquisition was fully automatic and remotely controlled. Near-surface temperature measurements from shallow boreholes (up to 0.8 m deep) were performed along the AERT profile and supplemented by climate data from three automated weather stations located 300 to 800 m horizontally and 50 to 400 m vertically from the AERT profile.
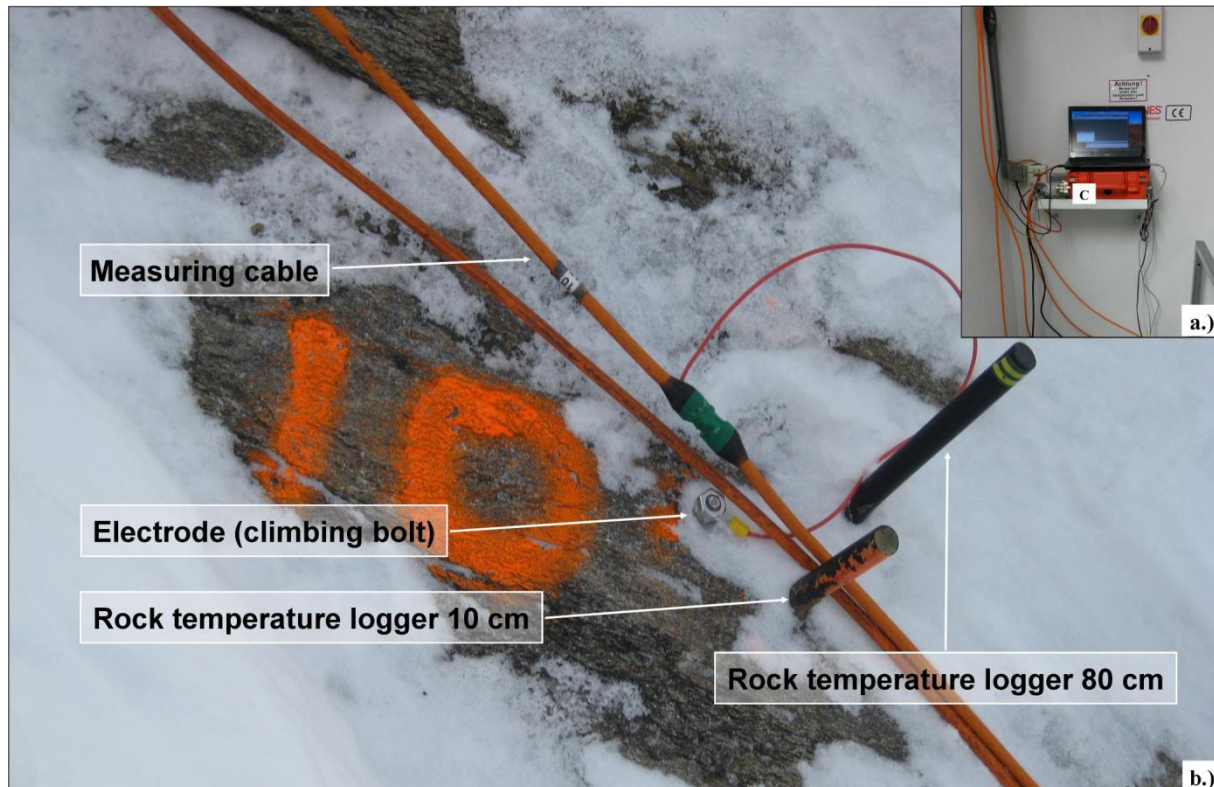
Figure 40: Permanent ERT installation with climbing bolts and rock temperature loggers (a, b). Control system with network access, power connection and overvoltage protection (b).

Datasets were recorded at 4-hr intervals and comprised six Wenner, Schlumberger and coupling test measurements per day, enabling checks of systematic measurement error. Prior test measurements were conducted at frequencies from 1 to 12.5 Hz in 2012. As measurements with 4.16 Hz provided the best compromise between quality and measurement time (i.e. also exposure time to lightning-related overvoltage), we used 4.16 Hz with a stack of 3.

Data acquisition

Following the prototype period (2012), continuous measurements commenced in February 2013. Software problems caused unsystematic short data gaps, and two lightning strikes led to serious hardware damages and data losses totalling 4.5 months (March − April and June −October 2013, Figure 41).
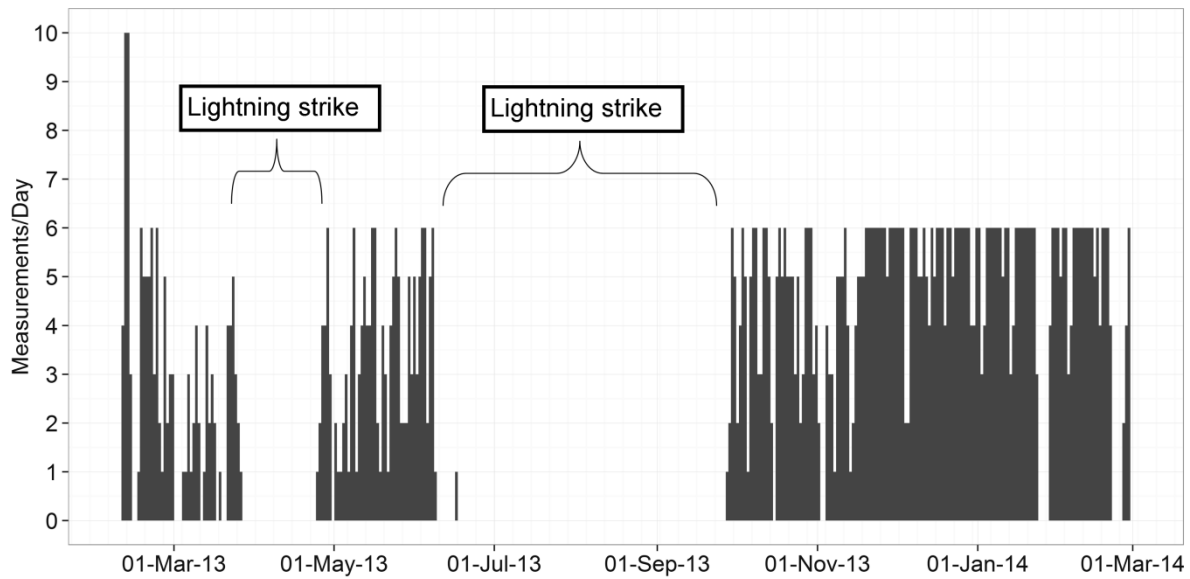
Figure 41: ERT measurements performed per day (Wenner). Software problems and lightning strikes indicate unsystematic periods of data loss.

Nevertheless, an extensive time series of more than 2,500 single datasets were recorded (Table 6). In this paper, we discuss only Wenner datasets, as this measurement configuration yields the highest signal-to-noise ratios for mountain permafrost environments (Hauck and Vonder Muhll, 2003; Krautblatter and Hauck, 2007).

Table 6: Overview of total measured datasets and apparent resistivities per measurement type (11 February 2013-28 February 2014).

Measurement type	Datasets (total)	Datapoints per dataset	Apparent resistivities (total)
Wenner	996	210	209160
Schlumberger	887	136	120632
Coupling	929	37	34373 (Resistance)

Data processing strategy

The data processing strategy was divided into two main parts. First, data pre-processing was based on unprocessed raw data, including (i) an initial data analysis; (ii) a physically-based plausibility check of the measured data range; and (iii) the detection, filtering and analysis of measurement errors and their influencing factors. Second, data post-processing included (i) analysis of the measurement interval and (ii) data inversion.

Data pre-processing

We initially analysed the data to clarify their general structure and to summarise the main statistical characteristics (e.g. measurement intervals) for further analysis (Adèr et al., 2008). The initial data analysis included (i) an Anderson Darling normality test with the R package "Nortest" (Gross and Ligges, 2012) to detect departures from a normal distribution (Stephens, 1974), (ii) plotting data in box plots and (iii) detection of outliers using 1.5 times the interquartile range (IQR) (Tukey, 1977). To test the validity of the measured data range we used a physically-based plausibility check (Supper et al., 2014). The apparent resistivities ρ_{app} obtained for the Wenner array (Equation 2, 3) are

$$\rho_{app}[Ohmm] = 2 * \pi * a[m] * R[Ohm] \qquad (2)$$

$$R = \frac{U[V]}{I_{inj}[mA]} \qquad (3)$$

where a is the electrode separation, R is the resistance, U is the potential difference and I_{inj} is the injected current (Koefoed, 1979).

Thus, the measured potential difference

$$U[V] = \frac{I_{inj}[A] * \rho_{app}[Ohmm]}{2 * \pi * a[m]} \qquad (4)$$

were used for a theoretical evaluation of the measured values (Supper et al., 2014).

The detection and filtering of measurement errors was based on the capability of the GeoTom data acquisition software (Schnaubelt, 2011). Three error types were marked in the raw data files: (1) The "SDρA error type" represents the standard deviation of the stacked measurements. If the SDρA in a stack of 3 exceeds 5%, the measurement was possibly influenced by random noise, based on the experience on bedrock ERT in this study. (2) The "current error" occurred when the injected current could not be kept constant over a measurement cycle defined by the measurement frequency of 4.16 Hz, beyond which the instrument switched between normal and reverse current injection. (3) The "voltage error type" occurred when the measured voltage was lower than a predefined threshold of 200 μV.

To check the viability of using ERT as a potential early warning signal, all signal distortion must be identified which would activate a warning. We compared the relative error distribution with possible influences such as rock and air temperatures, wind gusts or precipitation. Applying the described error detection, we calculated the relative error for each dataset and categorised the error type. The relative error represents the percentage of erroneous data points for each raw dataset. To analyse the robustness of the relationship between possible influencing factors and measurement errors, we used a simple random sample method as an unbiased surveying technique (Starnes et al., 2010). A linear model was applied to each subset to analyse the significance of the correlation. All of the analysis and filtering steps were performed with the software package R.

Data post-processing

The upper few metres of rock has the shortest response time to fluid water caused by precipitation or snowmelt and are well suited to test whether 4h time intervals are sufficient to monitor rapid changes. This area is covered by the first measured layer of the Wenner array and includes the largest number of apparent resistivity datum points of all measurement levels (n=34).

Before data inversion, we automatically detected datasets with large temporal changes > 20% of apparent resistivity within 4 hours to focus on rapid (process) changes. The > 20% threshold was user-defined and provided a first estimation for significant changes. All inversions were performed using the software package RES2DINV. The inversion routine was configured using the commonly applied ERT parameterisation for permafrost rock walls after Krautblatter and Hauck (2007) and Rosset et al. (2013), including robust inversion and mesh refinement.

7.1.5 Results

Data characteristics

The analysed Wenner time series consists of 996 single datasets with a total of 209,160 apparent resistivity datum points. The median value of 432 kΩm differs significantly from the mean value of 1,073 kΩm and indicates a deviation from the normal distribution. The mean value is higher than the median for all individual datasets, which indicates a positively skewed distribution. In most datasets, the mean value is slightly below the 75% percentile, and in some cases above it (Figure 42).
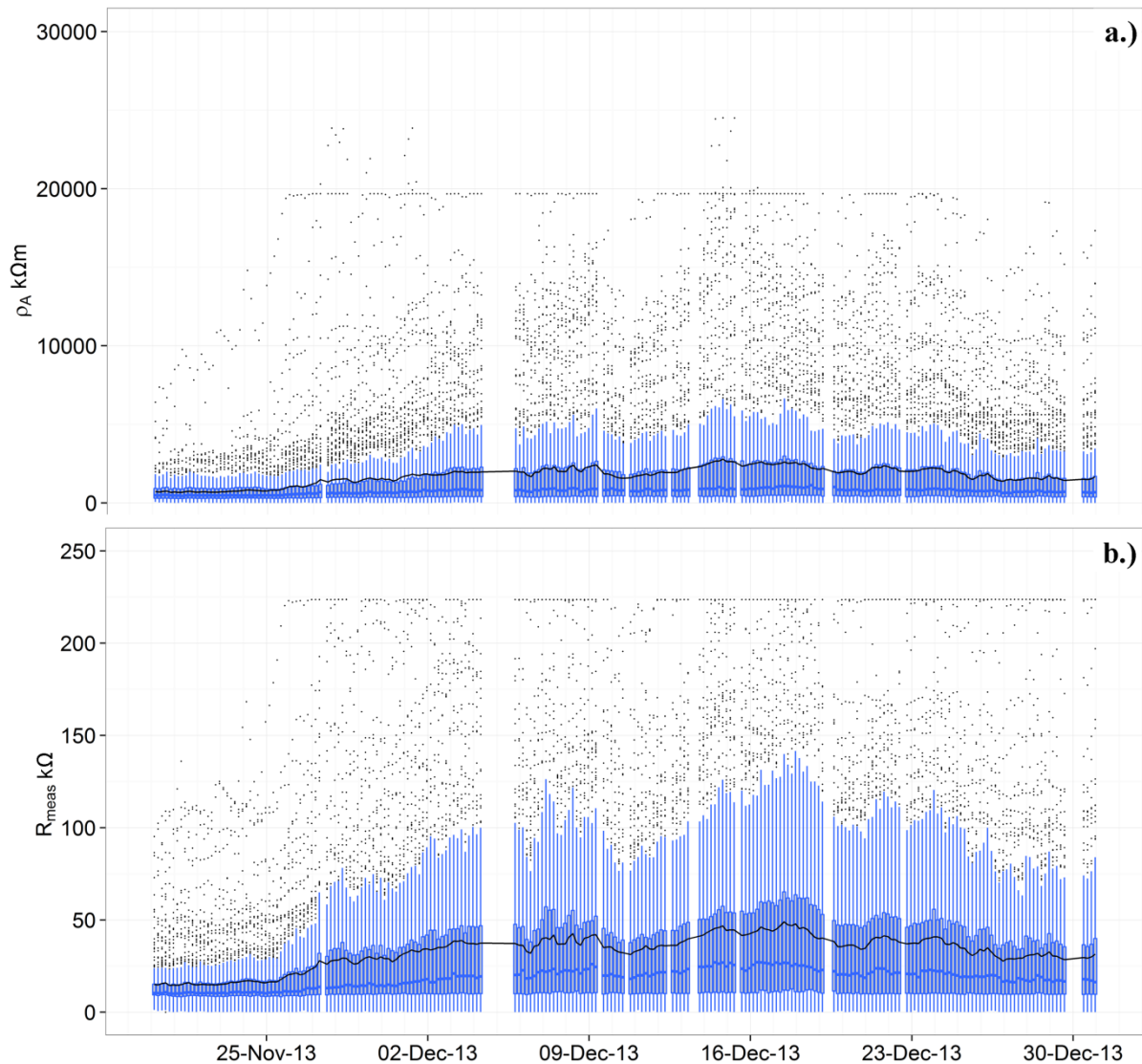
Figure 42: Time series and statistical distribution of apparent resistivities (a) and measured resistance (b) in terms of the median (blue line), the scatter (25% and 75% percentiles, blue box), the range of extreme values (1.5 times the interquartile range added to the 25% percentile and to the 75% percentile, blue whiskers), the outliers (black dots) and the mean values (black line), (20 November 2013-31 December 2013).

The Anderson Darling normality test results in a calculated p-value of $4.75e^{-12}$ for the entire time series, indicating a significant deviation from the normal distribution. As a consequence, the robust median instead of the mean value has to be taken into account for further analysis of the measurement interval and for change detection.

Data validity, detection and filtering of measurement errors
The initial data analysis indicates possible outliers with apparent resistivities up to 28 MΩm (Figure 42). Testing the validity of the data range, we inserted the maximum measured apparent resistivity of ρ_{app} = 28 MΩm, the injected current of I_{inj} = 1 µA and the electrode spacing of a = 20 m into the formula for the measured potential difference (Equation 4). The calculated value of U is 0.22 V, with a resistance of 0.22 MΩ.

A new error type was identified (Figure 43 a). The error type occurred when the hardware tried to inject a current of less than 0.1 μA with simultaneous voltages above 200 mV. In total 7,828 measurement errors were identified and, thus, 3.7% of the entire time series had to be filtered (Figure 43 b).
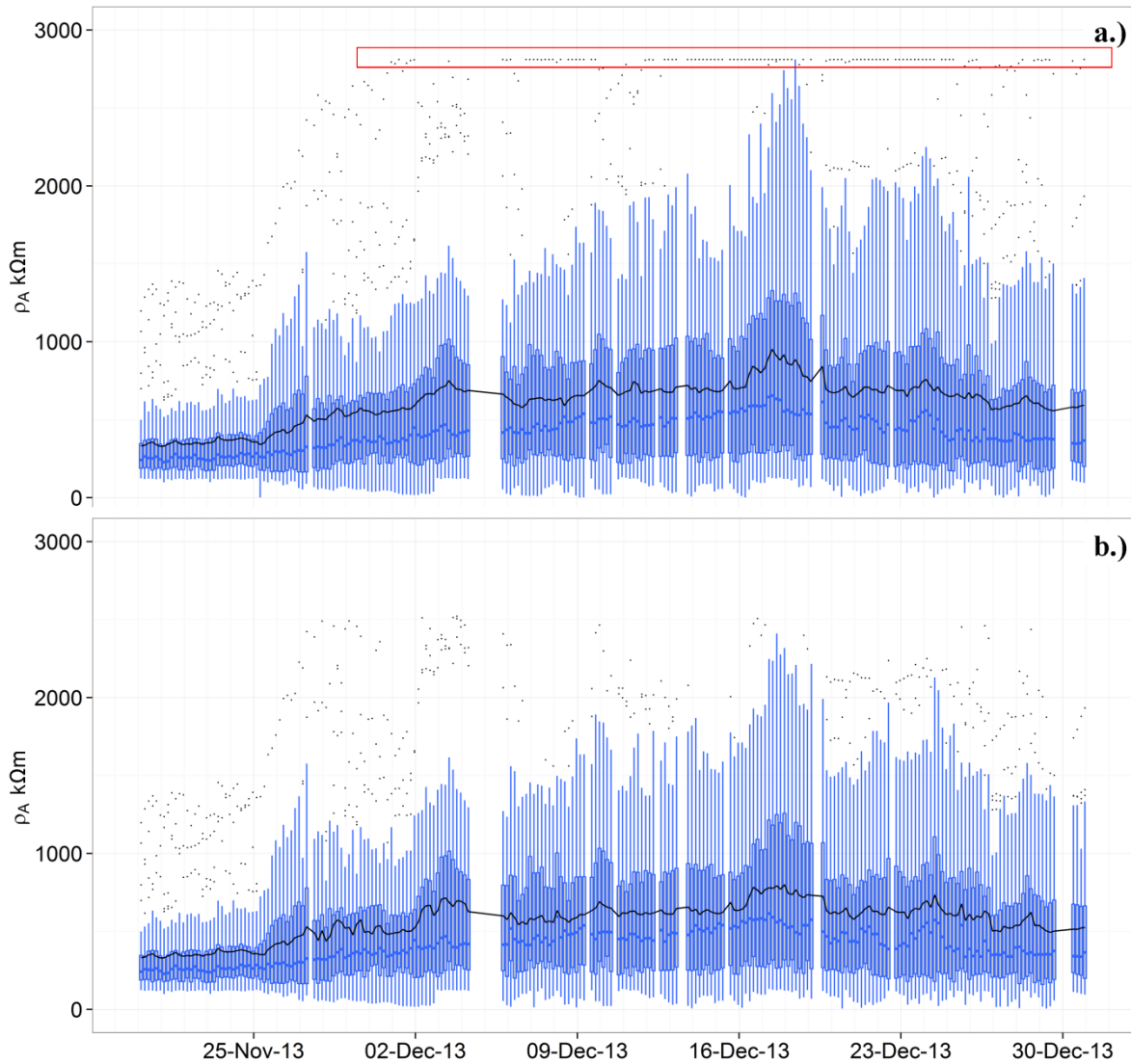
Figure 43: An example of the statistical distribution before (a) and after filtering of the measurement errors (b). The box in (a) marks the new hardware limit error type. (20 November 2013-31 December 2013).

Influencing factors on measurement errors

The relative error distribution shows limited periods of high values (Figure 44 b) and affects up to 40% (90 of 210 datapoints).
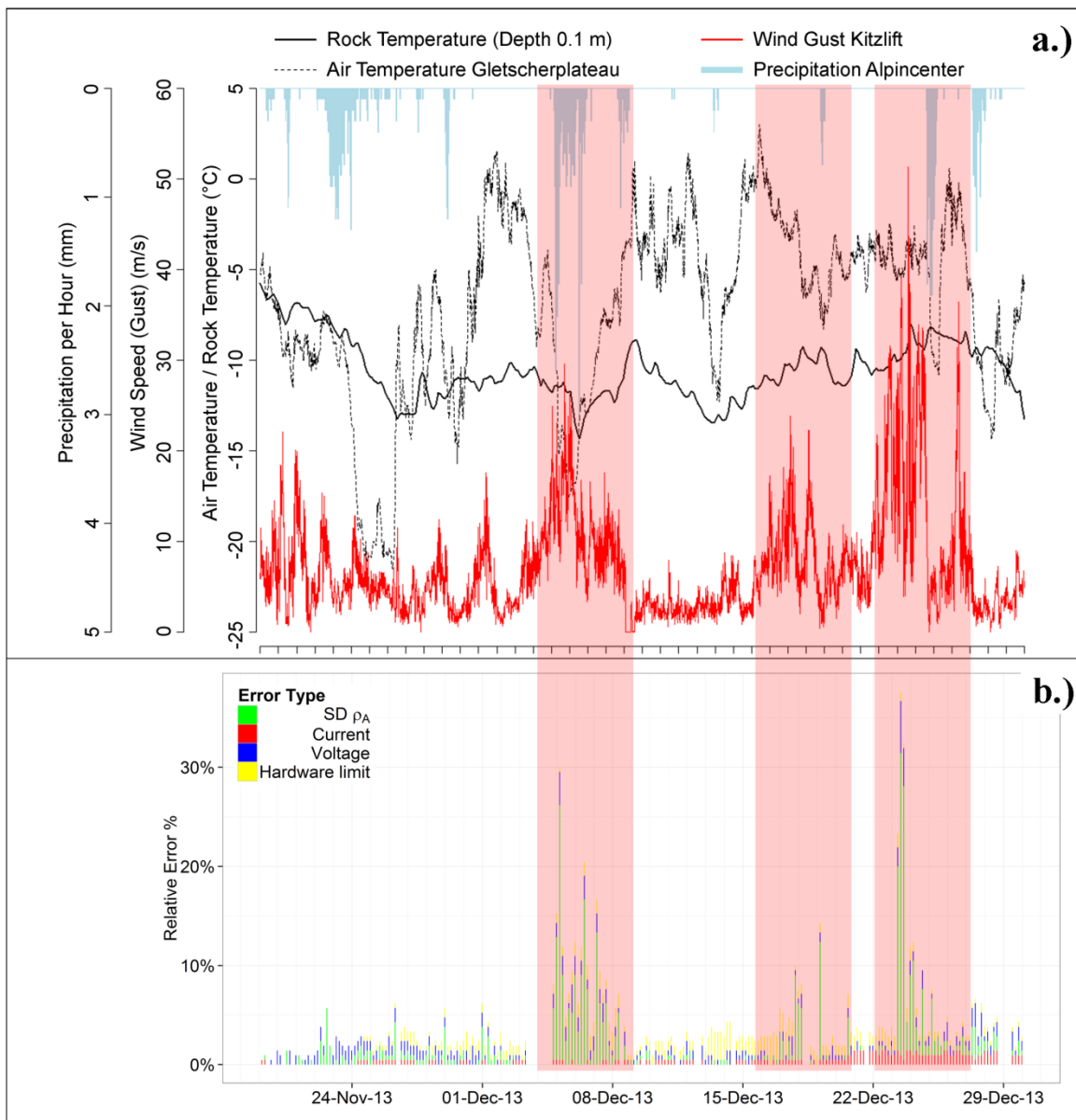
Figure 44: Relative measurement errors for each Wenner dataset classified by potential influencing factors (a) and error type (b). The three red boxes highlight periods of interest.

The measurement error distribution has limited periods of measurement error maxima with a coincident absolute and relative significant increase of the SDρA error type (Figure 44 b). A comparison with potential influencing factors (Figure 44 a, b) suggests a correlation between periods of high relative errors and wind gusts. Wind gusts represent the maximum wind speeds and are recorded for a sample period of two seconds in a measurement interval of 10 minutes. To analyse the robustness of the relationship between wind gusts and measurement errors, nine randomised subsets of 100 Wenner (population = 996) datasets were drawn (Figure 45 a-i). All of the randomised subsets confirm the significant correlation (p-value < 0.001) between the absolute datapoint errors and the wind gusts.
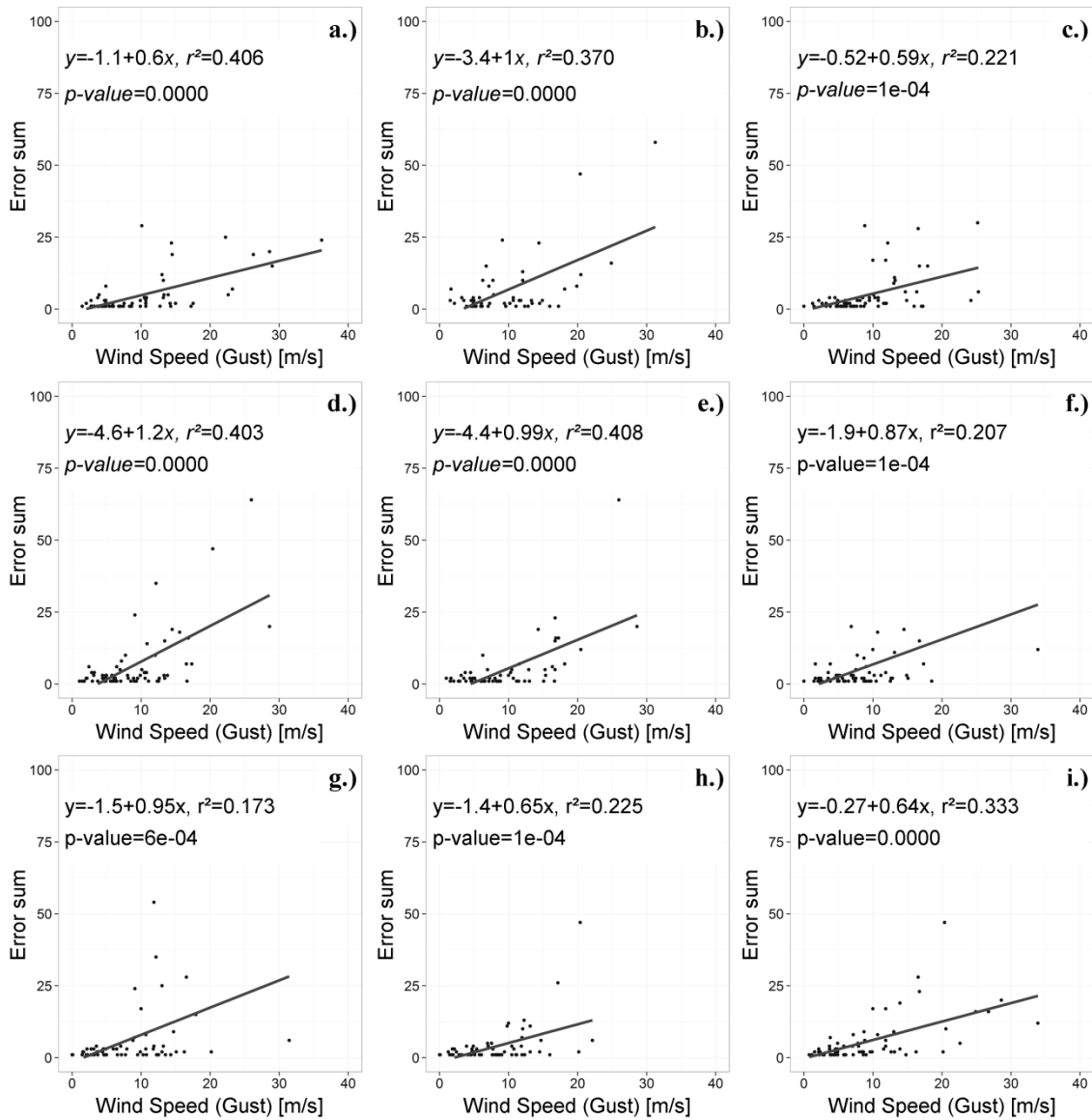
Figure 45: Correlations between the absolute datapoint errors and wind gusts using different randomised subsets (a-i).

Measurement interval

778 out of 996 Wenner measurements were recorded in a constant interval of four hours, without any data gaps, and only these were considered to avoid comparisons of different time intervals. Relative changes in apparent resistivity calculated based on the difference between the median values of the first layer (section data characteristics) range from 0.5 to 272.5% within four hours. 18.4% of the population have more than 10% and only 4.9% of the population have relative changes more than 20%. Krautblatter et al. (2010) have demonstrated a relative measurement error based on reciprocal measurements of 8% for large resistances above 5 KΩ. The resistances in the present study reach 250 KΩ (*Figure 42* b) and the error estimation E_{est} of 8% (Krautblatter et al., 2010) was used to calculate the relative uncertainty U_{rel} of 11.3% (Equation 5).

$$U_{rel} = \sqrt{2 * E_{est}^2} \qquad (5)$$

84.8% of the calculated relative changes between two datasets were within the uncertainty range (Figure 46).
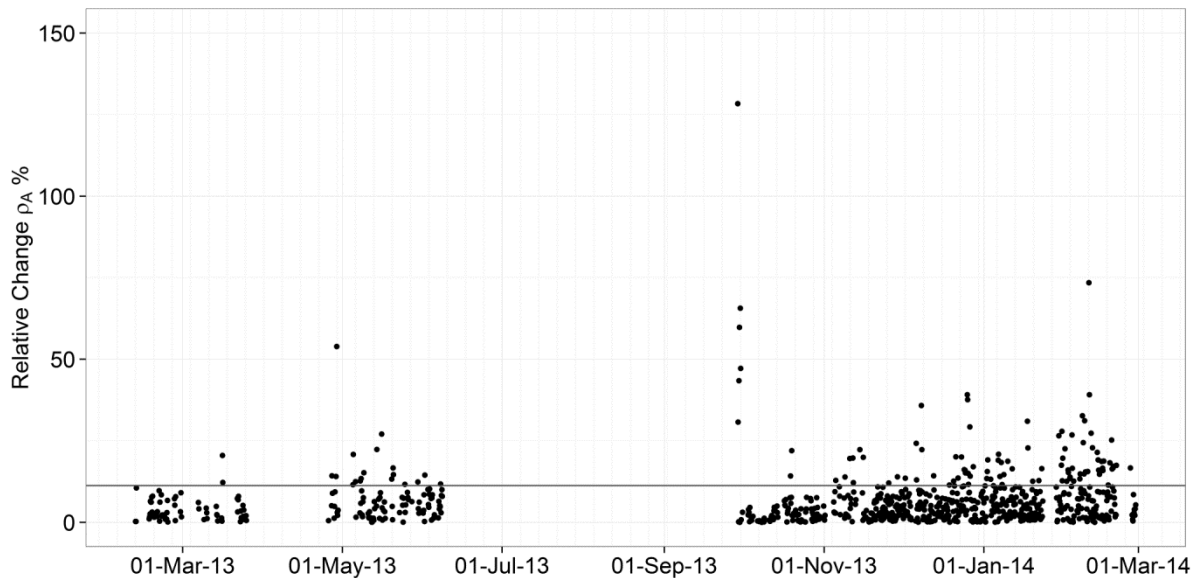
Figure 46: Relative changes of the median apparent resistivity of the first layer, measured in an interval of four hours. The black line indicates the 11.3% uncertainty level. High relative changes are mainly caused by water inundation during heavy precipitation.

ERT Monitoring results

Figure 47 is based on combined data from ERT tomographies, high resolution (10 cm) topography, geotechnical investigations and optical borehole scans (discontinuity mapping) as well as near-surface temperature data. Preferred paths of water in- and outflow were visually observed by the authors and the employees of the summit station at various times. Borehole photographs taken by an inspection camera (during an installation procedure) show a water table inside the borehole at a depth of around 5 m.
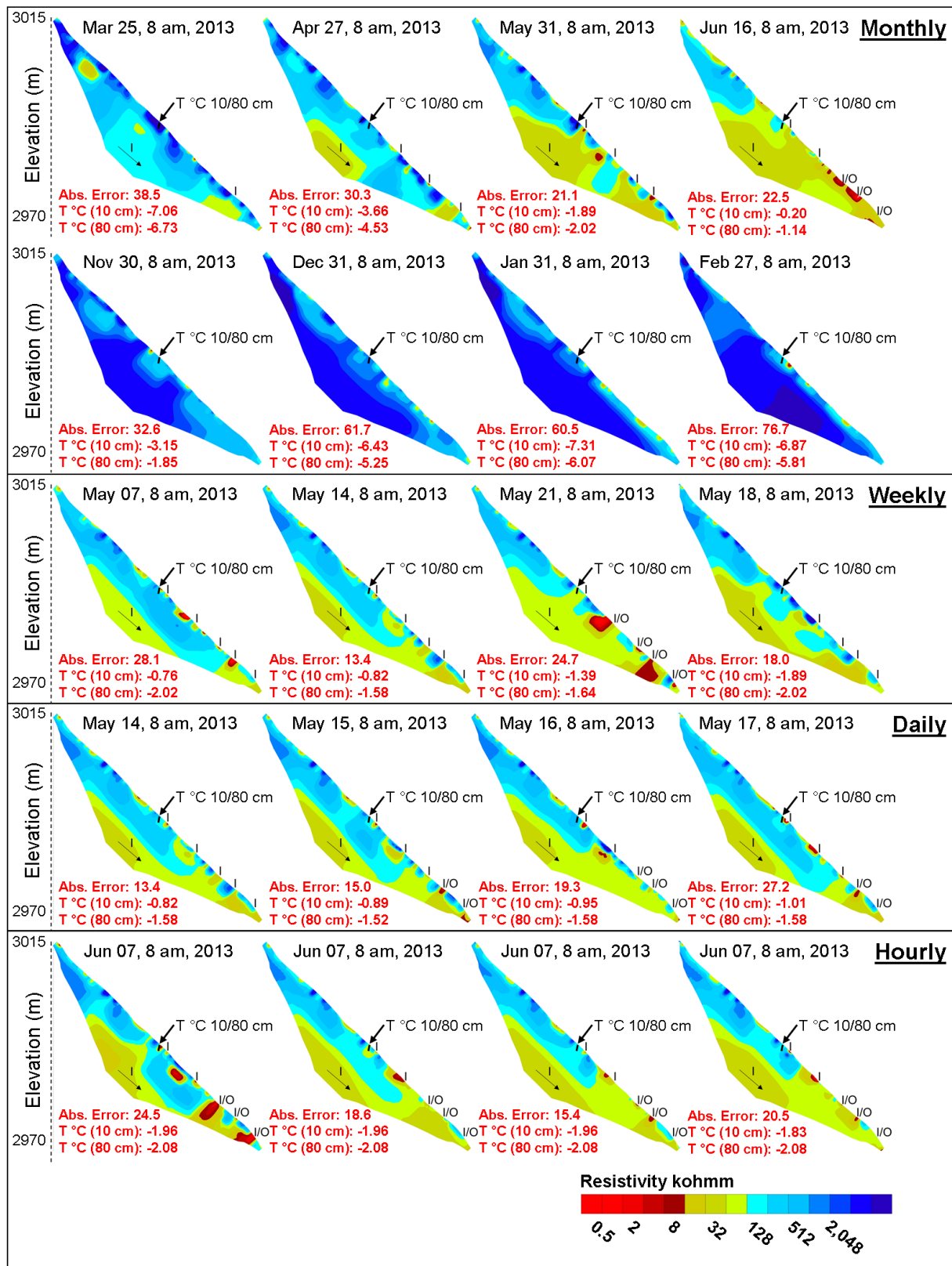
Figure 47: Selected tomographies representing monthly, weekly, daily and hourly evolution of the subsurface resistivity. "I" marks location of frequent water inflow and "I/O" water in- and outflow paths. The monthly, daily and hourly measurements show the thawing period in spring (Mar-Jun) and the monthly measurements the freezing period in winter (Nov-Feb).

The tomographies shown in Figure 47 examplify the monthly, weekly, daily and hourly evolution of the subsurface resistivity. During the freezing period the resistivities are high (≥ 128 kΩm), whereas the thawing period is characterised by a bottom-up trend in decreasing resistivities over time. The resistivity changes substantially during the thawing period in spring. Resistivities decrease to values below 32 kΩm, first at depths of 15-5 m from the rock face, before this low resistivity zone extends upwards. Subsequently, resistivities as low as 1 kΩm are directly observed around open fractures.

7.1.6   Discussion

Technical improvements, experiences and limitations
This study presents the first automated, permanently installed ERT in an unstable alpine rock wall. Compared to weekly and monthly measurements (Krautblatter and Hauck, 2007; Krautblatter et al., 2010), the system can monitor the subsurface continuously and reveal rapidly changing conditions at potential failure planes. Despite the relatively low costs of installing the system, the maintenance efforts are high, especially for unstable rock walls (Keuschnig et al., 2015). To improve system performance and avoid unstable measurements, the system was adapted to resist harsh environmental conditions. Climbing bolts used as electrodes have a high mechanical capacity and achieve constant coupling. Damage caused by overvoltage during thunderstorms is the main limiting factor for the monitoring system. The overvoltage can be transmitted by the measurement cables, the grounding, notebook connections or the power supply system of the used infrastructure. This makes overvoltage protection essential to minimize damages and costs.

Measurement errors, influencing factors and measurement interval

Measurement errors
Controlling and filtering routines are essential to guarantee consistent AERT data. Inversion routines critically depend on the quality of the pre-processed raw data. Changing measurement errors can significantly influence tomography results and inhibit comparability. The conditions at the study site (e.g. steep permafrost rockwall without debris cover) and the field setup (e.g. climbing bolts as electrodes) differ from those in similar ERT studies (Hilbich et al., 2011; Rosset et al., 2013; Supper et al., 2014). Consequently, the initial statistical analysis based on unprocessed raw data is an important step to clarify the general structure of the data and to summarise their main characteristics. Because of rapid subsurface changes, the data ranges of single datasets are highly variable and have different deviations from normal distribution for the observed time series (Figure 42). Also, the use of mean values to describe time-dependent changes has to be checked carefully.

The validity of the data range and the maximum measurable values depend strongly on the technical specifications of the applied hardware. The measured potential difference of the highest measured apparent resistivity (ρ_{app} = 28 MΩm) is in the voltage range of the hardware of 500 V and is clearly above the voltage resolution of 10 nV. The hardware has an input impedance of 20 MΩ, and according to common hardware recommendations for resistance measurements the measureable resistance should not exceed 1/10 of the input impedance, i.e. 2 MΩ. Figure 42 (b) demonstrates that all values of R_{meas} are below 250 kΩ and are, therefore, theoretically valid and have not been filtered.

All datasets were systematically checked for measurement errors. A new error type (Figure 43 a), which occurs if the hardware tries to inject current of less than 0.1 μA with simultaneous voltages

above 200 mV, has been reported to the ERT manufacturer and will be considered in future software updates. Measurement errors in steep fractured and exposed permafrost rock faces affect 3.7% of all measured datapoints, which is understandingly higher than the reported error rate of 1.62% in debris-covered rock slopes (Hilbich et al., 2011). The error rate is still appropriate for the intended purpose, with respect to the signal changes of ~30% resistivity change per °C temperature in frozen rock (Krautblatter et al., 2010).

Influencing factors on measurement errors
We have carefully analysed the factors that may influence measurement errors. Surprisingly, the analysis only suggests a correlation of measurement errors with wind gusts (Figure 44 a, b). The time-limited, absolute and relative increase of the SDρA error type (Figure 44 b) indicates an increase of external noise, possibly caused by fluctuating electromagnetic fields induced by natural (e.g. water circulation) or artificial sources (e.g. summit station). We infer that turbulence associated with high wind speeds persists for some hours during which high noise levels occur. Linear models based on randomised subsets show a significant correlation between measurement errors and wind gusts, especially at wind speeds over 10m/s (Figure 45 a-i). Strong wind gusts result from heavy atmospheric turbulence, which can induce direct or indirect vibrations (e.g. via infrastructure) into the ground. Wind gusts caused by convective atmospheric changes (e.g. thunderstorms) can also indicate high electric field strengths and potentially induce electrokinetic effects (Telford et al., 1990). During these periods measured electrical field strengths at the nearby Sonnblick Observatory can reach up to several thousand V/m instead of approximately 100-200 V/m under normal conditions (pers. communication, Niedermoser B., 21.03.2015). Both vibration- and atmospheric-induced currents influence the subsurface electrical field and so may affect ERT measurements.

Measurement interval
Krautblatter et al. (2010) have demonstrated a relative measurement error based on reciprocal measurements of 8% for large resistances above 5 kΩ. Based on this first assumption, we calculated a relative uncertainty U_{rel} of 11.3%. The user-defined threshold of > 20% for change detection significantly exceeds the uncertainty range and enables reliable results and interpretation. 84.8% of changes are within the uncertainty and therefore cannot be reliably interpreted by this automatic procedure alone. But trends in small apparent resistivity changes may result from slow processes such as temperature changes over a longer time period (> 4 hours). We assume that relative changes of more than 20% can result from increased water availability caused by snowmelt or rainfall. Similar behaviour has been observed before for water infiltrating permafrost at the Zugspitze (Krautblatter et al., 2010).

Monitoring of fluid flow in fractures
We interpret Figure 47 to show that during the thawing period meltwater infiltrates mainly along the slope, parallel to open cleavage fractures which are also apparent in the borehole scan (Figure 48).The infiltrating water significantly lowers the resistivity, from the base of the wetted layer upwards. The electrical resistivity is controlled mainly by temperature and water saturation of the measured material. The near-surface temperature measurements at 10 and 80 cm depth show no significant changes during periods with large variations in apparent resistivity (Figure 47, hourly, daily). Further, temperatures at depth respond very slowly to external changes and cannot explain major resistivity changes. Thus, major hourly changes in resistivity (Figure 47) are probably controlled by pressurised fluid flow in fractures. This results in an increasing (from the bottom upwards) saturation as well as slow warming of the rock mass around fractures. As a consequence hydrostatic

pressures increase until cleftwater pours out through open fractures. Similar forcing has been observed before the triggering of a recent rock slide detachment below the ERT transect (Figure 48, Keuschnig et al. 2015).
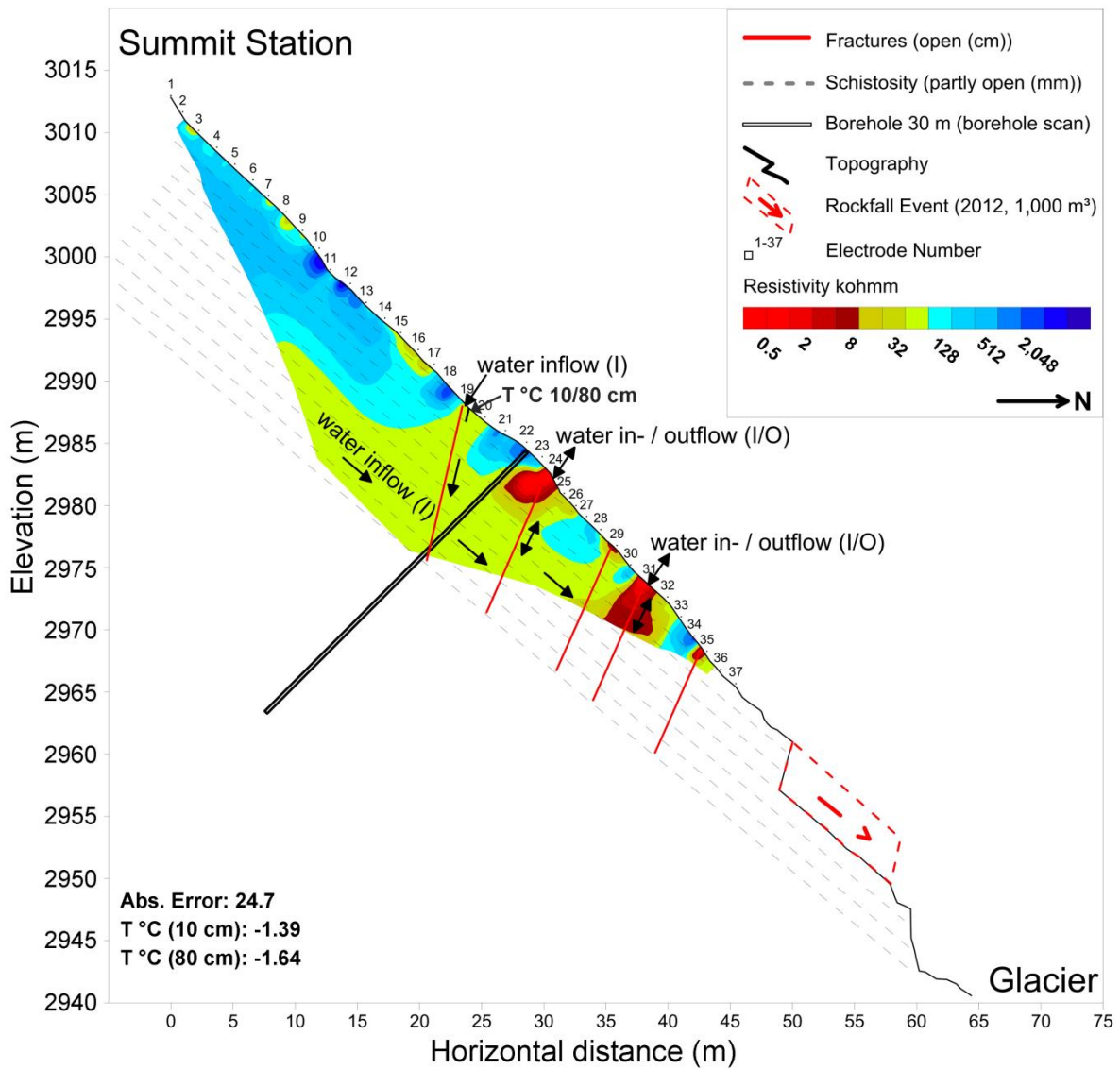
Figure 48: ERT Tomography (21 May 2013 08:00 am) combined with high resolution (10 cm) topography taken from a TLS scan two weeks after the rockfall event. Mapped fractures and schistosity are based on a geotechnical investigation and on optical borehole scans. Arrows mark location of frequent, visually observed water in- and outflow paths.

7.1.7 Conclusion and outlook: towards integrated and error-controlled continuous electrical resistivity tomography measurements

This study presents the first automated and continuously operating ERT monitoring system for steep unstable permafrost-affected rock walls. Along with seismic refraction tomography (Krautblatter and Draebing, 2014), ERT provides the only available spatial monitoring technique for permafrost rocks, but it is much better suited than seismic refraction tomography to develop continuous monitoring under extreme conditions. The Wenner time series consists of 996 single datasets with more than 200,000 apparent resistivity datum points, which represents the largest and highest temporally resolved (published) dataset so far (Supper et al., 2014). The relative measurement error distribution shows limited periods of enhanced measurement errors. Among disturbing factors, wind gusts cause the highest distortion, while changes in air temperature, precipitation or rock temperatures have less impact on the error levels and thus are not filtered out. Major changes in resistivity are attributed to fluid flow in fractures, resulting in saturation and warming of the rock mass from the bottom upwards.

Future developments in hard- and software are needed to enhance the reliability of the monitoring system. To implement such ERT measurements automatically in early warning systems, we need to improve:

1. Automatic error detection. Statistical methods, based on unprocessed raw data, can be used for an automated error control and are a prerequisite for optimal data inversion routines. The quantification of external influencing factors on automated ERT measurements needs further research to reliably interpret continuous AERT data sets with respect to subsurface temperature and saturation changes.
2. Evaluation of longer-term changes in the temperature-resistivity relationship, based on laboratory and field evidences.
3. Empirically constrained thresholds for fluid induced ERT changes.
4. Local validation measurements by piezometric information.

Overall, enhanced ERT monitoring systems have the potential to provide fundamental components for early warning systems in potentially hazardous permafrost-affected rock walls.

7.2 Near-surface rock temperature monitoring

Fully incorporated: KEUSCHNIG, M., HARTMEYER, I., SCHMIDJELL, A, MARBACH, M., SCHROTT, L. & KRAUTBLATTER, M. prepared for submission. A low-cost strategy for near-surface rock temperature measurements using iButtons. Cold Regions Science and Technology.

7.2.1 Abstract

Near-surface rock temperature (NSRT) measurements are a challenging task for numerous periglacial and permafrost research activities. This article presents a new designed low-cost strategy for NSRT measurements based on miniature temperature loggers (iButtons®) with the main goal to enable a hitherto unknown coverage of spatial and temporal variations of NSRT measurements. The strategy introduces an innovative adaptation procedure including preparation, installation and maintenance of the system. To meet the requirements for spatially and temporally distributed rock temperature measurements, the system was analysed regarding costs, reliability, accuracy and data quality. The costs for the new developed iButton measurement rod are about one sixth of conventionally used rock temperature loggers. Tested under field conditions, the developed iButton measurement rods deliver temperature data that is comparable with data measured by higher-priced, more precise logger systems.

7.2.2 Introduction

Near-surface rock temperature measured in high-alpine rock faces is highly relevant to a broad range of applications. It is an important parameter for the understanding of permafrost development and related processes (e.g. frost weathering). Beyond that, NSRT is relevant for slope stability considerations (Krautblatter et al., 2013; Draebing et al., 2014; Keuschnig et al., 2015), for the validation of geophysical measurements (Supper et al., 2014), and for the assessment of permafrost modelling approaches (Gruber, 2003; Gruber et al., 2004b; Hipp et al., 2014).

Near-surface rock temperatures display a significant spatial and temporal variability due to the heterogeneity of high-alpine topography. In order to assess the variability a considerable number of NSRT measurements is usually required (Hartmeyer et al., 2012b). The used method furthermore has to operate reliably under extremely harsh environmental conditions. Both of these requirements significantly raise the total costs for acquisition, installation and maintenance of the deployed loggers.

Based on the use of iButtons this study presents a low-cost alternative for NSRT measurement. iButtons are robust, low-priced, miniature temperature loggers, well-suited for monitoring purposes. Originally designed for the monitoring of thermally sensitive products, iButtons have already been used in numerous scientific studies (Safanda, 1999; Smith et al., 2010; Lewkowicz et al., 2012; Brabyn et al., 2014). Gubler et al. (2011) installed 390 spatially distributed iButtons to investigate small-scale ground temperature variability in loose material. The application of iButtons for rock temperature measurements has not been reported so far.

The presented study introduces the first implementation strategy of iButtons for rock temperature measurements. Based on four years of measurement experience the following research questions are addressed: (1) How can iButtons be adapted to provide spatially and temporally highly resolved

NSRT measurements? (2) What reliability and accuracy can be derived under field conditions in complex structured permafrost-affected rock walls?

7.2.3   Instrumentation strategy and costs

Study Site

The presented study was conducted at the Kitzsteinhorn (3,203 m), located in the Hohe Tauern Range, Austria, 47°11'17'' N, 12°41'15'' E. The Kitzsteinhorn has a horn-type summit pyramid with steep rock faces, well-suited for spatially distributed rock temperature measurements at different elevations and slope aspects. The investigated rock faces belong to the Penninic Bündner Schist formation and consist primarily of calcareous mica-schist. North-facing slopes above 2,500 m are likely to be affected by permafrost, whereas south-facing slopes are free of permafrost up to elevations of more than 3,000 m. Temperature data from 20-30 m deep boreholes located at 3,000 m indicate permafrost core temperatures of approx. -2 °C and an active layer thickness of 3 m for north-facing slopes.

For the presented NSRT measurement campaign a pairwise instrumentation strategy has been chosen. Each of the currently 16 measurement sites is provided with a pair of loggers, installed in depths of 10 cm and 80 cm. This strategy allows thermal offset calculations and modeling of rock temperatures at depth.

Logger properties and preparation

The iButton device is a commercial, self-sufficient system that measures temperature and records the result in a protected memory section. Battery and computer chip are enclosed in a 16 mm thick stainless steel can (Figure 49, a). The operating range of the used iButton model ('DS1922L') extends from -40 °C to +85 °C, measurement accuracy is ±0.5 °C (from -10 °C to +65 °C), and resolution is 0.0625 °C (MAXIM, 2016).

In order to enable logger installation in shallow boreholes, iButtons are glued to the ends of round polyethylene rods (diameter 17.35 mm) (Figure 49, c, d) with a 1-component polyurethane sealant (Figure 49, b, d). Polyethylene has a very low thermal conductivity (~0.4 W/mK), is elastic, and weather/UV-resistant.
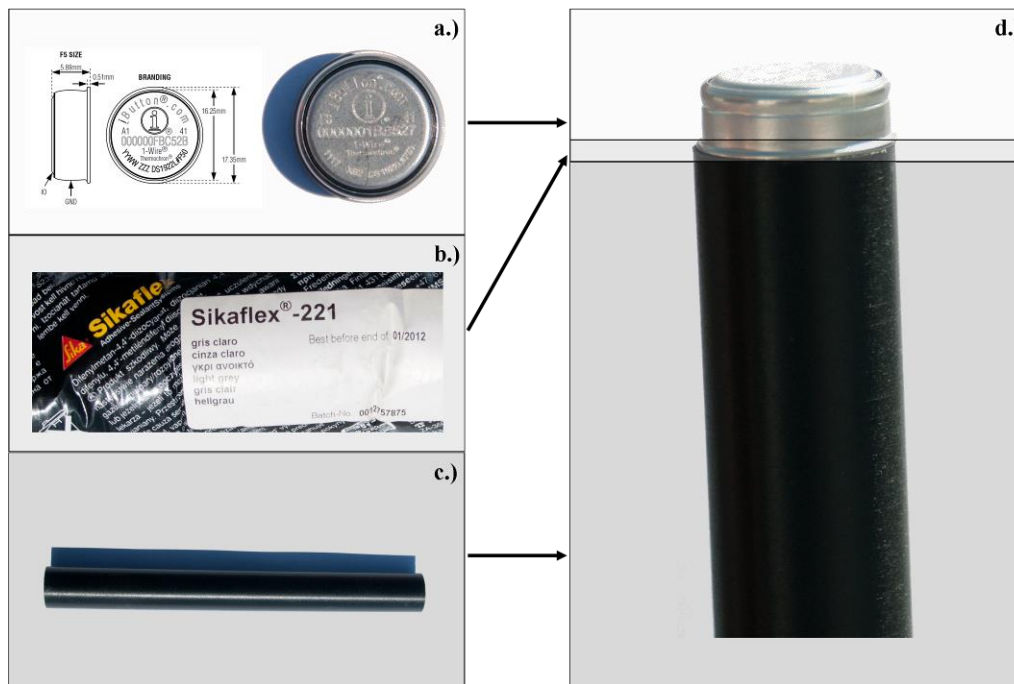
Figure 49: iButton measurement rod (d) consisting of the iButton (a), polyurethane sealant (b), and the polyethylene rod (c) (modified afterMAXIM (2016)).

Logger installation and maintenance

The installation starts with the drilling of a shallow borehole. In this study a battery-operated percussion drilling machine with a maximum drill length of 80 cm was used (Figure 50, a). The used drill diameter of 18 mm minimally exceeds the diameter of the logger. This enables smooth insertion of the logger into the borehole without creating a significant air-filled annulus. During and after drilling the cuttings have to be removed from the borehole with steel brushes and pressurized canned air (Figure 50, b, c). iButton devices are splash-water proof but do not operate under permanently wet conditions. For this reason each iButton is sealed with a silicon-based thermal paste (6 W/mK, Figure 50, d) prior to the insertion into the borehole. This protects the logger from water entry and improves the thermal coupling to the surrounding rock mass. After the logger is inserted into the borehole, the mouth of the borehole is sealed with weather/UV-resistant silicone to prevent water/air entry (Figure 50, e). Figure 50 (f) shows a pair of loggers with measurement depths of 10 and 80 cm after the completion of the installation.

In order to read out the recorded temperature data, the logger has to be retrieved from the borehole. For this purpose the silicone cover is removed and the logger is pulled out of the borehole by hand. During readout the iButton is inserted into an adapter that connects to the target device (notebook, smartphone) via USB.
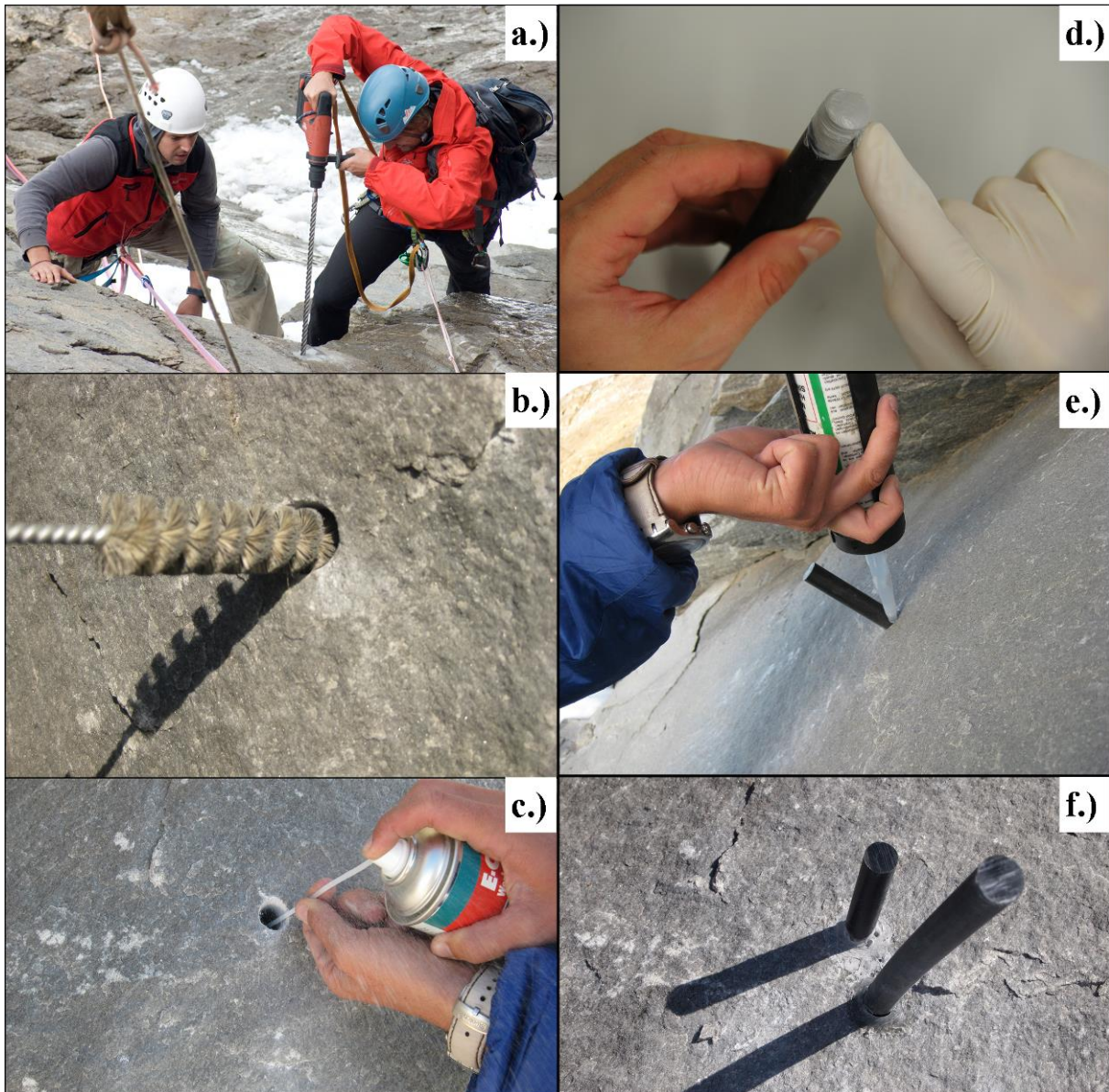
Figure 50: Installation of iButton measurement rods.

Costs

The application of iButtons facilitates rock temperature measurements whose costs lie well below the costs of alternative measurement techniques. Table 7 provides a cost comparison for iButtons and three alternative methods that are widely used in geoscientific studies.

Table 7: Comparison of approximate costs (price of 2015) for iButtons (DS 1922 L), M-Log5W-DALLAS (GeoPrecision), UTL-3 (Geotest), and Hobo U12-015 (Onset). Costs for software, accessories, and drilling are not included as they do not differ significantly for the four listed methods.

	iButton DS 1922L (Maxim Integrated)		M-Log5W-DALLAS (Geoprecision)	UTL-3 (Geotest)	Hobo U12-015 (Onset)
Acquisition costs	iButton DS 1922L (±0.5 °C): Polyethylene Rod (80 cm): Sealing works:	25 € 15 € 10 €	M-Log5W-DALLAS (±0.25 °C, external sensor 2 m, wireless logger)	UTL-3 Datalogger (±0.1 °C, external sensor 2 m)	Hobo U12-015 (±0.25 °C)
		~ 50 €	~ 380 €	~300 €	~220 €
Maintenance costs*	Logger replacement required after 3 years (battery cannot be replaced)		Battery replacement required after 3 years	Battery replacement required after 3 years	Battery replacement required after 3 years (factory replacement)
		~50 €	~5 €	~20 €	~? €
Total Costs 3 years 6 years		~50 € ~100 €	~380 € ~385 €	~300 € ~320 €	220 € > 220 €

*Battery life under perennially cold conditions tends to be substantially shorter than specified by the manufacturer. For this reason a reduced battery life of 3 years is assumed for all listed methods.

7.2.4 Measurement reliability and accuracy

Following a prototype period in 2010/2011, first continuous measurements were started in September 2011. Particularly during the first year of operation water entry is most likely to be responsible for serious hardware damage – 6 out of 16 loggers (38 %) were affected by data loss. In response to this problem loggers were sealed with a water-repellent, silicon-based thermal paste (Figure 50, d), which contributed significantly to an increase of their functional reliability and lifespan. Currently, a failure rate of about 10 % has to be taken into account. Up to now 32 iButton measurement rods were installed resulting in a hitherto unknown coverage of spatial and temporal variations of NSRT measurements (*Figure 51*).
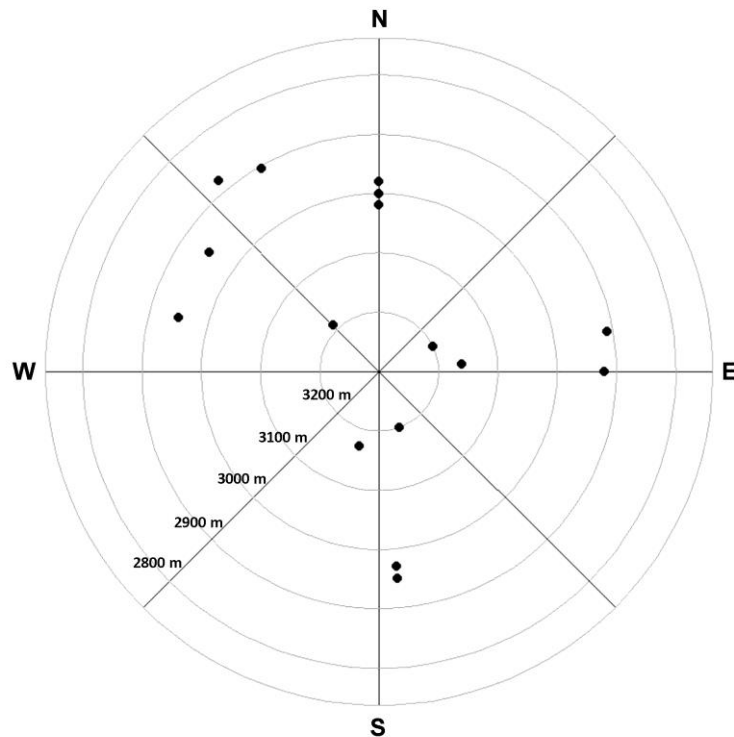
Figure 51: Spatial distribution of 32 installed iButton measurement rods (Open Air Lab Kitzsteinhorn, Austria).

The iButton does not allow battery change. Hence, the entire iButton measurement rod has to be replaced as the battery nears the end of its life span. While this increases the total operation costs over long measurement periods (Table 7), it adds the significant benefit of systematically introducing fresh, factory-calibrated loggers. Thus, the substantial risk of unnoticed long-term temperature drifts is eliminated.

In comparison to other temperature loggers (Table 7) iButtons have a lower measurement accuracy of ±0.5 °C (from -10 °C to +65 °C). In order to analyse the measurement performance of iButtons under field conditions they were compared with a UTL3 data logger with an accuracy of ±0.1 °C. Both data loggers were placed at the same location (10 cm depth) inside a tunnel ("Hanna Stollen") with highly stable environmental conditions (±1 °C / year). The measurements were taken at one-hour intervals. During a measurement period of three months, all temperature data from the iButton© remained clearly within the accuracy range of the UTL3 logger (±0.1 °C, Figure 52).
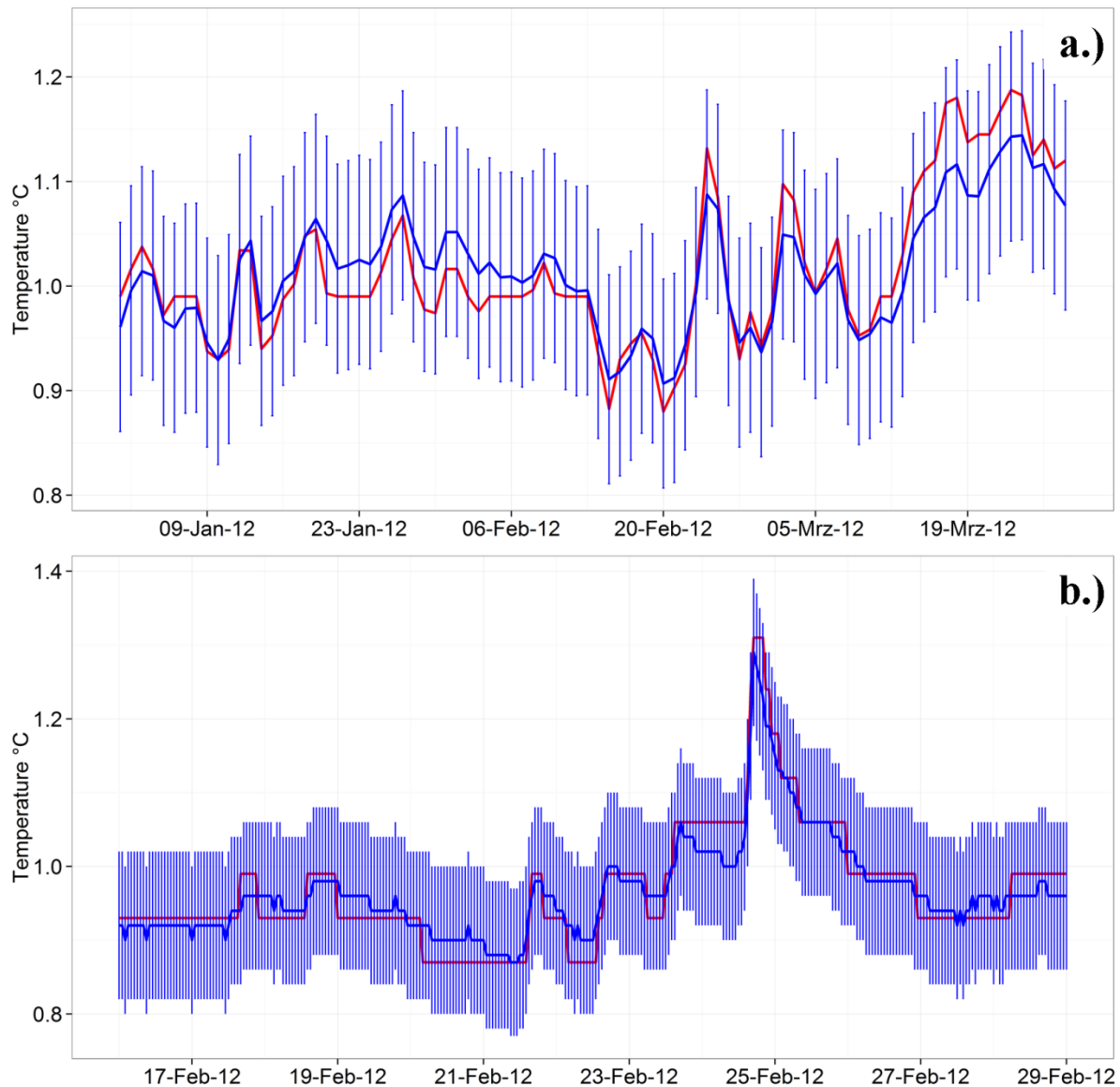
Figure 52: Daily mean temperature time series (a) and hourly temperature evolution (b), comparison between UTL3 temperature logger with an accuracy of ±0,1 °C (blue line) and an iButton measurement rod with an accuracy of ±0,5 °C (red line). Both measurement units were placed at the same site and the same depth of 10 cm. Error bars (blue) in both charts are showing the accuracy range of the UTL 3 logger.

7.2.5 Conclusions

In this study a simple adaptation procedure was presented, which allows the implementation of iButtons for NSRT measurements. Due to the miniature dimensions of the developed iButton measurement rod, drilling and installation works are reduced to a minimum. Costs for acquisition are about one sixth of the costs of conventionally used rock temperature loggers. Thus, damage to the logger – a significant risk for sensitive instruments exposed to rough, high-alpine environmental conditions – is financially manageable. Currently, a failure rate of about 10 % has to be taken into account which is comparable to the reliability of other temperature loggers. Up to now 32 iButton measurement rods were installed resulting in a hitherto unknown coverage of spatial and temporal

variations of NSRT measurements. Tested under field conditions, the developed iButton measurement rods deliver temperature data that is almost identical with data measured by higher-priced, more precise loggers, possibly indicating similar accuracy ranges. Even though further testing under different environmental conditions is required to confirm this trend, the presented iButton measurement rods are well suited for cost effective, long-term NSRT measurements.

7.3 Combining monitoring approaches: towards a temperature-resistivity calibrated electrical resistivity system

Fully incorporated: KEUSCHNIG, M., KRAUTBLATTER, M. & HARTMEYER, I. prepared for submission. Field evidence for temperature-resistivity relationship of permafrost-affected alpine rock walls. The Cryosphere.

7.3.1 Abstract

Temperature-resistivity relationships (T-ρ) provide a proxy for the thermal state and in further consequence stability-relevant information of permafrost rock walls. Here, we present the first temperature-resistivity relationship for permafrost rock walls measured under field conditions. Based on 1,485 Wenner and rock temperature datasets we analysed the T-ρ characteristics considering different depths of temperature investigation. We can demonstrate that the analysed T-ρ relationships show a well fitted linear regression. A comparison between T-ρ gradients of this field study with T-ρ gradients based on laboratory measurements under frozen conditions show similar results. In this study, we show the characteristics of T-ρ relationships under field conditions and the potential to provide stability-relevant information for potential early warning systems.

7.3.2 Introduction

Numerous rockfall events have been observed and reported recently from permafrost-affected areas (Rabatel et al., 2008; Huggel, 2009; Ravanel and Deline, 2011; Fischer et al., 2013; Keuschnig et al., 2015) representing a serious risk factor for man and infrastructure. Laboratory studies show that thermal changes in frozen rock significantly alter the mechanical properties of rock and ice along potential failure planes (Krautblatter et al., 2013). As a consequence for rock slope failures in permafrost-affected rock walls the thermal state is a key factor and a prerequisite for slope stability analysis. Therefore, the development and refinement of methods capable of providing information on thermal subsurface properties has gained major importance (Harris et al., 2009; Krautblatter et al., 2012).

Electrical resistivity tomography (ERT) has become increasingly popular in this field as electrical resistivity of frozen rock is highly temperature-dependent and reacts sensitively to the gradual freezing of water in pores and fissures in bedrock from 0 to ca. -8 °C (Mellor, 1973; Krautblatter et al., 2010). Automated ERT (AERT) has the ability to provide more than 1D data and has been demonstrated as a powerful method for continuously monitoring the state of permafrost (Hilbich et al., 2011; Supper et al., 2014; Keuschnig et al., accepted).

Laboratory studies show that electrical resistivity is an accurate proxy for rock temperature (Seguin, 1978). Krautblatter (2009) demonstrates a bilinear temperature-resistivity (T-ρ) relationship based on sedimentary, metamorphic and igneous rock samples from permafrost areas. A comparable field study of T-ρ relationships have not been reported yet due to the lack of accurate field monitoring data. The main objective of this study is to close the gap between quasi-homogenous laboratory and field measurements. Based on the AERT measurement strategy reported by Keuschnig et al. (accepted) the following research questions are addressed in this study: (1) What are the characteristics of a T-ρ relationship under field conditions? (2) Is the T-ρ gradient comparable with laboratory results?

7.3.3   Methods

This study uses the permanently installed AERT system reported by (Keuschnig et al., accepted). This system includes a GeoTom-MK1E100 multielectrode resistivity system (GEOLOG2000), designed to operate in high-mountain conditions. It is robust and weather resistant, protected by a hard-case and includes all required components such as transmitter, receiver, µ-controller, AD-converter, power supply and charging unit.

The AERT profile consists of 37 electrodes and follows the rock face topography, with an overall length of 72 m. The AERT profile is a compromise between permafrost-relevant investigation depths of more than 10 m and the required resolution for active-layer measurements with a median depth of investigation of ca. 1 m. Stainless steel climbing bolts 90 mm long and 10 mm in diameter, rather than fixed stainless screws of the same size (Krautblatter and Hauck, 2007) were drilled into the bedrock to enhance mechanical resistance and consistent electric coupling. Measurement cables were attached to anchors and aligned to minimise damage from rockfall and snow pressure. The control system was deployed inside the summit station with network access, power connection and overvoltage protection. Data acquisition was fully automatic and remotely controlled. Near-surface temperature measurements from shallow boreholes (up to 0.8 m deep) were performed along the AERT profile and supplemented by climate data from three automated weather stations located 300 to 800 m horizontally and 50 to 400 m vertically from the AERT profile.

Rock temperatures were taken with specifically adapted iButtons (Keuschnig et al., 2012; Keuschnig et al., prepared for submission-a) with an accuracy of ±0.5 °C. NSRT sensors are placed at three locations in a depth of 10 to 80 cm located along the ERT profile (T in Figure 53 c, d).
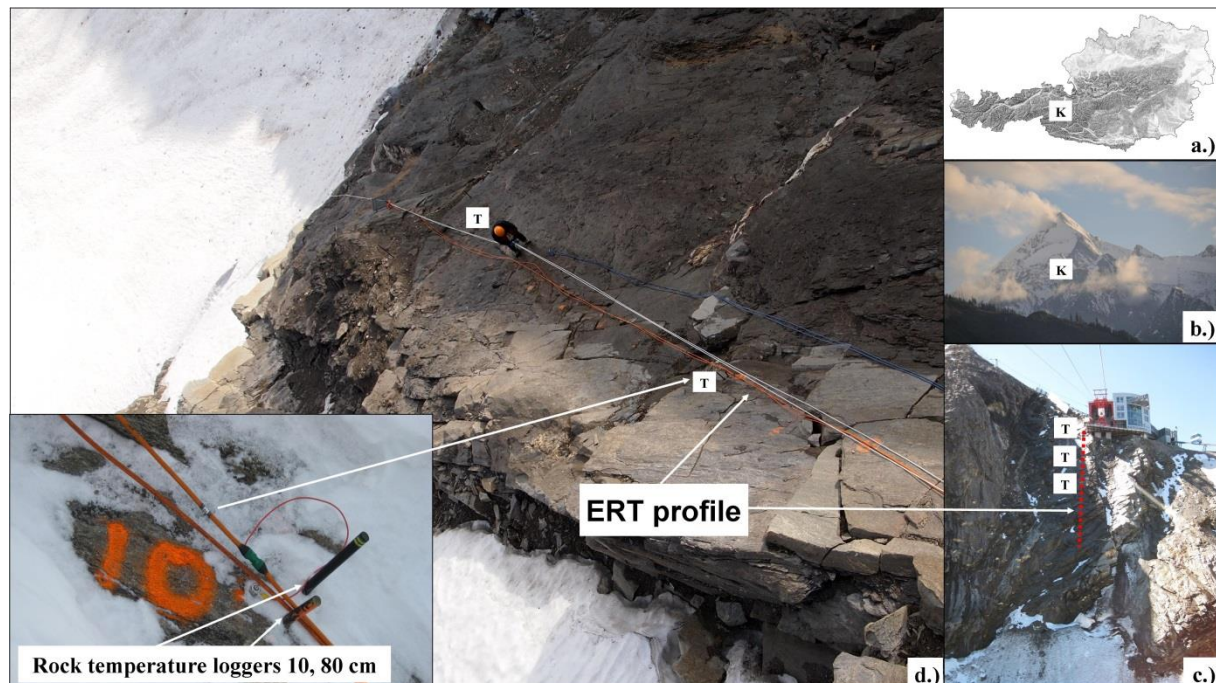
Figure 53: ERT profile located at the Kitzsteinhorn (K in a, b, 3,203 m), Hohe Tauern Range, Austria. Letters show the position of the 10 and 80 cm NSRT measurements (T in c, d).

The quasi-continuous monitoring consists of datasets recorded at 4-hr intervals which is most likely the minimum interval at which changes greater than the measurement noise become evident (Keuschnig et al., accepted). Various software problems caused short data gaps, lightning strike events led to serious hardware damages and to data losses. The whole time series was analysed and processed using the software package R. The resistivities were taken from the first layer of the measured Wenner arrays which provides field analogue to four-electrode geometry of laboratory measurements (Krautblatter, 2009) and due to the highest number of resistivity measurement points (n=34). A data quality check which includes exploratory statistics, a physically based plausibility check and the identification of measurement errors according to Keuschnig et al. (accepted) was applied.

7.3.4   Study site

The study site is located in the summit region of the Kitzsteinhorn, Hohe Tauern Range, Austria (Figure 53 a, b). The Kitzsteinhorn summit pyramid (K in Figure 53 a, b; 3,203 m above sea level (a.s.l.); 47°11'17'' N, 12°41'15'' E), consists of rocks of the Penninic Bündner Schist Formation in the Tauern Window. This formation belongs to the Glockner Facies of the Glockner Nappe and comprises calcareous mica schist, prasinite, amphibolite, phyllite and serpentinite (Hoeck et al., 1994; Schober et al., 2012).

The rock face contains a permafrost body whose core temperature is approximately -2 °C, as evidenced by five boreholes up to 30 m deep and by the thermal regime of dozens of near-surface temperature measurements close to the ERT array (T in Figure 53 c, d) (Hartmeyer et al., 2012). Over the last decades the rock face below the cable car has been affected by a rapid glacier retreat at the base and the complete loss of its ice cover on the rock surface recorded by orthophotographs. Several rockfall detachments with single blocks of up to 100 m³ were observed in the past few years. One major event (1,000 m³) occurred directly below the ERT survey, and subsurface conditions during its detachment were recorded by ERT measurements (Schober et al. (2012); Keuschnig et al. (2015)).

7.3.5   Results

The calculated T-ρ relationship consists of 1,485 Wenner datasets including 345,870 resistivity data points and rock temperature measurements. In total 2,626 data points which represents 4.7 % of the whole dataset were detected and filtered. The filtered apparent resistivities range from 3.5 Ωm to 2.5 MΩm with a median of 236.3 kΩm and a mean of 411.3 kΩm. For all individual datasets the mean value is higher than the median which indicates a deviation from normal distribution (Figure 54). As a consequence and to avoid major influences of outliers the robust median was used for further analysis.
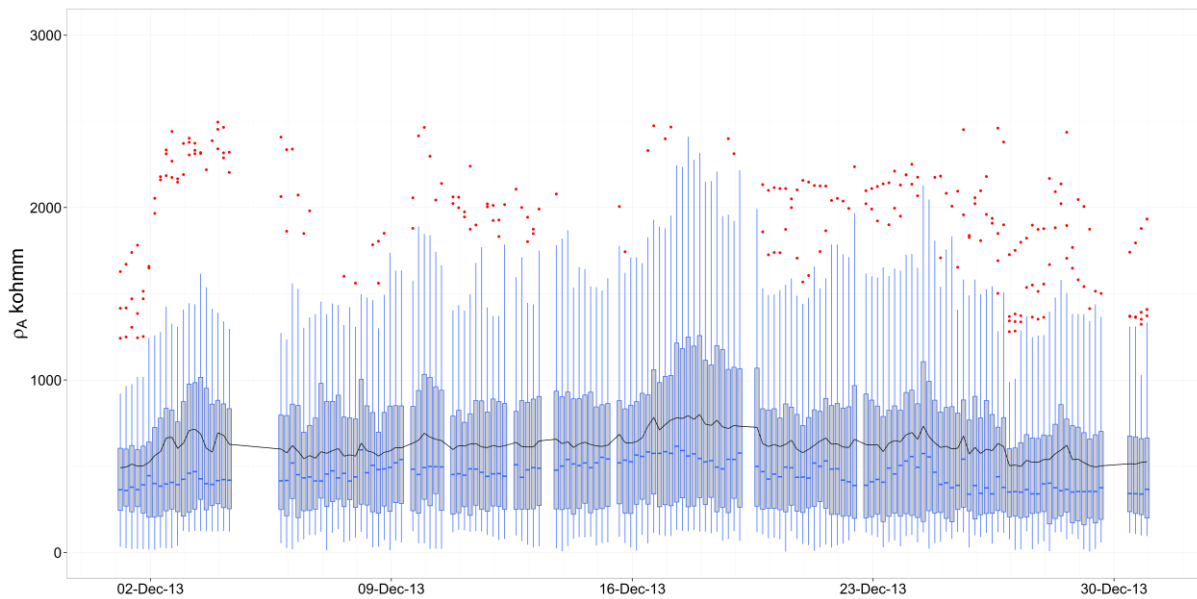
Figure 54: Time series and statistical distribution of apparent resistivities in terms of the median (blue line), the scatter (25% and 75% percentiles, blue box), the range of extreme values (1.5 times the interquartile range added to the 25% percentile and to the 75% percentile, blue whiskers), the outliers (red dots) and the mean values (black line), (20 November 2013-31 December 2013).

Rock temperatures were correlated to each Wenner dataset. Linear regression models were fitted on datasets with temperatures <= 0 °C to represent permafrost conditions and to allow a comparison with laboratory measured values for permafrost rocks according to Krautblatter (2009). T-ρ relationships have been calculated on different rock temperature depths along the profile. In addition to the 10 cm rock temperatures only one 80 cm temperature dataset has been analysed due to data gaps and damages of the other 80 cm logger (Figure 55).
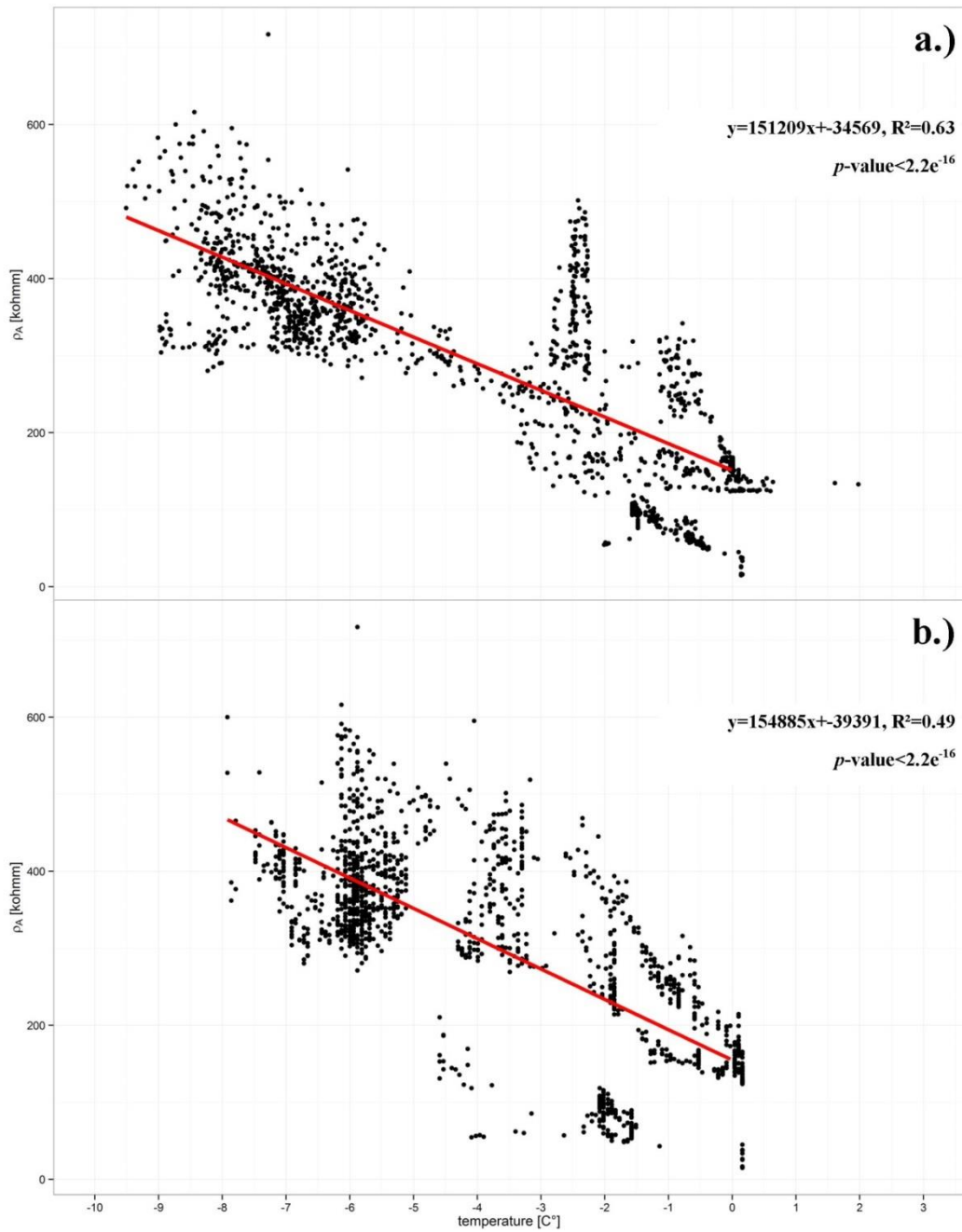
Figure 55: T-ρ relationships different depths, temperatures consist of the mean value of three 10 cm rock temperature measurements along the ERT profile (a) and the 80 cm logger (b). Red line indicates a linear model for rock temperature values <= 0 °C.

To assess the whole temperature field the mean value of the rock temperature in 10 and 80 cm were calculated (Figure 56).
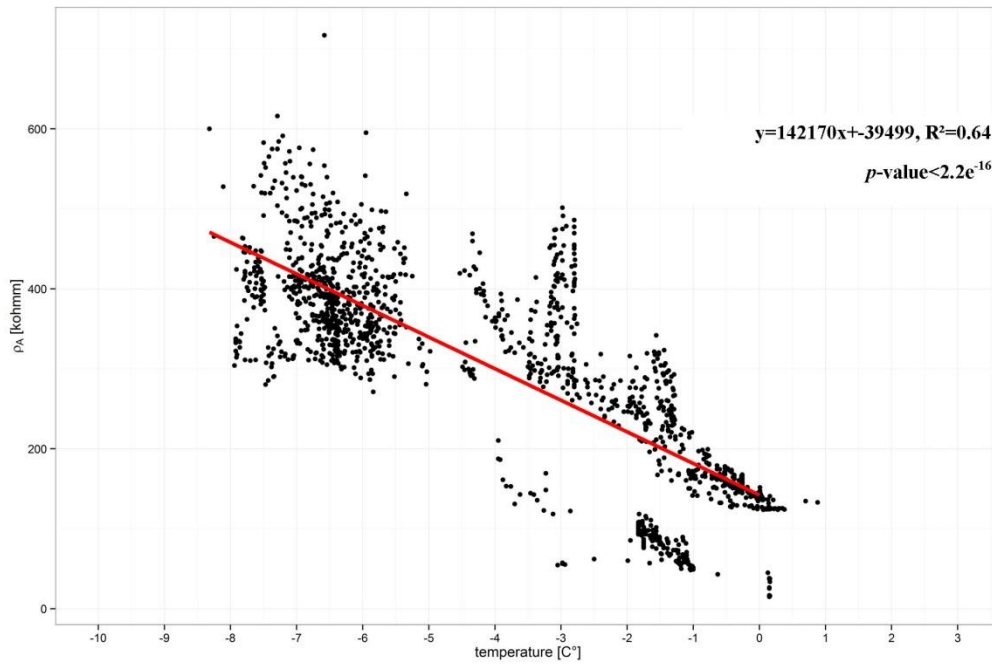
Figure 56: T-ρ relationship, temperatures consist the mean rock temperatures in 10 and 80 cm depth. Red line indicates a linear model for rock temperature values <= 0 °C.

Table 8 shows the T-ρ characteristics for different rock temperature depths. To get a representative value for the 0 °C and 2 °C resistivity, temperatures were sampled in a range of ±0.05 °C.

Table 8: Temperature-resistivity characteristics for mica schist under permafrost conditions.

T-ρ relationship	*p*-value	R^2	0° Resistivity (ρ) [kΩm]	-2° Resistivity (ρ) [kΩm]	T-ρ gradient frozen [%/°C]
10 cm (mean)	***, <2.2e^{-16}	0.63	177.2±33.4	270.0±98.3	**22.9**
80 cm	***, <2.2e^{-16}	0.49	227.8±33.0	169.3±120.6	**25.4**
10 and 80 cm (mean)	***, <2.2e^{-16}	0.64	164.6±21.9	312.4±103.3	**27.8**

7.3.6 Discussion

As shown in Figure 56 and Table 8, the temperature-resistivity data represent a strong linear T-ρ relationship with a three star significance, a *p*-value<2.2e^{-16} and a R² of up to 0.64. Taking into account the 2 m spacing of the Wenner array the maximum depth of rock temperature investigation is approximately between the medium depth of electric current flow according to Barker (1989) with 102 cm and the more pessimistic results after Roy and Apparao (1971) with 66 cm. The rock temperature at 80 cm fulfil this assumption but the T-ρ characteristics show the weakest model fit and the largest standard deviations (Figure 55 (b), Table 8) of all tested relationships. On the other hand the T-ρ characteristics at 10 cm represent a well fitted linear model (Figure 55 (a), Table 8). The measured resistivities are highly variable over time with a resistivity maximum of 2.5 MΩm resulting in lower temperature investigation depths during high resistivity periods and higher temperature investigation depths during low resistivity periods. As a consequence we propose the presented T-ρ relationship based on the mean value of the 10 and 80 cm rock temperatures (Figure 56, Table 8). The measured T-ρ gradients of 22.9 to 27.9 %/°C under permafrost conditions (T <= 0 °C), are in the range of the laboratory results of 29.8±10.6 %/°C (Krautblatter, 2009).

7.3.7 Conclusion and outlook

1,485 Wenner datasets and rock temperature measurements of different depths have been analysed. Linear regression modelling shows that analysed T-ρ relationships are highly significant with a *p*-value<2.2e^{-16} and a R² of up to 0.64. A comparison between the field and laboratory results show a similar T-ρ gradient under permafrost conditions which emphasizes the dominant influence on temperature on the resistivity of permafrost rocks. For rock slope failures in permafrost-affected rock walls the thermal state is a key factor. Here, we show the first temperature-resistivity relationship for permafrost rock walls measured under field conditions. This represents an important step to enhance the applicability of ERT monitoring to provide subsurface temperature changes e.g. for early warning systems for potentially hazardous permafrost-affected rock walls.

7.4   Case study: implications from a permafrost-affected rockslide

Fully incorporated: KEUSCHNIG, M., HARTMEYER, I., HÖFER-ÖLLINGER, G., SCHOBER, A., KRAUTBLATTER, M. & SCHROTT, L. 2015. Permafrost-Related Mass Movements: Implications from a Rock Slide at the Kitzsteinhorn, Austria. In: LOLLINO, G., MANCONI, A., CLAGUE, J., SHAN, W. & CHIARLE, M. (eds.) Engineering Geology for Society and Territory - Volume 1. Springer International Publishing.

7.4.1   Abstract

Rock instability in high mountain areas poses an important risk for man and infrastructure. At 03:00 pm on August 18th 2012 a rock slide event was documented at the Kitzsteinhorn, Austria. The release zone was detected on a north-exposed rock face below the cable car summit station (3.029 m). Analysis of terrestrial laser scanning (TLS) data delivered an accurate identification of the release area and a rockfall volume of approximately 500 m³. Cubic blocks with lengths of up to 4 m and masses of up to 125 t were released during the event. The failure plane is located in a depth of approximately 3 to 4 m and runs parallel to the former rock surface (mean inclination 47°). Comparison with borehole data located less than 50 metres from the release zone shows that failure plane depth is consistent with active layer depth. The event documentation is supplemented with observations of rock and air temperature, data on precipitation and snow depth, electrical resistivity tomography data, observed active layer depth and geological/geotechnical background data. The comprehensive ambient data suggests the influence of high temperatures and water availability for the triggering of the rock slide.

7.4.2   Introduction

Numerous rockfall events in the European Alps suggest an increasing occurrence of mass movements due to rising temperatures. In recent years particularly during extensive hot periods large numbers of rockfall events have been reported (e.g. hot summers of 2003 and 2005). However, in most cases reconstruction of triggering mechanisms is problematic due to a lack of information on physical in-situ conditions before and during the event. Preparatory factors of subsurface (e.g. geological setting, permafrost conditions), surface (e.g. topography, snow cover) and atmospheric conditions (e.g. climatic and meteorological conditions) and their complex relationships play a key role and must be taken into account.

The presented activities have been carried out within the research project MOREXPERT ('Developing a Monitoring Expert System for Hazardous Rock Walls') funded by Competence Centers for Excellent Technologies (COMET). MOREXPERT, which was started in September 2010, has initiated a new long-term monitoring site focusing on permafrost and rockfall interaction in steep bedrock in the Austrian Alps (Keuschnig et al., 2011; Hartmeyer et al., 2012b).

7.4.3   Study site

The study site is located at the Kitzsteinhorn (3,203 m, Hohe Tauern Range, Austria), a particularly interesting site for the monitoring of glacier retreat, potential permafrost degradation and their respective consequences for the stability of alpine rock faces. The Kitzsteinhorn is constituted of rock of the Bündner schist formation and belongs to the Glockner Nappe, specifically the Glockner Facies, which consists of calcareous mica schist, prasinite, amphibolite, phyllite and serpentinite (Schober et

al., 2012). The affected slope is a north-facing back wall of a glacial cirque with a mean inclination of 47°. It extends from the cable car summit station (3,029 m) down to the upper margin of the Schmiedingerkees glacier (2,950 m). The rock face is underlain by permafrost, over the last decades it has been affected by intense glacier retreat at the base and the complete loss of its ice cover.

7.4.4 Localization and quantification of the rock slide event

The blockslide occurred on August 18th 2012 at 03:00 pm. Touristic visitors and employees, who were present at the cable car summit station at the time of the event, registered the blockslide acoustically and visually. The release area is situated approximately 50 metres below the summit station (3,029 m, Figure 57) at the base of the rock slope, directly above the glacier. The failure plane is located in a depth of approximately 3 to 4 m and runs parallel to the terrain surface. Ice was visible on the failure plane immediately after the event. The release area and the volume of 500 m³ were investigated and quantified with TLS. Cubic blocks with lengths of up to 4 m and a weight of up to 125 t were released and slid over the glacier surface for more than 200 m.
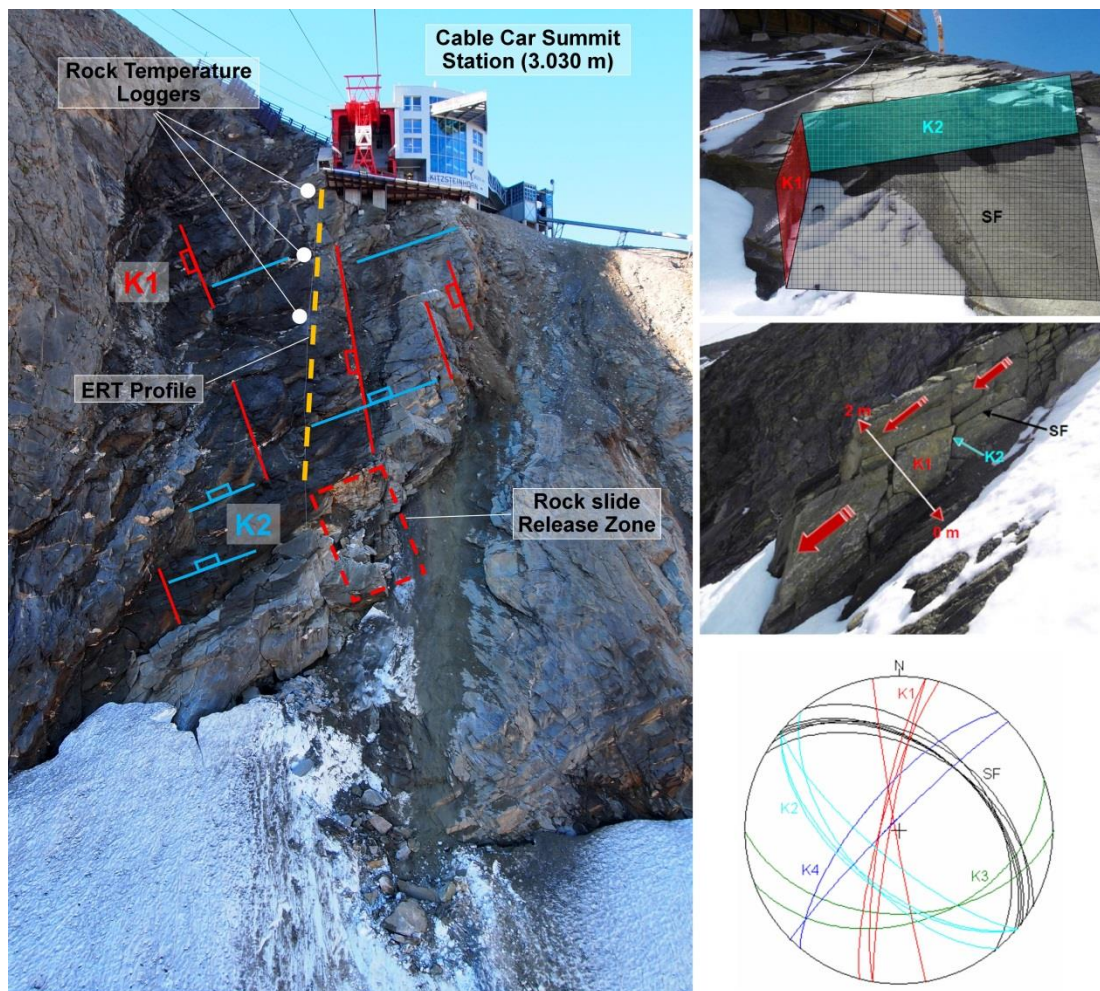
Figure 57: On the left side: Frontal view of the affected rock face with position of permanently installed monitoring instruments (ERT, rock temperature loggers). On the left and right side: Geotechnical setting and orientation of discontinuities.

7.4.5   Disposition and type of movement

The north face has an inclination of 23-67° and a mean value of 47°. The rock mass (calcareous mica schist) at the affected slope shows distinct schistosity (SF). The schistosity dips parallel to the slope, flat to medium steeply in direction NNE-NE and acts as an open interface structure. In addition to the schistosity, the joint sets K1 and K2 represent the main interface sets. K1 dips steeply to W and K2 dips medium-steeply to steeply to SW. The joint sets K3 and K4 are less frequent. The former dips medium-steeply to flat to S-SSE, the latter steeply to NW. K1 and K2 are oriented approximately orthogonal to the schistosity and constitute cubic to rhomboidal rock bodies. During the event several of these joint-bordered rock bodies were detached resulting in a blockslide.

7.4.6   Destabilising factors

Preparatory factors

Rising temperatures have led to substantial glacier retreat that has been particularly pronounced since the 1980s. Due to intense ablation the surface of the Schmiedingerkees glacier has been lowered by approximately 30 m over the last 40 years (Figure 58). Glacial debuttressing is therefore assumed to be a major long-term destabilizing factor for the discussed rock face. Excavated rock faces have been exposed to atmospheric influences, likely inducing intensified mechanical weathering. During the transition from subglacial to subaerial conditions geological discontinuities have become subject to a different thermal regime which includes the development of an active layer and convective heat transport in unfrozen clefts.
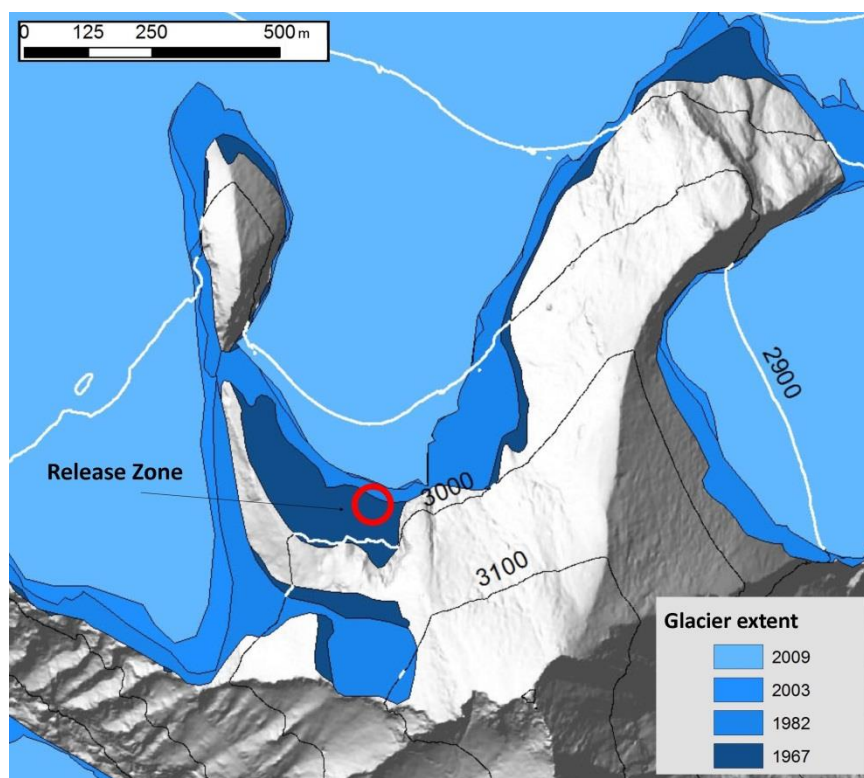
Figure 58: Decreasing glacier extent and ice cover in the area of the release zone during the last decades.

The initial fracture occurred clearly above the glacier surface (Figure 59). Thus, the triggering of the event cannot be explained by glacial debuttressing alone, despite the close proximity of the release zone to the upper glacier margin and the seasonal minimum of the snow height at the glacier at the time of the event.

Figure 59: Detachment of the blockslide: 18. August 2011 (left) - intact rock, 17. August 2012 - crack visible in the tensile zone (middle), 19. August 2012 – situation after the release (right).

Trigger factors

According to Krautblatter et al. (2013) the destabilisation mechanism can be discussed using driving and resisting forces. Rock temperature (Davies et al., 2001) and water pressures are stability-relevant factors for permafrost-affected rock walls. Subsurface temperature variations, for instance, affect ice pressures (driving force) and the strength of ice and rock (resisting force). High water pressures in fractures can reduce friction and exert high stresses on the surrounding rock mass.

Meteorological data from a weather station (Figure 60) located less than 500 m from the release area show that air temperatures remain above 0 °C for more than two weeks (01 August 2012-18 August 2012) before the blockslide event. Rock temperature measurements at a depth of 80 cm which were performed less than 50 m from the release zone also delivered values well above 0°C for the same time period (Figure 60).
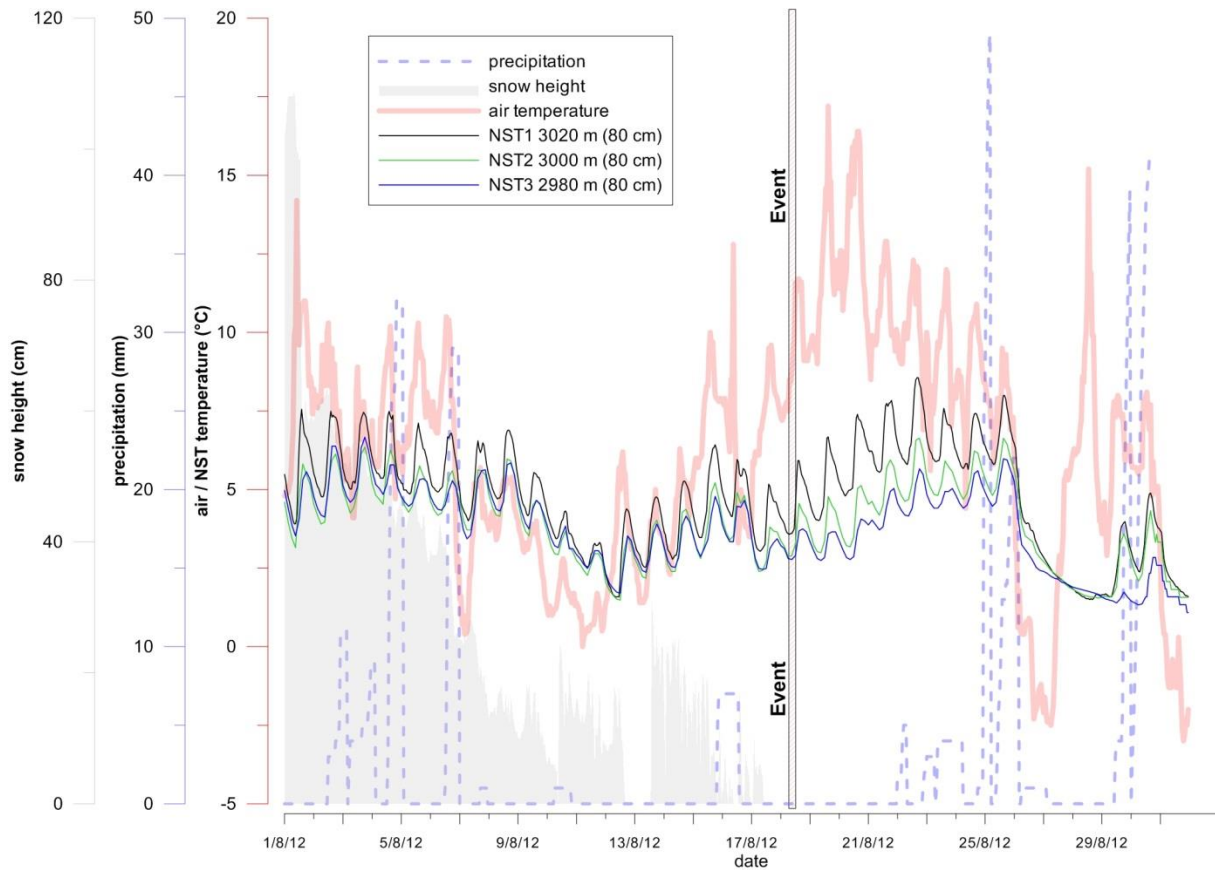
Figure 60: Time series of air temperature, near-surface rock temperature, precipitation and snow height for August 2012. The rock slide event occurred on 18. August at 03:00 PM.

Close to the release area, visible ice has been observed in a deep borehole in a depth of 3 m. This corresponds very well with the depth of the failure plane and the active layer during the time of the rockfall event. At the same time, data from a permanently installed Electrical Resistivity Tomography (ERT) profile show a strong decrease of electrical resistivity less than 30 m from the release zone (Figure 61). The lower resistivities are the result of higher temperatures and/or increased water availability. Near surface rock temperatures show no positive or negative temperature trend before the event (Figure 60). Thus, increased (cleft) water availability has to be responsible for the observed decrease in resistivity.
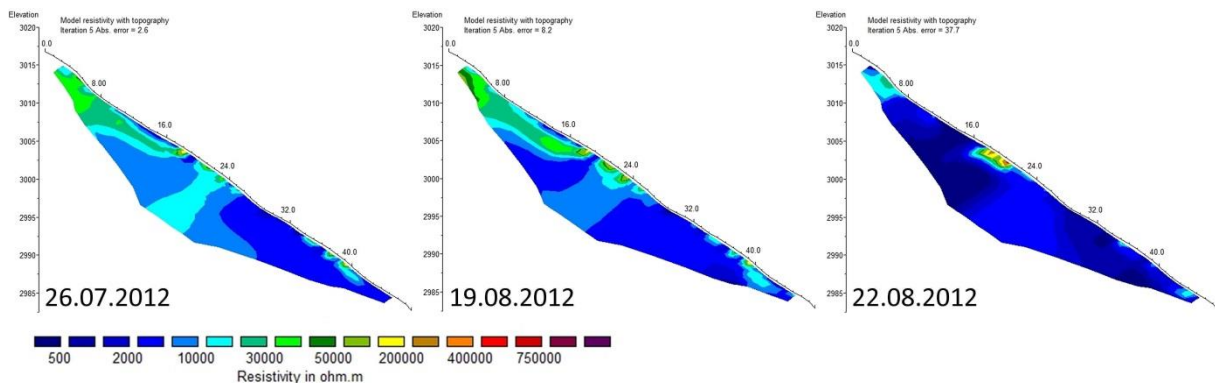
Figure 61: ERT data; decreasing resistivity indicates higher temperatures and/or higher water content.

7.4.7 Conclusion

High air temperatures led to intensified snow and ice melt and to an increase of active layer thickness. After the blockslide event, ice was visible on the failure plane. Combined analysis of rock temperature and ERT data show increased water availability before and after the rockfall event. We infer that increased water pressures in combination with decreased rock and ice strength caused by warming were the main trigger factors for the observed blockslide event.

8 Synoptic discussion

This chapter combines and discusses the overall outcome of this thesis. As all chapters include a separate discussion, cross references to the related chapter and postulated research question (Chapter 3.3) are given in brackets.

On the one hand an increasing number of rockfall events of different magnitudes has been observed and reported recently from permafrost-affected rock faces (Rabatel et al., 2008; Huggel, 2009; Ravanel and Deline, 2011; Fischer et al., 2013; Stoffel et al., 2014; Keuschnig et al., 2015) posing a serious risk factor to man and infrastructure (Höfer-Öllinger et al., 2015). These studies are based on field observations and suggest an increasing occurrence of rockfall events due to rising temperatures. On the other hand laboratory studies show that thermal changes in frozen rock significantly alter the mechanical properties of rock and ice along potential failure planes (Mellor, 1973; Fischer et al., 2013; Krautblatter et al., 2013). However, for single rockfall events, the reconstruction of the failure- and the triggering mechanism is problematic due to different response times of slope stability-relevant parameters and a lack of atmospheric, surface and subsurface data at and before the event.

To reduce the scientific gap between laboratory evidences on "rock sample scale" and field observations on "rock mass scale", long-term monitoring of slope stability-relevant parameters in permafrost-affected rock walls is essential. During the course of this Ph.D.-thesis, an open air laboratory (OpAL) for long-term monitoring of permafrost and mass movements was established in the summit region of the Kitzsteinhorn (3,203 m) (Keuschnig et al., 2011; Hartmeyer et al., 2012b) and is now the best instrumented long-term monitoring site for permafrost and mass movements in Austria. The development and refinement of monitoring methods capable of providing information on thermal and hydrostatic subsurface properties has gained major importance (Harris et al., 2009; Haeberli et al., 2010; Krautblatter et al., 2012). This is especially true as boreholes provide 1D thermal data in a complex 3D terrain and cannot be installed in actively unstable rock masses. Electrical resistivity of frozen rock is highly temperature-dependent and reacts sensitively to the gradual freezing of water in pores and fissures in bedrock between 0 and ca. -8 °C (Mellor, 1973; Krautblatter et al., 2010). However, continuous monitoring by automated electrical resistivity tomography in steep unstable bedrock has not been achieved yet as it imposes stringent demands for near-vertical electrode and cable setups, accessibility and infrastructure, and regular maintenance and safety.

This Ph.D.-thesis presents the first automated, permanently installed ERT in an unstable alpine rock wall **(Research Question 1.1 and Chapter 7.1.6)** for potential early warning systems. Compared to weekly and monthly measurements (Krautblatter and Hauck, 2007; Krautblatter et al., 2010), the system can monitor relevant changes in subsurface properties continuously and reveal rapidly changing conditions at potential failure planes. Despite the relatively low installation costs, the maintenance efforts are high, especially for unstable rock walls (Keuschnig et al., 2015). To improve system performance and avoid unstable measurements, the system was adapted to resist harsh environmental conditions. Climbing bolts used as electrodes have a high mechanical capacity and achieve constant coupling. Damage caused by overvoltage during thunderstorms is the main limiting factor for the monitoring system. The overvoltage can be transmitted by the measurement cables, the grounding, notebook connections or the power supply system of the used infrastructure. This makes overvoltage protection essential to minimize damages and costs.

To check the viability of ERT as a potential early warning signal, all signal distortions must be identified which would activate an inadvertent warning **(Research question 1.2 and Chapter 7.1.6)**. Therefore, controlling and filtering routines are essential to guarantee consistent AERT data. Especially inversion routines critically depend on the quality of the pre-processed raw data because changing measurement errors can significantly influence tomography results and inhibit comparability (Rosset et al., 2013). Consequently, the initial statistical analysis based on unprocessed raw data is an important step to clarify the general structure of the data and to summarise their main characteristics. The validity of the data range and the maximum measurable values depend strongly on the technical specifications of the applied hardware. All datasets were systematically checked for measurement errors. Measurement errors in steep fractured and exposed permafrost rock faces affect 3.7% of all measured data points, which is understandingly higher than the reported error rate of 1.62% in debris-covered rock slopes (Hilbich et al., 2011), probably also due to different data pre-filtering. The error rate is still appropriate for the intended purpose, with respect to the signal changes of ca. 30% resistivity change per °C temperature in frozen rock (Krautblatter et al., 2010). Influencing factors on measurement errors were carefully analysed. Surprisingly, the analysis only suggests a correlation of measurement errors with wind gusts. The time-limited, absolute and relative increase of the SDpA random error indicates an increase of external noise, possibly caused by fluctuating electromagnetic fields induced by natural (e.g. water circulation) or artificial sources (e.g. summit station). Linear models based on randomised subsets show a significant correlation between measurement errors and wind gusts with a p-value < 0.001. Strong wind gusts result from heavy atmospheric turbulence, which can induce direct or indirect vibrations (e.g. via infrastructure) into the ground. Wind gusts caused by convective atmospheric changes (e.g. thunderstorms) can also indicate high electric field strengths and potentially induce electrokinetic effects (Telford et al., 1990). During these periods measured electrical field strengths at the nearby Sonnblick Observatory can reach up to several thousand V/m instead of approximately 100-200 V/m under normal conditions (pers. communication, Niedermoser B., 21.03.2015). Both vibration- and atmospheric-induced currents influence the subsurface electrical field and so may affect ERT measurements.

For quasi-continuous monitoring of subsurface changes, ERT was conducted every 4h. The relative changes in apparent resistivity calculated based on the difference between the median values of the first layer range from 0.5 to 272.5% within four hours. Krautblatter et al. (2010) have demonstrated a relative measurement error based on reciprocal measurements of 8% for large resistances above 5 kΩ. Based on this first assumption, the calculated relative uncertainty U_{rel} = 11.3%. The user-defined threshold of > 20% for change detection significantly exceeds the uncertainty range and enables reliable results and interpretation. 84.8% of changes are within the uncertainty and therefore cannot be reliably interpreted by this automatic procedure alone. But trends in small apparent resistivity changes may result from slow processes such as temperature changes over a longer time period (> 4 hours). It can be assumed that relative changes of more than 20% can result from increased water availability caused by snowmelt or rainfall and for small subsurface temperature changes, 4h interval measurements of ERT monitoring are probably the highest sensible temporal resolution since otherwise noise is larger than systematic changes between repeated measurements.

Strong resistivity changes with more than 20% within 4h coincided with rapid freezing or water inundating rock fractures **(Research question 3.2 and Chapter 7.1.6)**. Automatically detected periods with large resistivity changes produce ERT time series with low resistivities extending from the bottom upwards during times of snowmelt. During the thawing period meltwater infiltrates mainly

along the slope, parallel to open cleavage fractures. The infiltrating water significantly lowers the resistivity, from the base of the wetted layer upwards. The electrical resistivity is controlled mainly by temperature and water saturation of the measured material. The NSRT measurements at 10 and 80 cm depth show no significant changes during periods with large variations in apparent. Furthermore, temperatures at depth respond very slowly to external changes and cannot explain major resistivity changes. Thus, major hourly changes in resistivity are probably controlled by pressurised fluid flow in fractures. This results in an increasing (from the bottom upwards) saturation as well as slow warming of the rock mass around fractures. As a consequence, hydrostatic pressures increase until cleftwater pours out through open fractures. Similar forcing has been observed before the triggering of a recent rock slide detachment below the ERT transect (Chapter: 7.4, Keuschnig et al. 2015).

The NSRT are measured using a newly developed low-cost alternative based on miniature temperature loggers (iButtons) **(Research question 2.1 and Chapter 7.2.3)**. Due to the miniature dimensions of the developed iButton measurement rod, drilling and installation works are reduced to a minimum. Costs for acquisition are about one sixth of the costs of conventionally used rock temperature loggers. Thus, damage to the logger – a significant risk for sensitive instruments exposed to rough, high-alpine environmental conditions – is financially manageable. 32 iButton measurement rods were installed resulting in a hitherto unknown coverage of spatial and temporal variations of NSRT measurements **(Research question 2.2 and Chapter 7.2.4)**. A failure rate of about 10 % has to be taken into account which is comparable to the reliability of other temperature loggers. Tested under field conditions, the developed iButton measurement rods deliver temperature data that is almost identical with data measured by higher-priced, more precise loggers, possibly indicating similar accuracy ranges. Even though further testing under different environmental conditions is required to confirm this trend, the presented iButton measurement rods are well suited for cost effective, long-term NSRT measurements.

The combination of AERT and NSRT measurements leads to the first comprehensive field evidence of a bi-linear temperature-resistivity (T-ρ) relationship **(Research question 4.1 and Chapter 7.3.6)**. The T-ρ relationship can be used as a proxy for the thermal state (Seguin, 1978) and in further consequence for stability-relevant information on the mechanical state of permafrost rock walls. Based on 1,485 Wenner and rock temperature datasets, the T-ρ characteristics were analysed considering different depths of temperature investigation. Linear regression modelling shows that analysed T-ρ relationships are highly significant with a *p*-value $< 2.2e^{-16}$ and a R² of up to 0.64. The measured T-ρ gradients of 22.9 to 27.9 %/°C under permafrost conditions, are in the range of the laboratory results of 29.8±10.6 %/°C (Krautblatter, 2009) **(Research question 4.2 and Chapter 7.3.6)**.

9 Conclusion and outlook

In this Ph.D.-thesis, the first automatic, continuous ERT monitoring system (AERT) for steep, permafrost-affected rockwalls, a new low-cost strategy for spatially and temporally highly resolved NSRT measurements and the first field evidence of a temperature-resistivity relationship were presented. The analysed ERT time series consists of more than 1,000 single Wenner datasets with more than 300,000 apparent resistivity datum points, which represents the largest and highest temporally resolved (published) dataset so far (Supper et al., 2014). Along with seismic refraction tomography (Krautblatter and Draebing, 2014), ERT provides the only available spatial monitoring technique for permafrost rocks, but it is much better suited than seismic refraction tomography to develop continuous monitoring under extreme conditions (AERT). The AERT system is able to detect short-term trigger mechanisms like pressurised fluid flow as well as long-term temperature trends as proxy for the mechanical state of permafrost rocks on a decimetre- to metre-scale. It can be concluded that major changes in resistivity are attributed to water flow in fractures, resulting in saturation and warming of the rock mass from the bottom upwards. This leads to (i) an increasing hydrostatic pressure until cleftwater pours out through open fractures and (ii) decreasing strengths of rock and ice and as a consequence to possible major instabilities and rock fall events.

Future developments in hard- and software are needed to enhance the reliability of the monitoring system. To implement such ERT measurements automatically in early warning systems, we need to improve:

1. Automatic error detection. Statistical methods, based on unprocessed raw data, can be used for an automated error control and are a prerequisite for optimal data inversion routines. The quantification of external influencing factors on automated ERT measurements needs further research to reliably interpret continuous AERT data sets with respect to subsurface temperature and saturation changes.
2. Evaluation of longer-term changes in the temperature-resistivity relationship, based on laboratory and field evidences.
3. Empirically constrained thresholds for fluid flow induced ERT changes.
4. Local validation measurements by piezometric information.

Overall, enhanced ERT monitoring systems have the potential to provide fundamental components for early warning systems in potentially hazardous permafrost-affected rock walls.

Acknowledgements

Figure 62: A perfect team.

Abbreviations

2D	two-dimensional
3D	three-dimensional
a	annum (year)
AERT	Automatic Electrical Resistivity Tomography
ALS	Airborne Laser Scanning
APCC	Austrian Panel for Climate Change
approx.	approximate
a.s.l.	above sea level
BTS	Bottom Temperature of the winter Snow cover
ca.	circa
DGPS	Differential Global Positioning System
e.g.	exempli gratia, for example
ERT	Electrical Resistivity Tomography
Figure	Figure
GCOS	Global Climate Observing System
GPR	Ground Penetrating Radar
GST	Ground Surface Temperature
GTOS	Global Terrestrial Observing Network
i.e.	id est, that is
IPA	International Permafrost Association
IPCC	Intergovernmental Panel for Climate Change
LIA	Little Ice Age
m	metre
MAAT	Mean Annual Air Temperature
MAGST	Mean Annual Ground Surface Temperature
NSRT	Near Surface Rock Temperature
NST	Near Surface Temperature
OpAL	Open Air Lab
PERMOS	Swiss Permafrost Network
T	Temperature
Tab.	Table
TLS	Terrestrial Laser Scanning
WEqT	Winter Equilibrium Temperature
ZAA	Zero Annual Amplitude
ρ	Resistivity

SI-units are used in accordance with their established abbreviations.

Index of Tables

Index of Figures

Bibliography

ACGR. 1988. *Glossary of permafrost and related ground ice terms. Permafrost Subcommittee of the Associate Committee on Geotechnical Research (ACGR),* Ottawa, National Research Council of Canada.

Adèr H, Mellenbergh GJ, Hand DJ. 2008. *Advising on research methods : a consultant's companion*, Johannes van Kessel Pub.

APCC. 2014. *Österreichischer Sachstandsbericht Klimawandel 2014 (AAR14). Austrian Panel on Climate Change (APCC),* Wien, Österreich, Verlag der Österreichischen Akademie der Wissenschaften.

Barker RD. 1989. DEPTH OF INVESTIGATION OF COLLINEAR SYMMETRICAL 4-ELECTRODE ARRAYS. *Geophysics,* **54,** 1031-1037, DOI: 10.1190/1.1442728.

Berthling I, Melvold K. 2008. Ground penetrating radar. *In:* HAUCK, C, KNEISEL, C (eds.) *Applied Geophysics in Periglacial Environments.* Cambridge: Cambridge University Press.

Böhm R, Auer I, Korus E. 2008. Das Klima der letzten beiden Jahrhunderte in Flattach. A tale of two valleys.

Bommer C, Phillips M, Keusen HR, Teysseire P. 2009. *Bauen im Permafrost: Ein Leitfaden für die Praxis.,* Birmensdorf, Eidgenössische Forschungsanstalt für Wald, Schnee und Landschaft - WSL.

Bottino G, Chiarle M, Joly A, Mortara G. 2002. Modelling rock avalanches and their relation to permafrost degradation in glacial environments. *Permafrost and Periglacial Processes,* **13,** 283-288, DOI: 10.1002/ppp.432.

Brabyn L, Zawar-Reza P, Stichbury G, Cary C, Storey B, Laughlin DC, Katurji M. 2014. Accuracy assessment of land surface temperature retrievals from Landsat 7 ETM + in the Dry Valleys of Antarctica using iButton temperature loggers and weather station data. *Environmental Monitoring and Assessment,* **186,** 2619-2628, DOI: 10.1007/s10661-013-3565-9.

Brenning A, Gruber S, Hoelzle M. 2005. Sampling and statistical analyses of BTS measurements. *Permafrost and Periglacial Processes,* **16,** 383-393, DOI: 10.1002/ppp.541.

Brown J, Ferrians Jr. OJ, Heginbottom JA, Melnikov ES. 1997. Circum-Arctic map of permafrost and ground-ice conditions. *U.S. Geological Survey in Cooperation with the Circum-Pacific Council for Energy and Mineral Resources,* **Circum-Pacific Map Series CP-45, scale 1:10,000,000, 1 sheet**.

Budd WF, Jacka TH. 1989. A review of ice rheology for ice sheet modelling. *Cold Regions Science and Technology,* **16,** 107-144, DOI: 10.1016/0165-232x(89)90014-1.

Christiansen HH, Etzelmuller B, Isaksen K, Juliussen H, Farbrot H, Humlum O, Johansson M, Ingeman-Nielsen T, Kristensen L, Hjort J, Holmlund P, Sannel ABK, Sigsgaard C, Akerman HJ, Foged N, Blikra LH, Pernosky MA, Odegard RS. 2010. The Thermal State of Permafrost in the Nordic Area during the International Polar Year 2007-2009. *Permafrost and Periglacial Processes,* **21,** 156-181, DOI: 10.1002/ppp.687.

Conacher A. 1988. The geomorphic significance of process measurements in an ancient landscape. *Catena Supplement,* **13,** 147-164.

Davies MCR, Hamza O, Harris C. 2001. The effect of rise in mean annual temperature on the stability of rock slopes containing ice-filled discontinuities. *Permafrost and Periglacial Processes,* **12,** 137-144, DOI: 10.1002/ppp.378.

Delaloye R, Lambiel C. 2005. Evidence of winter ascending air circulation throughout talus slopes and rock glaciers situated in the lower belt of alpine discontinuous permafrost (Swiss Alps). *Norsk Geografisk Tidsskrift – Norwegian Journal of Geography,* **59,** 194-203, DOI: 10.1080/00291950510020673.

Deline P. 2009. Interactions between rock avalanches and glaciers in the Mont Blanc massif during the late Holocene. *Quaternary Science Reviews,* **28,** 1070-1083, DOI: http://dx.doi.org/10.1016/j.quascirev.2008.09.025.

Draebing D, Haberkorn A, Krautblatter M, Phillips M. 2016. Spatial and temporal snow cover variability and resulting thermal and mechanical response in a steep permafrost rock wall. *11th International Conference on Permafrost 2016, At Potsdam.* Potsdam.

Draebing D, Krautblatter M, Dikau R. 2014. Interaction of thermal and mechanical processes in steep permafrost rock walls: A conceptual approach. *Geomorphology,* **226,** 226-235.

Dwivedi RD, Soni AK, Goel RK, Dube AK. 2000. Fracture toughness of rocks under sub-zero temperature conditions. *International Journal of Rock Mechanics and Mining Sciences,* **37,** 1267-1275, DOI: 10.1016/s1365-1609(00)00051-4.

Ebohon B, Schrott L. 2008. Modeling Mountain Permafrost Distribution. A New Permafrost Map of Austria. *In:* KANE, DL, HINKEL, KM (eds.) *Proceedings of the 9th International Conference on Permafrost.* Fairbanks, Alaska, USA.

Etzelmüller B, Berthling I, Sollid JL. 2003. Aspects and concepts on the geomorphological significance of Holocene permafrost in southern Norway. *Geomorphology,* **52,** 87-104, DOI: http://dx.doi.org/10.1016/S0169-555X(02)00250-7.

Etzelmuller B, Odegard RS, Berthling I, Sollid JL. 2001. Terrain parameters and remote sensing data in the analysis of permafrost distribution and periglacial processes: Principles and examples from southern Norway. *Permafrost and Periglacial Processes,* **12,** 79-92, DOI: 10.1002/ppp384.

Fischer L, Huggel C, Kaab A, Haeberli W. 2013. Slope failures and erosion rates on a glacierized high-mountain face under climatic changes. *Earth Surface Processes and Landforms,* **38,** 836-846, DOI: 10.1002/esp.3355.

Fischer L, Kaab A, Huggel C, Noetzli J. 2006. Geology, glacier retreat and permafrost degradation as controlling factors of slope instabilities in a high-mountain rock wall: the Monte Rosa east face. *Natural Hazards and Earth System Sciences,* **6,** 761-772.

French HM. 2007. Permafrost. *The Periglacial Environment.* John Wiley & Sons Ltd,.

Geertsema M, Clague JJ, Schwab JW, Evans SG. 2006. An overview of recent large catastrophic landslides in northern British Columbia, Canada. *Engineering Geology,* **83,** 120-143, DOI: http://dx.doi.org/10.1016/j.enggeo.2005.06.028.

Gorbunov AR, Marchenko SS, Seversky EV. 2004. The thermal environment of blocky materials in the mountains of central Asia. *Permafrost and Periglacial Processes,* **15,** 95-98, DOI: 10.1002/ppp.478.

Grohmann CH, Smith MJ, Riccomini C. 2011. Multiscale Analysis of Topographic Surface Roughness in the Midland Valley, Scotland. *Ieee Transactions on Geoscience and Remote Sensing,* **49,** 1200-1213, DOI: 10.1109/tgrs.2010.2053546.

Gross J, Ligges U. 2012. Tests for Normality. R package version 1.0-2.

Gruber S, Haeberli W. 2007. Permafrost in steep bedrock slopes and its temperature-related destabilization following climate change. *Journal of Geophysical Research-Earth Surface,* **112,** 10, DOI: 10.1029/2006jf000547.

Gruber S, Hoelzle M. 2008. The cooling effect of coarse blocks revisited: a modeling study of a purely conductive mechanism. *In:* KANE, DL, HINKEL, KM (eds.) *Proceedings of the 9th International Conference on Permafrost.* Fairbanks, Alaska, USA.

Gruber S, Hoelzle M, Haeberli W. 2004a. Permafrost thaw and destabilization of Alpine rock walls in the hot summer of 2003. *Geophysical Research Letters,* **31,** 4, DOI: 10.1029/2004gl020051.

Gruber S, Hoelzle M, Haeberli W. 2004b. Rock-wall temperatures in the Alps: modelling their topographic distribution and regional differences. *Permafrost and Periglacial Processes,* **15,** 299-307, DOI: 10.1002/ppp.501.

Gruber S, King L, Kohl T, Herz T, Haeberli W, Hoelzle M. 2004c. Interpretation of geothermal proffies perturbed by topography: The Alpine Permafrost boreholes at Stockhorn Plateau, Switzerland. *Permafrost and Periglacial Processes,* **15,** 349-357, DOI: 10.1002/ppp.503.

Gruber S, Peter M, Hoelzle M, Woodhatch I, Haeberli W. 2003. Surface temperatures in steep alpine rock faces – A strategy for regional-scale measurement and modelling. *In:* PHILLIPS, M, SPRINGMAN, SM, ARENSON, L (eds.) *Proc. 8th International Conference on Permafrost, 21-25 July, Zurich, Switzerland.*

Gruber SP, M.; Hoelzle, M.; Woodhatch, I.; Haeberli, W. . 2003. Surface temperatures in steep Alpine rock faces - a strategy for regional-scale measurement and modelling. *Proceedings of the 8th International Conference on Permafrost 2003, Zurich, Switzerland***,** 325–330.

Grunewald T, Schirmer M, Mott R, Lehning M. 2010. Spatial and temporal variability of snow depth and ablation rates in a small mountain catchment. *Cryosphere,* **4,** 215-225, DOI: 10.5194/tc-4-215-2010.

GTN-P. 2015. *The Global Terrestrial Network for Permafrost* [Online]. Available: http://gtnp.arcticportal.org/ [Accessed 07.02 2015].

Gubler S, Fiddes J, Keller M, Gruber S. 2011. Scale-dependent measurement and analysis of ground surface temperature variability in alpine terrain. *Cryosphere,* **5,** 431-443, DOI: 10.5194/tc-5-431-2011.

Guodong C, Dramis F. 1992. Distribution of mountain permafrost and climate. *Permafrost and Periglacial Processes,* **3,** 83-91, DOI: 10.1002/ppp.3430030205.

Haeberli W. 1973. Die Basis Temperatur der winterlichen Schneedecke als möglicher Indikator für die Verbreitung von Permafrost in den Alpen. *Zeitschrift für Gletschologie und Glazialgeologie,* **9,** 221-227.

Haeberli W. 1978. Special aspects of high mountain permafrost methology and zonation in the Alps. *Permafrost, Proceedings of the Third International Conference on Permafrost, Edmonton, Alberta, Canada.* National Research Council of Canada, Ottawa.

Haeberli W, Huggel C, Kääb A, Zgraggen-Oswald S, Polkvoj A, Galushkin I, Zotikov I, Osokin N. 2004. The Kolka-Karmadon rock/ice slide of 20 September 2002: an extraordinary event of historical dimensions in

North Ossetia, Russian Caucasus. *Journal of Glaciology,* **50,** 533-546, DOI: 10.3189/172756504781829710.

Haeberli W, Noetzli J, Arenson L, Delaloye R, Gartner-Roer I, Gruber S, Isaksen K, Kneisel C, Krautblatter M, Phillips M. 2010. Mountain permafrost: development and challenges of a young research field. *Journal of Glaciology,* **56,** 1043-1058.

Haneberg WC, Creighton AL, Medley EW, Jonas DA. Use of LIDAR to assess slope hazards at the Lihir gold mine, Papua New Guinea. *In:* HUNGR, O, FELL, R, COUTURE, R, EBERHARDT, E, eds. International Conference on Landslide Risk Management, 2005 Vancouver BC, Canada.

Hanson S, Hoelzle M. 2004. The thermal regime of the active layer at the Murtel rock glacier based on data from 2002. *Permafrost and Periglacial Processes,* **15,** 273-282, DOI: 10.1002/ppp.499.

Harris C, Arenson LU, Christiansen HH, Etzelmuller B, Frauenfelder R, Gruber S, Haeberli W, Hauck C, Hoelzle M, Humlum O, Isaksen K, Kaab A, Kern-Luetschg MA, Lehning M, Matsuoka N, Murton JB, Noezli J, Phillips M, Ross N, Seppala M, Springman SM, Muehll DV. 2009. Permafrost and climate in Europe: Monitoring and modelling thermal, geomorphological and geotechnical responses. *Earth-Science Reviews,* **92,** 117-171, DOI: 10.1016/j.earscirev.2008.12.002.

Harris C, Haeberli W, Vonder Muhll D, King L. 2001. Permafrost monitoring in the high mountains of Europe: the PACE project in its global context. *Permafrost and Periglacial Processes,* **12,** 3-11, DOI: 10.1002/ppp.377.

Harris C, Isaksen K. 2008. Recent Warming of European Permafrost: Evidence from Borehole Monitoring. *In:* KANE, DL, HINKEL, KM (eds.) *Ninth International Conference on Permafrost. Institute of Northern Engineering, University of Alaska Fairbanks.*

Harris C, Vonder Muhll D, Isaksen K, Haeberli W, Sollid JL, King L, Holmlund P, Dramis F, Guglielmini M, Palacios D. 2003. Warming permafrost in European mountains. *Global and Planetary Change,* **39,** 215-225.

Harris SA, Pedersen DE. 1998. Thermal regimes beneath coarse blocky materials. *Permafrost and Periglacial Processes,* **9,** 107-120, DOI: 10.1002/(sici)1099-1530(199804/06)9:2<107::aid-ppp277>3.0.co;2-g.

Hartmeyer I, Keuschnig M, Delleske R, Schrott L. 2012a. Reconstruction of the Magnetköpfl event - Detecting rock fall release zones using terrestrial laser scanning, Hohe Tauern, Austria. *Geophysical Research Abstracts* **14**.

Hartmeyer I, Keuschnig M, Schrott L. 2012b. A Scale-Oriented Approach for the Long-Term Monitoring of Ground Thermal Conditions in Permafrost-Affected Rock Faces, Kitzsteinhorn, Hohe Tauern Range, Austria. *Austrian Journal of Earth Sciences,* **105,** 128-139.

Hasler A, Gruber S, Beutel J. 2012. Kinematics of steep bedrock permafrost. *Journal of Geophysical Research-Earth Surface,* **117,** 17, DOI: 10.1029/2011jf001981.

Hauck C, Kneisel C. 2008. *Applied geophysics in periglacial environments,* London, Cambridge University Press.

Hauck C, Vonder Muhll D. 2003. Inversion and interpretation of two-dimensional geoelectrical measurements for detecting permafrost in mountainous regions. *Permafrost and Periglacial Processes,* **14,** 305-318, DOI: 10.1002/ppp.462.

Heritage GL, Milan DJ. 2009. Terrestrial Laser Scanning of grain roughness in a gravel-bed river. *Geomorphology,* **113,** 4-11, DOI: 10.1016/j.geomorph.2009.03.021.

Herz T. 2006. *Das Mikroklima grobblockiger Schutthalden der alpinen Periglazialstufe und seine Auswirkungen auf Energieaustauschprozesse zwischen Atmosphäre und Lithosphäre.* University of Gießen.

Hilbich C, Fuss C, Hauck C. 2011. Automated Time-lapse ERT for Improved Process Analysis and Monitoring of Frozen Ground. *Permafrost and Periglacial Processes,* **22,** 306-319, DOI: 10.1002/ppp.732.

Hilbich C, Hauck C, Hoelzle M, Scherler M, Schudel L, Voelksch I, Muehll DV, Maeusbacher R. 2008. Monitoring mountain permafrost evolution using electrical resistivity tomography: A 7-year study of seasonal, annual, and long-term variations at Schilthorn, Swiss Alps. *Journal of Geophysical Research-Earth Surface,* **113,** 12, DOI: 10.1029/2007jf000799.

Hilbich C, Marescot L, Hauck C, Loke MH, Mausbacher R. 2009. Applicability of Electrical Resistivity Tomography Monitoring to Coarse Blocky and Ice-rich Permafrost Landforms. *Permafrost and Periglacial Processes,* **20,** 269-284, DOI: 10.1002/ppp.652.

Hiller C, Keuschnig M, Hartmeyer I, Goetz J. 2014. Assessment of the temperature variability at the snow-ground interface – concept and first results. *Geophysical Research Abstracts* **16**.

Hipp T, Etzelmüller B, Westermann S. 2014. Permafrost in Alpine Rock Faces from Jotunheimen and Hurrungane, Southern Norway. *Permafrost and Periglacial Processes,* **25,** 1-13, DOI: 10.1002/ppp.1799.

Hodge R, Brasington J, Richards K. 2009. Analysing laser-scanned digital terrain models of gravel bed surfaces: linking morphology to sediment transport processes and hydraulics. *Sedimentology,* **56,** 2024-2043, DOI: 10.1111/j.1365-3091.2009.01068.x.

Hoeck V, Pestal G, Brandmaier P, Clar E, Cornelius H, Frank W, Matl H, Neumayer P, Petrakakis K, Stadlmann T, Steyrer H. 1994. Geologische Karte der Republik Österreich, Blatt 153 Großglockner. Geologische Bundesanstalt, Wien.

Hoelzle M. 1992. Permafrost occurrence from BTS measurements and climatic parameters in the eastern Swiss Alps. *Permafrost and Periglacial Processes,* **3,** 143-147, DOI: 10.1002/ppp.3430030212.

Hoelzle M. 1994. Permafrost und Gletscher im Oberengadin. Grundlagen und Anwendungsbeispiele automatisierter Schätzverfahren. *Mitteilungen, Versuchsanstalt für Wasserbau, Hydrologie und Glaziologie der ETH Zürich,* **119**.

Hoelzle M, Wegmann M, Krummenacher B. 1999. Miniature temperature dataloggers for mapping and monitoring of permafrost in high mountain areas: First experience from the Swiss Alps. *Permafrost and Periglacial Processes,* **10,** 113-124, DOI: 10.1002/(sici)1099-1530(199904/06)10:2<113::aid-ppp317>3.0.co;2-a.

Höfer-Öllinger G, Keuschnig M, Krautblatter M, Schober A. 2015. Climate Change Impacts on High Alpine Infrastructures: An Example from the Kitzsteinhorn (3200 m), Salzburg, Austria. *In:* LOLLINO, G, MANCONI, A, CLAGUE, J, SHAN, W, CHIARLE, M (eds.) *Engineering Geology for Society and Territory - Volume 1.* Springer International Publishing.

Huggel C. 2009. Recent extreme slope failures in glacial environments: effects of thermal perturbation. *Quaternary Science Reviews,* **28,** 1119-1130, DOI: 10.1016/j.quascirev.2008.06.007.

Huggel C, Clague JJ, Korup O. 2012. Is climate change responsible for changing landslide activity in high mountains? *Earth Surface Processes and Landforms,* **37,** 77-91, DOI: 10.1002/esp.2223.

Huggel C, Gruber S, Caplan-Auerbach J, Wessels RL, Molnia BF. 2008. The 2005 Mt. Steller, Alaska, rock-ice avalanche: A large slope failure in cold permafrost. *In:* KANE, DL, HINKEL, KM (eds.) *Ninth International Conference on Permafrost. Institute of Northern Engineering, University of Alaska Fairbanks.*

Huggel C, Zgraggen-Oswald S, Haeberli W, Kääb A, Polkvoj A, Galushkin I, Evans SG. 2005. The 2002 rock/ice avalanche at Kolka/Karmadon, Russian Caucasus: assessment of extraordinary avalanche formation and mobility, and application of QuickBird satellite imagery. *Nat. Hazards Earth Syst. Sci.,* **5,** 173-187, DOI: 10.5194/nhess-5-173-2005.

Ikeda A, Matsuoka N. 1999. Measurement of bottom temperature of the winter snow cover (BTS) in relation to rock-glacier activity, Corviglia, Swiss Alps: a preliminary report. *Annual report, Institute of Geosciences, University of Tsukuba,* **25,** 13-19.

IPA. 2015. *What is permafrost?* [Online]. Available: http://ipa.arcticportal.org/resources/what-is-permafrost [Accessed 26.01 2015].

IPCC. 2013. *Climate Change 2013: The Physical Science Basis. Contribution of Working Group I to the Fifth Assessment Report of the Intergovernmental Panel on Climate Change,* Cambridge, United Kingdom and New York, NY, USA, Cambridge University Press.

IPCC. 2014. Summary for Policymakers. *In:* FIELD, CB, BARROS, VR, DOKKEN, DJ, MACH, KJ, MASTRANDREA, MD, BILIR, TE, CHATTERJEE, M, EBI, KL, ESTRADA, YO, GENOVA, RC, GIRMA, B, KISSEL, ES, LEVY, AN, MACCRACKEN, S, MASTRANDREA, PR, WHITE, LL (eds.) *Climate Change 2014: Impacts, Adaptation, and Vulnerability. Part A: Global and Sectoral Aspects. Contribution of Working Group II to the Fifth Assessment Report of the Intergovernmental Panel on Climate Change.* Cambridge, United Kingdom, and New York, NY, USA: Cambridge University Press.

Isaksen K, Sollid JL, Holmlund P, Harris C. 2007. Recent warming of mountain permafrost in Svalbard and Scandinavia. *Journal of Geophysical Research-Earth Surface,* **112,** 11, DOI: 10.1029/2006jf000522.

Isaksen K, Vonder Muhll D, Gubler H, Kohl T, Sollid JL. 2000. Ground surface-temperature reconstruction based on data from a deep borehole in permafrost at Janssonhaugen, Svalbard. *In:* STEFFEN, K (ed.) *Annals of Glaciology, Vol 31, 2000.* Cambridge: Int Glaciological Soc.

Ishikawa M. 2003. Thermal regimes at the snow-ground interface and their implications for permafrost investigation. *Geomorphology,* **52,** 105-120, DOI: 10.1016/s0169-555x(02)00251-9.

Ishikawa M, Hirakawa K. 2000. Mountain permafrost distribution based on BTS measurements and DC resistivity soundings in the Daisetsu Mountains, Hokkaido, Japan. *Permafrost and Periglacial Processes,* **11,** 109-123, DOI: 10.1002/1099-1530(200004/06)11:2<109::aid-ppp343>3.0.co;2-o.

Jaesche P. 1999. Bodenfrost und Solifluktionsdynamik in einem alpinen Periglazialgebiet (Hohe Tauern, Osttirol). *Naturwissenschaftliche Gesellschaft Bayreuth,* **136**.

Jaesche P, Huwe B, Stingl H. 2002. Temporal variability of alpine solifluction. a modelling approach. *Geographica Helvetica,* **57,** 157-169.

Jaesche P, Veit H, Huwe B. 2003. Snow cover and soil moisture controls on solifluction in an area of seasonal frost, eastern Alps. *Permafrost and Periglacial Processes,* **14,** 399-410, DOI: 10.1002/ppp.471.

Keller F. 1992. Automated mapping of mountain permafrost using the program PERMAKART within the geographical information system ARC/INFO. *Permafrost and Periglacial Processes,* **3,** 133-138.

Keller F. 1994. Interaktion zwischen Schnee und Permafrost. Eine Grundlagenstudie im Oberengadin. *Mitteilungen, Versuchsanstalt für Wasserbau, Hydrologie und Glaziologie der ETH Zürich,* **127**.

Keller F, Tamas M. 2003. Enhanced ground cooling in periods with thin snow cover in the Swiss National Park. *In:* PHILLIPS, M, SPRINGMAN, SM, ARENSON, L (eds.) *Proc. 8th International Conference on Permafrost, 21-25 July, Zurich, Switzerland.*

Kellerer-Pirklbauer A, Avian A, Lieb GK, Rieckh M. 2008. Temperatures in Alpine Rockwalls during the Warm Winter 2006/2007 in Austria and their Significance for Mountain Permafrost: Preliminary Results. *In:* KANE, DL, HINKEL, KM (eds.) *Extended Abstracts, Ninth International Conference on Permafrost (NICOP), University of Alaska, Fairbanks, USA, June – July 2008.*

Keuschnig M, Hartmeyer I, Höfer-Öllinger G, Schober A, Krautblatter M, Schrott L. 2015. Permafrost-Related Mass Movements: Implications from a Rock Slide at the Kitzsteinhorn, Austria. *Engineering Geology for Society and Territory - Volume 1***,** 255-259, DOI: 10.1007/978-3-319-09300-0_48.

Keuschnig M, Hartmeyer I, Krautblatter M. prepared for submission-a. A low-cost strategy for near-surface rock temperature measurements using iButtons. *Cryosphere*.

Keuschnig M, Hartmeyer I, Otto JC, Schrott L. 2011. A new permafrost and mass movement monitoring test site in the Eastern Alps—concept and first results of the MOREXPERT project. *In:* BORSDORF, A, STÖTTER, J, VEULLIET, E (eds.) *Managing Alpine future II—inspire and drive sustainable mountain regions. Proceedings of the Innsbruck Conference, 21–23 November 2011.* IGF-Forschungsberichte 4: Austrian Academy of Sciences.

Keuschnig M, Hartmeyer I, Schmidjell A, Schrott L. 2012. The adaptation of iButtons® for near-surface rock temperature and thermal offset measurements in a high alpine environment – Instrumentation and first results, Kitzsteinhorn (3203 m), Hohe Tauern, Austria. *Geophysical Research Abstracts* **14**.

Keuschnig M, Krautblatter M, Hartmeyer I. prepared for submission-b. Field evidence for temperature-resistivity relationship of permafrost-affected alpine rock walls. *The Cryosphere*.

Keuschnig M, Krautblatter M, Hartmeyer I, Fuss C, Schrott L. accepted. Automated Electrical Resistivity Tomography testing for Early Warning in Unstable Permafrost Rock Walls around Alpine Infrastructure. *Permafrost and Periglacial Processes*.

King L. 1983. High mountain permafrost in Scandinavia. *Permafrost, Proceedings of the Fourth International Conference on Permafrost, 17–22 July, Fairbanks, Alaska.* National Academy Press, Washington, DC.

King L. 1986. Zonation and Ecology of High Mountain Permafrost in Scandinavia. *Geografiska Annaler. Series A, Physical Geography,* **68,** 131-139, DOI: 10.2307/521452.

Klee A, Riedl C. 2011. Case studies in the European Alps - Hoher Sonnblick, Central Austrian Alps. *In:* KELLERER-PIRKLBAUER, A, LIEB, GK, SCHOENREICH, P, DELINE, P, POGLIOTTI, P (eds.) *Thermal and geomorphic permafrost response to present and future climate change in the European Alps. PermaNET project, final report of Action 5.3.*

Kneisel C, Hauck C, Fortier R, Moorman B. 2008. Advances in geophysical methods for permafrost investigations. *Permafrost and Periglacial Processes,* **19,** 157-178, DOI: 10.1002/ppp.616.

Kneisel C, Rödder T, Schwindt D. 2014. Frozen ground dynamics resolved by multi-year and year-around electrical resistivity monitoring at three alpine sites in the Swiss Alps. *Near Surface Geophysics,* **12,** 117-132, DOI: 10.3997/1873-0604.2013057.

Koefoed O. 1979. *Geosounding principles, 1: Resistivity sounding measurements*, Elsevier/North-Holland.

Koestel J, Kemna A, Javaux M, Binley A, Vereecken H. 2008. Quantitative imaging of solute transport in an unsaturated and undisturbed soil monolith with 3-D ERT and TDR. *Water Resources Research,* **44,** 17, DOI: 10.1029/2007wr006755.

Krautblatter M. 2009. *Detection and quantification of permafrost change in alpine rock walls and implications for rock instability.* Ph.D.-Thesis, University of Bonn.

Krautblatter M, Dikau R. 2007. TOWARDS A UNIFORM CONCEPT FOR THE COMPARISON AND EXTRAPOLATION OF ROCKWALL RETREAT AND ROCKFALL SUPPLY. *Geografiska Annaler: Series A, Physical Geography,* **89,** 21-40, DOI: 10.1111/j.1468-0459.2007.00305.x.

Krautblatter M, Draebing D. 2014. Pseudo 3D - P-wave refraction seismic monitoring of permafrost in steep unstable bedrock. *J. Geophys. Res. - Earth Surface,* **VOL. 119,** 287-299, DOI: 10.1002/2012JF002638.

Krautblatter M, Funk D, Gunzel FK. 2013. Why permafrost rocks become unstable: a rock-ice-mechanical model in time and space. *Earth Surface Processes and Landforms,* **38,** 876-887, DOI: 10.1002/esp.3374.

Krautblatter M, Hauck C. 2007. Electrical resistivity tomography monitoring of permafrost in solid rock walls. *Journal of Geophysical Research-Earth Surface,* **112**, DOI: 10.1029/2006jf000546.

Krautblatter M, Huggel C, Deline P, Hasler A. 2012. Research Perspectives on Unstable High-alpine Bedrock Permafrost: Measurement, Modelling and Process Understanding. *Permafrost and Periglacial Processes,* **23,** 80-88, DOI: 10.1002/ppp.740.

Krautblatter M, Moore JR. 2014. Rock slope instability and erosion: toward improved process understanding. *Earth Surface Processes and Landforms,* **39,** 1273-1278, DOI: 10.1002/esp.3578.

Krautblatter M, Verleysdonk S, Flores-Orozco A, Kemna A. 2010. Temperature-calibrated imaging of seasonal changes in permafrost rock walls by quantitative electrical resistivity tomography (Zugspitze, German/Austrian Alps). *Journal of Geophysical Research-Earth Surface,* **115**, DOI: 10.1029/2008jf001209.

LaBrecque DJ, Miletto M, Daily W, Ramirez A, Owen E. 1996. The effects of noise on Occam's inversion of resistivity tomography data. *Geophysics,* **61,** 538-548, DOI: 10.1190/1.1443980.

Lachenbruch AH, Marshall BV. 1986. CHANGING CLIMATE - GEOTHERMAL EVIDENCE FROM PERMAFROST IN THE ALASKAN ARCTIC. *Science,* **234,** 689-696, DOI: 10.1126/science.234.4777.689.

Lambiel C, Pieracci K. 2008. Permafrost distribution in talus slopes located within the alpine periglacial belt, Swiss Alps. *Permafrost and Periglacial Processes,* **19,** 293-304, DOI: 10.1002/ppp.624.

Lewkowicz AG. 2008. Evaluation of miniature temperature-loggers to monitor snowpack evolution at mountain permafrost sites, northwestern Canada. *Permafrost and Periglacial Processes,* **19,** 323-331, DOI: 10.1002/ppp.625.

Lewkowicz AG, Bonnaventure PP, Smith SL, Kuntz Z. 2012. SPATIAL AND THERMAL CHARACTERISTICS OF MOUNTAIN PERMAFROST, NORTHWEST CANADA. *Geografiska Annaler: Series A, Physical Geography,* **94,** 195-213, DOI: 10.1111/j.1468-0459.2012.00462.x.

Lewkowicz AG, Etzelmuller B, Smith SL. 2011. Characteristics of Discontinuous Permafrost based on Ground Temperature Measurements and Electrical Resistivity Tomography, Southern Yukon, Canada. *Permafrost and Periglacial Processes,* **22,** 320-342, DOI: 10.1002/ppp.703.

Lipovsky P, Evans S, Clague J, Hopkinson C, Couture R, Bobrowsky P, Ekström G, Demuth M, Delaney K, Roberts N, Clarke G, Schaeffer A. 2008. The July 2007 rock and ice avalanches at Mount Steele, St. Elias Mountains, Yukon, Canada. *Landslides,* **5,** 445-455, DOI: 10.1007/s10346-008-0133-4.

Luetschg M, Lehning M, Haeberli W. 2008. A sensitivity study of factors influencing warm/thin permafrost in the Swiss Alps. *Journal of Glaciology,* **54,** 696-704, DOI: 10.3189/002214308786570881.

Magnin F, Deline P, Ravanel L, Noetzli J, Pogliotti P. 2015. Thermal characteristics of permafrost in the steep alpine rock walls of the Aiguille du Midi (Mont Blanc Massif, 3842 m a.s.l). *The Cryosphere,* **9,** 109-121, DOI: 10.5194/tc-9-109-2015.

Mair V, Zischg A, Lang K, Tonitandel D, Krainer K, Kellerer-Pirklbauer A, Deline P, Schoenreich P, Cremonese E, Pogliotti P, Gruber S, Böckli L. 2011. PermaNET - Permafrost Long-term Monitoring Network. Synthesis report. *INTERPRAEVENT Journal series 1.*

Matsuoka N. 2008. Frost weathering and rockwall erosion in the southeastern Swiss Alps: Long-term (1994-2006) observations. *Geomorphology,* **99,** 353-368, DOI: 10.1016/j.geomorph.2007.11.013.

Matsuoka N, Murton J. 2008. Frost weathering: Recent advances and future directions. *Permafrost and Periglacial Processes,* **19,** 195-210, DOI: 10.1002/ppp.620.

MAXIM. 2016. *DSL1922L iButton Temperature Loggers with 8KB Data-Log Memory* [Online]. Available: https://www.maximintegrated.com/en/products/digital/data-loggers/DS1922L.html [Accessed 12.07.2016.

Mcquillin R, Bacon M, Barclay W. 1984. *An Introductions to Seismic Interpretation,* London, Graham & Trotman.

Mellor M. 1973. Mechanical properties of rocks at low temperatures. Paper presented at 2nd International Conference on Permafrost, Int. Permafrost Association, Yakutsk, Russia. 334-344.

Moore JR, Gischig V, Katterbach M, Loew S. 2011. Air circulation in deep fractures and the temperature field of an alpine rock slope. *Earth Surface Processes and Landforms,* **36,** 1985-1996, DOI: 10.1002/esp.2217.

Murton JB, Peterson R, Ozouf JC. 2006. Bedrock fracture by ice segregation in cold regions. *Science,* **314,** 1127-1129, DOI: 10.1126/science.1132127.

Musil M, Maurer H, Green AG, Horstmeyer H, Nitsche FO, Vonder Muhll D, Springman S. 2002. Shallow seismic surveying of an Alpine rock glacier. *Geophysics,* **67,** 1701-1710, DOI: 10.1190/1.1527071.

Noetzli J, Vonder Muehll D. 2010. Permafrost in Swizerland 2006/2007 and 2007/2008. Glaciological Report (Permafrost) No. 8/9 of the Cryospheric Commission of the Swiss Academy of Sciences.

Nogués-Bravo D, Araújo MB, Errea M, Martinez-Rica J. 2007. Exposure of global mountain systems to climate warming during the 21st Century. *Global Environmental Change,* **17,** 420-428.

Nyenhuis M. 2006. *Permafrost und Sedimenthaushalt in einem alpinen Geosystem.* Ph.D., Department of Geography, University of Bonn.

Oldenburg DW, Li YG. 1999. Estimating depth of investigation in dc resistivity and IP surveys. *Geophysics,* **64,** 403-416, DOI: 10.1190/1.1444545.

Otto JC, Keuschnig M. 2014. Permafrost-Glacier Interaction - Process Understanding of Permafrost Reformation and Degradation. *In:* RUTZINGER, M, HEINRICH, K, BORSDORF, A, STÖTTER, J (eds.) *permAfrost – Austrian Permafrost Research Initiative - Final Report.* IGF-Forschungsberichte 6: Austrian Academy of Sciences.

Otto JC, Keuschnig M, Gotz J, Marbach M, Schrott L. 2012. Detection of Mountain Permafrost by Combining High Resolution Surface and Subsurface Information - an Example from the Glatzbach Catchment, Austrian Alps. *Geografiska Annaler Series a-Physical Geography,* **94A,** 43-57, DOI: DOI 10.1111/j.1468-0459.2012.00455.x.

Otto JC, Sass O. 2006. Comparing geophysical methods for talus slope investigations in the Turtmann valley (Swiss Alps). *Geomorphology,* **76,** 257-272, DOI: 10.1016/j.geomorph.2005.11.008.

Park H, Walsh J, Fedorov AN, Sherstiukov AB, Iijima Y, Ohata T. 2013. The influence of climate and hydrological variables on opposite anomaly in active-layer thickness between Eurasian and North American watersheds. *Cryosphere,* **7,** 631-645, DOI: 10.5194/tc-7-631-2013.

PermaNET. 2015. *Permafrost Monitoring Network* [Online]. Available: http://www.permanet-alpinespace.eu/ [Accessed 30.01 2015].

PERMOS. 2013. Permafrost in Switzerland 2008/2009 and 2009/2010. *In:* NOETZLI, J (ed.) *Glaciological Report (Permafrost) 10/11.* Cryospheric Commission of the Swiss Academy of Sciences.

PERMOS. 2015. *Swiss Permafrost Monitoring Network* [Online]. Available: http://www.permos.ch/ [Accessed 30.01 2015].

Phillips M, Mutter EZ, Kern-Luetschg M, Lehning M. 2009. Rapid Degradation of Ground Ice in a Ventilated Talus Slope: Fluela Pass, Swiss Alps. *Permafrost and Periglacial Processes,* **20,** 1-14, DOI: 10.1002/ppp.638.

Pudasaini SP, Krautblatter M. 2014. A two-phase mechanical model for rock-ice avalanches. *Journal of Geophysical Research: Earth Surface,* **119,** 2272-2290, DOI: 10.1002/2014JF003183.

Rabatel A, Deline P, Jaillet S, Ravanel L. 2008. Rock falls in high-alpine rock walls quantified by terrestrial lidar measurements: A case study in the Mont Blanc area. *Geophysical Research Letters,* **35**, DOI: 10.1029/2008gl033424.

Ravanel L, Deline P. 2011. Climate influence on rockfalls in high-Alpine steep rockwalls: The north side of the Aiguilles de Chamonix (Mont Blanc massif) since the end of the 'Little Ice Age'. *Holocene,* **21,** 357-365, DOI: 10.1177/0959683610374887.

Ravanel L, Deline P, Magnin F, Malet E, Noetzli J. 2011. The first year of borehole measurements in the rock permafrost at Aiguille du Midi (3842 m a.s.l., Mont Blanc massif). *Geophysical Research Abstracts* **13**.

Rennert R. 1991. *Geoökologische Untersuchungen zur Bodengefrornis an der Untergrenze des alpinen Permafrostes.* University of Bayreuth.

Robertson EC. 1988. Thermal Properties of Rocks. *Open-File Report 88-441.* United States Department of the Interior, Geological Survey, Reston, Virginia.

Rodder T, Kneisel C. 2012. Influence of snow cover and grain size on the ground thermal regime in the discontinuous permafrost zone, Swiss Alps. *Geomorphology,* **175,** 176-189, DOI: 10.1016/j.geomorph.2012.07.008.

Rosset E, Hilbich C, Schneider S, Hauck C. 2013. Automatic filtering of ERT monitoring data in mountain permafrost. *Near Surface Geophysics,* **11,** 423-433, DOI: 10.3997/1873-0604.2013003.

Roy A, Apparao A. 1971. DEPTH OF INVESTIGATION IN DIRECT CURRENT METHODS. *Geophysics,* **36,** 943-&, DOI: 10.1190/1.1440226.

Safanda J. 1999. Ground surface temperature as a function of slope angle and slope orientation and its effect on the subsurface temperature field. *Tectonophysics,* **306,** 367-375, DOI: 10.1016/s0040-1951(99)00066-9.

Sanderson T. 1987. *Ice mechanics and risks to offshore structures*, Springer Netherlands.

Sass O. 2004. Rock moisture fluctuations during freeze-thaw cycles: Preliminary results from electrical resistivity measurements. *Polar Geography,* **28,** 13-31.

Sass O. 2005. Spatial patterns of rockfall intensity in the northern Alps. *In:* SCHMIDT, KH, BECHT, M, BRUNOTTE, E, EITEL, B, SCHROTT, L (eds.) *Geomorphology in Environmental Application:.* Stuttgart: Gebruder Borntraeger.

Sättele M, Krautblatter M, Bründl M, Straub D. 2015. Forecasting rock slope failure: how reliable and effective are warning systems? *Landslides***,** 1-14, DOI: 10.1007/s10346-015-0605-2.

Schnaubelt G. 2011. GeoTom. 7.24 ed.: Geolog2000.

Schneider S, Hoelzle M, Hauck C. 2012. Influence of surface and subsurface heterogeneity on observed borehole temperatures at a mountain permafrost site in the Upper Engadine, Swiss Alps. *Cryosphere,* **6,** 517-531, DOI: 10.5194/tc-6-517-2012.

Schober A, Bannwart C, Keuschnig M. 2012. Rockfall modelling in high alpine terrain – validation and limitations / Steinschlagsimulation in hochalpinem Raum – Validierung und Limitationen. *Geomechanics and Tunnelling,* **5,** 368-378, DOI: 10.1002/geot.201200025.

Schoenrich P, Bodin X, Krysiecki J-M, Deline P, Ravanel L. 2010. Permafrost in France. *PermaFRANCE Network Report.* Grenoble: PermaFRANCE.

Schoner W, Boeckli L, Hausmann H, Otto JC, Reisenhofer S, Riedl C, Seren S. 2012. SPATIAL PATTERNS OF PERMAFROST AT HOHER SONNBLICK (AUSTRIAN ALPS) - EXTENSIVE FIELD-MEASUREMENTS AND MODELLING APPROACHES. *Austrian Journal of Earth Sciences,* **105,** 154-168.

Schrott L. 1994. *Die Solarstrahlung als steuernder Faktor im Geosystem der subtropischen semiariden Hochanden (Agua Negra, San Juan, Argentinien).*

Schrott L. 1996. Some geomorphological-hydrological characteristics of rock glaciers in the Andes, San Juan, Argentina. *Zeitschrift für Geomorphologie,* **Supplementband 104,** 161-173.

Schrott L, Otto JC, Keller F. 2012. MODELLING ALPINE PERMAFROST DISTRIBUTION IN THE HOHE TAUERN REGION, AUSTRIA. *Austrian Journal of Earth Sciences,* **105,** 169-183.

Schrott L, Sass O. 2008. Application of field geophysics in geomorphology: Advances and limitations exemplified by case studies. *Geomorphology,* **93,** 55-73, DOI: 10.1016/j.geomorph.2006.12.024.

Seguin MK. 1978. Temperature-electrical resistivity relationship in continuous permafrost at Purtuniq, Ungava Peninsula, paper presented at 3rd Int. Conf. on Permafrost, NRC, Edmonton, Canada.

Selby MJ. 1993. *Hillslope Materials and Processes. Second Edition*, Oxford University Press.

Slater L, Binley AM, Daily W, Johnson R. 2000. Cross-hole electrical imaging of a controlled saline tracer injection. *Journal of Applied Geophysics,* **44,** 85-102, DOI: http://dx.doi.org/10.1016/S0926-9851(00)00002-1.

Slaymaker O, Kelly REJ. 2009. The cryosphere and global environmental change. *Area,* **41,** 112-113, DOI: 10.1111/j.1475-4762.2008.875_5.x.

Smith ADH, Crabtree DR, Bilzon JLJ, Walsh NP. 2010. The validity of wireless iButtons (R) and thermistors for human skin temperature measurement. *Physiological Measurement,* **31,** 95-114, DOI: 10.1088/0967-3334/31/1/007.

Sosio R, Crosta GB, Hungr O. 2008. Complete dynamic modeling calibration for the Thurwieser rock avalanche (Italian Central Alps). *Engineering Geology,* **100,** 11-26, DOI: http://dx.doi.org/10.1016/j.enggeo.2008.02.012.

Starnes DS, Yates D, Moore DS. 2010. *The Practice of Statistics*, W. H. Freeman.

Stephens MA. 1974. EDF Statistics for Goodness of Fit and Some Comparisons. *Journal of the American Statistical Association,* **69,** 730-737, DOI: 10.2307/2286009.

Stingl H. 1971. Zur Verteilung von Groß- und Miniaturformen von Strukturböden in den Ostalpen. *Nachrichten Akademische Wissenschaften in Göttingen, Mathematisch-Physikalische Fakultät. Vandenhoeck & Ruprecht, Göttingen.,* **2,** 25-40.

Stingl H, Garleff K, Höfner T, Huwe B, Jaesche P, John B, Veit H. 2010. Grundfragen des alpinen Periglazials – Ergebnisse, Probleme und Perspektiven periglazialmorphologischer Untersuchungen im Langzeitprojekt „Glorer Hütte" in der Südlichen Glockner-/ Nördlichen Schobergruppe (Südliche Hohe Tauern, Osttirol). *Salzburger Geographische Arbeiten***,** 15-42.

Stoffel M, Tiranti D, Huggel C. 2014. Climate change impacts on mass movements - Case studies from the European Alps. *Science of the Total Environment,* **493,** 1255-1266, DOI: 10.1016/j.scitotenv.2014.02.102.

Supper R, Ottowitz D, Jochum B, Romer A, Pfeiler S, Kauer S, Keuschnig M, Ita A. 2014. Geoelectrical monitoring of frozen ground and permafrost in alpine areas: field studies and considerations towards an improved measuring technology. *Near Surface Geophysics,* **12,** 93-115, DOI: 10.3997/1873-0604.2013057.

Telford W, Geldart L, Sheriff R. 1990. *Applied Geophysics,* Cambridge, Cambridge University Press.

Tollner H. 1951. Über Schwankungen von Mächtigkeit und Dichte ostalpiner Firnfelder. *Theoretical and Applied Climatology,* **3,** 189-208.

Trabant PK. 1988. *Applied High-Resolution Geophysical Methods,* Prentice Hall, Upper Saddle River.

Tukey JW. 1977. *Exploratory Data Analysis*, Addison-Wesley Publishing Company.

Veit H. 1993. Holocene solifluction in the Austrian and Southern Tyrolian Alps: dating and climatic implications. *Palaeoclimate Research,* **11,** 23-32.

Wakonigg H. 1996. *Unterkühlte Schutthalden.* University of Graz.

Whalley WB. 1974. The mechanics of high-magnitude low-frequency rock failure. *Reading Geographical Papers,* **27**.

Whalley WB. 1984. Rockfalls. *In:* BRUNDSDEN, D, PRIOR, DB (eds.) *Slope Instability.* Chinchester: Wiley.

Williams Jr. RS, Ferrigno JG. 2012. State of the Earth's cryosphere at the beginning of the 21st century–Glaciers, global snow cover, floating ice, and permafrost and periglacial environments. *U.S. Geological Survey Professional Paper 1386–A*, 546.

Williams PJ, Smith MW. 1989. *The frozen earth – fundamentals of geocryology*, Cambridge University Press.

Zhang TJ. 2005. Influence of the seasonal snow cover on the ground thermal regime: An overview. *Reviews of Geophysics,* **43,** 26, DOI: 10.1029/2004rg000157.

Zhao L, Wu QB, Marchenko SS, Sharkhuu N. 2010. Thermal State of Permafrost and Active Layer in Central Asia during the International Polar Year. *Permafrost and Periglacial Processes,* **21,** 198-207, DOI: 10.1002/ppp.688.

Zhou J, Kinzelbach W, Cheng GD, Zhang W, He XB, Ye BS. 2013. Monitoring and modeling the influence of snow pack and organic soil on a permafrost active layer, Qinghai-Tibetan Plateau of China. *Cold Regions Science and Technology,* **90-91,** 38-52, DOI: 10.1016/j.coldregions.2013.03.003.